Fall 2012

Development and application of a two-dimensional hydrodynamic model for assessment of modern and historical flow conditions of Upper Mississippi River Pool 8 near La Crosse, Wisconsin

Brice E Stafne
University of Iowa

DEVELOPMENT AND APPLICATION OF A TWO-DIMENSIONAL HYDRODYNAMIC MODEL FOR ASSESSMENT OF MODERN AND HISTORICAL FLOW CONDITIONS OF UPPER MISSISSIPPI RIVER POOL 8 NEAR LA CROSSE, WISCONSIN

by

Brice E. Stafne

A thesis submitted in partial fulfillment
of the requirements for the Master of
Science degree in Civil and Environmental Engineering
in the Graduate College of
The University of Iowa

December 2012

Thesis Supervisors: Professor Larry J. Weber
Adjunct Assistant Professor Douglas J. Schnoebelen

Graduate College
The University of Iowa
Iowa City, Iowa

CERTIFICATE OF APPROVAL

MASTER'S THESIS

This is to certify that the Master's thesis of

Brice E. Stafne

has been approved by the Examining Committee
for the thesis requirement for the Master of Science
degree in Civil and Environmental Engineering at the December 2012
graduation.

Thesis Committee: _____
Larry J. Weber, Thesis Supervisor

_____
Douglas J. Schnoebelen, Thesis Supervisor

_____
A. Jacob Odgaard

ACKNOWLEDGMENTS

First of all I would like to acknowledge and thank the faculty and staff at IIHR – Hydroscience and Engineering for the help and support they have provided during my time at the institute. Drs. Doug Schnoebelen and Larry Weber, especially, have mentored me both professionally and personally. Additionally, I would like to thank Dr. A. Jacob Odgaard for being on my thesis committee. Others at the institute, including Oscar Hernandez, Jesse Piotrowski, and Dr. Nate Young provided invaluable modeling and GIS assistance.

Additionally, I would like to thank the RCS staff, including Brian Miller and Mark Wilson, for providing computer support, the administrative staff for keeping the institute running smoothly, and Nick Thornburg for helping with digitization of the historic maps. I would also like to thank my fellow IIHR students, including Rebecca Sheler, Matt Wunsch, Ben Reith, and Nick Thomas for making my time here fun and memorable.

I would like to acknowledge the passionate group of engineers and scientists working on the Upper Mississippi, including Chuck Theiling, Jon Hendrickson and Kevin Landwehr at the Army Corps of Engineers, Jeff Janvrin at the Wisconsin DNR, and various staff at the USGS Upper Midwest Environmental Science Center who provided specific help for this project. Their dedication to understanding and protection of the river is admirable.

I would also like to thank my family. My parents, Bruce and Rachel Stafne, have always supported me and made countless sacrifices as I've pursued my dreams, educational or otherwise. Finally, I want to acknowledge the grace of God, Who has blessed me with wonderful family, mentors, and friends, and opened opportunities I could never have imagined.

ABSTRACT

The Upper Mississippi River System (UMRS) is a diverse and dynamic ecosystem that includes the main stem river channel, side channels, backwater floodplains and lakes, islands, wetlands, grasslands, and floodplain forests. The hydrology of this rich ecosystem is one of the key drivers for physical, chemical and biological processes. However, the hydrology and hydraulics of the UMRS has been drastically altered from its natural state as a result of the construction of the locks and dams in the 1930s. Beginning with the Water Resources Development Act of 1986, biologists, ecologists, and engineers have been working to restore the river to a more natural state within the current constraints imposed by the lock and dam system. In an effort to restore rivers to a more natural state, the determination of a hydraulic reference condition is essential to understanding the "why and how" of historical river system function. Understanding the fundamental processes of historical conditions will help prioritize resources and better quantify possible outcomes for riverine restoration.

The main goal of this study was to construct a hydrodynamic reference condition for Pool 8 of the Upper Mississippi River System using hydrodynamic computational fluid dynamic (CFD) modeling. The CFD model will provide a better understanding of pre-impoundment flow conditions as compared to post-impoundment conditions today. The numerical model was constructed and developed primarily from a pre-impoundment 1890s topographic map with bathymetric cross-sections in the channels. The 1890s map and other sources from the U.S. Army Corps of Engineers provided historic elevation and hydraulic reference data for model calibration. The calibrated historic model was then compared with a current model of similar scale representing post-impoundment conditions, allowing for quantitative analysis of the differences between the two conditions.

Model results indicated large changes in average depth and average velocity between historic and current conditions in certain parts of the pool, while others remained relatively unchanged. For example, velocities decreased in main channel aquatic areas in the lower part of Pool 8 from an average of 0.6 m/s (2.0 ft/s) under historic conditions to 0.1 m/s (0.3 ft/s) under current conditions. In the same part of the pool, however, velocities in contiguous backwater areas remained relatively constant, with most remaining less than 0.25 m/s (0.82 ft/s). Additionally, in the lower part of the pool, discharge distribution between the floodplain areas and the main channel was historically much more dynamic, with flow concentrated in the main and secondary channels at discharges less than 2265 m^3/s and in the floodplains at greater than 2265 m^3/s. Under current conditions, discharge distribution is much less dynamic, with approximately 2/3 of the total discharge conveyed on the floodplain for all discharges modeled (283 m^3/s to 2832 m^3/s or 10,000 ft^3/s to 100,000 ft^3/s).

TABLE OF CONTENTS

LIST OF TABLES

LIST OF FIGURES

CHAPTER 1: INTRODUCTION

1.1 The Upper Mississippi River

The Upper Mississippi River System (UMRS) is recognized as both an important resource for commercial navigation and as a diverse ecosystem. In the Upper Mississippi River Management Act of 1986, Congress emphasizes this dual purpose distinction, stating "To ensure the coordinated development and enhancement of the Upper Mississippi River system, it is hereby declared to be the intent of Congress to recognize that system as a nationally significant ecosystem and a nationally significant commercial navigation system." (USGS, 1999)

Historically, flood plains have been very important both culturally and economically. Early civilizations were established in fertile flood plains, which later became focal points for urban development and exploitation of their resources (Tockner and Stanford, 2002). Similarly, society has tried to harness the UMR for navigation, utilize its resources (agricultural land, water, timber, and wildlife), and control it to protect human development from flooding. Attempts to improve navigation on the Mississippi River began in the early 1800s with the first dredging and snag removal projects, continued through the construction of the lock and dam system in the 1930s, and still occur today with the maintenance of the system. Along the way, the characteristics of many parts of the river have been drastically altered.

Today, the five UMRS states of Minnesota, Wisconsin, Iowa, Illinois, and Missouri, along with Federal agencies including the U.S. Army Corps of Engineers, U.S. Fish and Wildlife Service, and the U.S. Geological Survey work collaboratively to manage the river to meet both navigation and habitat rehabilitation objectives. Rehabilitation and restoration projects involve an extensive planning process to assess goals and determine the best alternative to meet those goals. It can often be difficult to assess the alternatives without an understanding of how the system historically

functioned, however. Computer generated hydrodynamic models, coupled with historic reference data, can help river managers better understand the fundamental hydraulics of the river as it existed prior to construction of the lock and dam system.

1.2 Motivation

Natural hydrologic processes and hydraulic patterns fundamentally influence the high productivity characteristics of river floodplain ecosystems and form the framework for many biological and chemical processes (Gore and Shields, 1995; Opperman et al., 2010; Tockner and Stanford, 2002). Currently, naturalization of the hydrologic regime is identified as one of the five system-wide objectives for restoration in the UMRS as described in the essential ecosystem characteristic (EEC) framework identified by the Navigation and Ecosystem Sustainability Program (NESP) Science Panel (Galat et al., 2007). Galat et al. (2007) outlines five objectives that are to be managed for in the UMRS:

1. A more natural hydrologic regime (hydrology and hydraulics)
2. Processes that shape a diverse and dynamic river channel (geomorphology)
3. Processes that input, transport, assimilate, and output materials within the UMR basin river-floodplains: water quality, sediments, and nutrients (biogeochemistry)
4. A diverse and dynamic pattern of habitats to support native biota (habitat)
5. Viable populations of native species and diverse plant and animal communities (biota)

The EEC framework describes how physical processes and structure (hydrology/hydraulics, biogeochemistry, and geomorphology) affect habitat structure, which in turn supports plant and animal species. Figure 1.1, which is reproduced in different forms in many UMRS planning study reports (Galat et al., 2007; USACE – RI, 2011), illustrates these relationships.

Development of levee systems, construction of channel training structures, and construction and operation of the locks and dams have significantly altered the hydraulic

conditions throughout the UMRS. The NESP Science Panel recognizes that restoration and maintenance of native river biota requires reestablishing a more natural hydrograph. Likewise, it recognizes that hydrodynamic conditions and hydraulic residence times in channels, backwaters, and floodplains will have to be restored to the extent possible to meet requirements of native species (Galat et al., 2007).

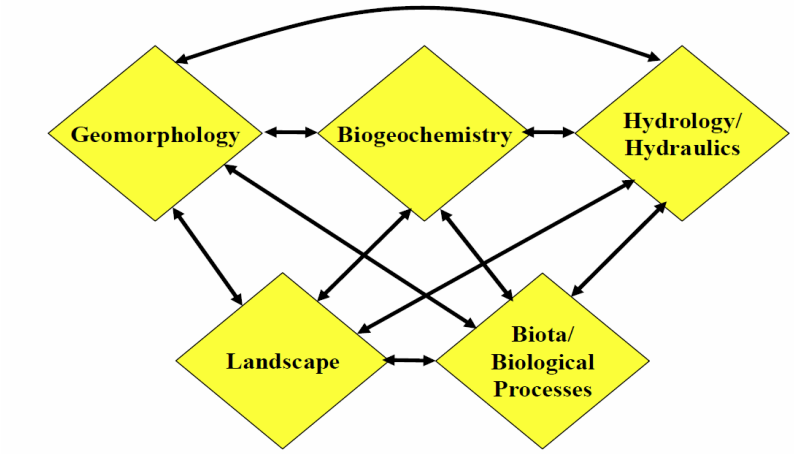

Figure 1.1: Upper Mississippi River System Essential Ecosystem Characteristic conceptual model.

Source: Upper Mississippi River System Ecosystem Restoration Objectives. U.S. Army Corps of Engineers – Rock Island District, 2011.

In order to restore the river ecosystem to support those native species, it is important to understand the physical characteristics of the system in its pre-altered state, or, what might have been the historical condition for the UMRS. Those physical characteristics can be defined in a broad sense as reference conditions. There is strong interest in the scientific community responsible for managing the river in determining the hydrodynamic reference conditions (water velocities and depths at the fundamental level) for pre-impoundment conditions on the UMRS. However, until this point, no research

has been performed with that specific goal in mind (Weber, 2011-2012; Schnoebelen, 2011-2012).

The reference condition concept is widely used in ecosystem planning and regulatory framework (Nestler, et al. 2010). Nestler et al. (2010) also explain a variety of ways to define the reference condition, including:

- *Reference condition for biological integrity* preserves the original concept of reference condition.
- *Best attainable condition (A_{BAC})* is the best condition available today and in the immediate future.
- *Minimally disturbed condition* is the absence of significant human disturbance, and likely the best approximation or estimate of biotic integrity.
- *Historical condition* any one of a number of pre-existing conditions or possibly the Reference Condition for Biological Integrity.
- *Least disturbed condition* is the best available physical, chemical and biological habitat conditions given today's state of the landscape.
- *Self reference* is based on data collected on a minimally impacted part of the greater system.
- *Evaluation of ambient conditions* to identify locally limiting conditions or stressors.

The value of quantitative reference condition analysis has already been demonstrated in the UMRS by other researchers. Nestler, et al. (2010) asserts that the UMRS requires a quantitative framework to organize possible management actions into a strategic implementation plan that is scientifically defensible and internally consistent. They developed a quantitative restoration framework and applied it to an example in the UMRS. In that application, hydrologic summary variables derived from stage data in Geomorphic Reach 3 were used to characterize conditions in each gage reach. Nestler et

al. also argue that the mathematical framework can be applied to the other EECs identified by researchers.

In particular, mathematical models can be useful for determining and assessing reference conditions because historical observations of flow events (low and high) are often lacking or poorly defined. Once a model has been shown to accurately reproduce known flow events, it becomes a powerful predictive tool for other flow scenarios. However, this predictive ability depends on the use of physically correct, deterministic hydraulic equations that aren't limited to use by empirical relationships (Cunge, Holly and Verwey, 1980, 133). This study applies such a numerical model based on physical processes, rather than relying on empirical relationships alone. The resulting model can yield a wealth of data for different flow scenarios, allowing comparisons of historical, current, and future flow events.

1.3 Objectives

The main goal of this study was to provide a hydrodynamic reference condition for Pool 8 for pre-impoundment conditions using two-dimensional numerical modeling. The study used the best historical data available (maps, river stages, flow) combined with the latest computer and computational methods available. The necessity of trying to determine hydrodynamic reference conditions to native species for use in the adaptive management framework is well recognized, but often difficult to achieve. This study built on the work of Smith (2011), who created a model of current conditions in Pool 8, by now creating a model of similar scale and scope for pre-impoundment (historical) conditions. With a library of both pre-impoundment and current hydrodynamic conditions compiled, a spatially correlated comparison of historic and current conditions will enable researchers and managers to better manage Pool 8. Specifically, the goals of this study were as follows:

- Create a seamless digital elevation model in the form of a raster image from historic floodplain maps to serve as the elevation source for the hydrodynamic model
- Gather and compare the available reference data describing historic hydraulic conditions
- Generate a two-dimensional hydraulic model representing historic hydrodynamic conditions in the area that is now Pool 8
- Determine model sensitivity to roughness coefficients and river bed topography
- Compile a library of discharge scenarios for historic conditions
- Perform quantitative comparisons between similar discharges in current conditions versus historic conditions

1.4 Study Area

The UMR is broken down into three floodplain reaches (not including the Illinois River). These include the Upper and Lower Impounded reaches and the Unimpounded Reach. The study area is located in the Upper Impounded reach, which extends from St. Paul, MN to Clinton, IA and includes the Upper and Lower St. Anthony Falls dams, and Lock and Dams one through thirteen. The Upper Impounded reach is characterized by narrow, island-filled floodplains that are bounded by steep bluffs (USGS, 1999). More specifically, the area now known as Pool 8 is located in Geomorphic Reach 3, which includes present day Pools 5 through 9. Historically, the reach exhibited classic island-braided morphology and today includes either the highest or near highest total absolute acreage of islands in the UMRS on a per pool basis (WEST Consultants, 2000).

Pool 8 was chosen as the location for this study because of the importance of this pool for both navigation and ecosystem restoration activities in the UMR. The present research builds on previous modeling work of current conditions in Pool 8 by Smith (2011), which then allows for comparison of modern and historical conditions. In

addition, Pool 8 is located near the U.S. Geological Survey (USGS) Upper Midwest Environmental Science Center (UMESC) and, as a result, has been the subject of many biological studies together with navigation improvement and habitat restoration work by the U.S. Army Corps of Engineers (USGS, 2012; Janvrin et al. [no date]; USACE – SP, 2012a; USACE – RI, 2011; Hendrickson and Hrdlicka, 2003; Hendrickson, 2010 for example). Additionally, because Pool 8 is part of the Long Term Resource Monitoring (LTRM) component of the Environmental Management Program (EMP), it will continue to be of interest for river managers and scientists (USGS, 2012).

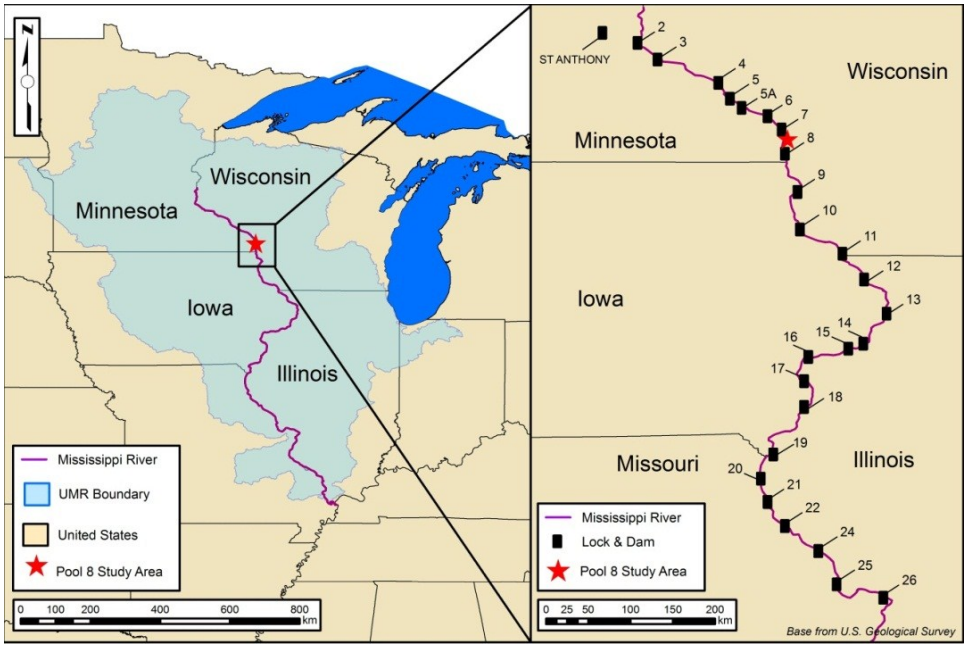

Figure 1.2: Aerial map of the study area showing the location of the present day Pool 8 within the UMR basin and the lock and dam system.

Source: Smith, T. J. "Simulation of spatial and temporal trends in hydrodynamic conditions of Upper Mississippi River Pool 8." *MS Thesis*. Iowa City, IA: The University of Iowa, 2011.

Figure 1.2 above shows the location of the study area in the UMR basin. Pool 8 divides the states of Minnesota and Wisconsin, and runs from Lock and Dam 7 near Onalaska and La Crosse, WI south past Brownsville, MN and Stoddard, WI and ends at

Lock and Dam 8 near Genoa, WI. Figure 1.3 shows river mile measurements that are used for linear reference on the river. Present day Lock and Dam 8 is located at River Mile 679.2 and Lock and Dam 7 is located at River Mile 702.5.

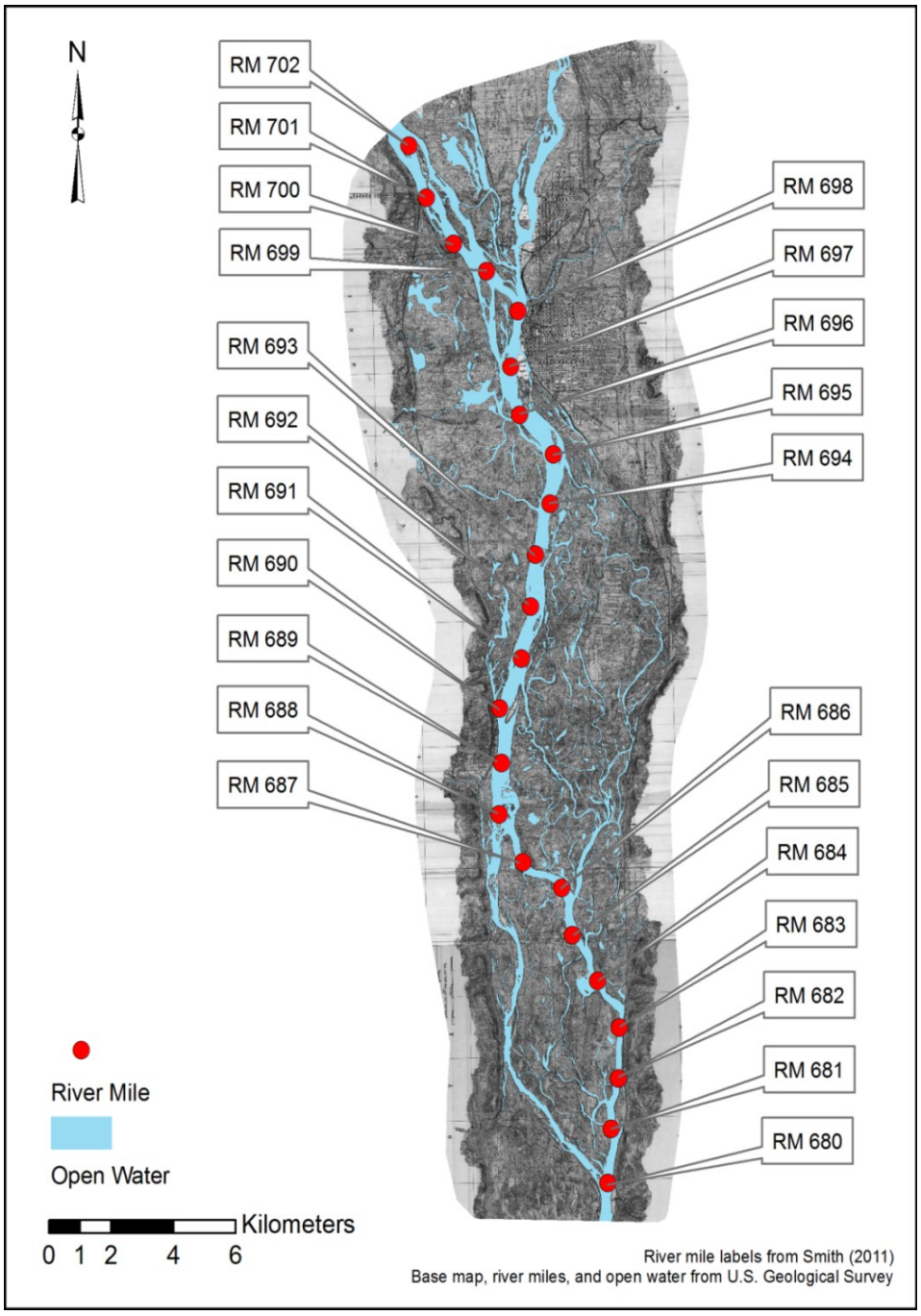

Figure 1.3: River miles referenced throughout the report overlaid over historic base map.

CHAPTER 2: LITERATURE REVIEW

2.1 Upper Mississippi River Navigation Projects – Historical Overview

A brief timeline of the history of the navigation improvements on the Upper Mississippi River is presented to better understand the hydrology of the present river. This section is not meant to be comprehensive, but rather to provide a framework for the reader on how the Upper Mississippi River has evolved to its present condition. Much of the channelization history of the Upper Mississippi River is detailed by John Anfinson (2003), a historian with the National Park Service in his book "*The River We Have Wrought.*"

The first Federal funding for navigation improvements on the Mississippi River was authorized in the 1824 Rivers and Harbors Act. It included $75,000 for removing snags and clearing sandbars (Anfinson, 2003, p. 23-25). In the Rivers and Harbors Act of 1866, Congress directed the Corps to survey the Upper Mississippi with the goal of establishing a 4-foot navigational channel. The Major of Engineers, Gouverneur K. Warren issued his first annual report in 1867, in which he requested funding for, among other things, the purchase and operation of two dredge and snag boats and the construction of two experimental wing dams. In his report, Warren was skeptical of channel constriction in the form of wing dams and closing dams, in part because he argued the whole upper river would need to be channelized to prevent sand from depositing where the channel constrictions stopped. Warren recommended the use of dredging instead of channel constriction as the main focus to achieve his objective.

Congress authorized two dredges, the Montana and the Caffrey. Along with dredging, the two ships were tasked with removing snags and cutting down overhanging trees that threatened to sweep cargo and passengers from the passing steamboats. Together, they removed more than 2,600 leaning trees in 1872, 3,100 in 1876, and over

6,300 in 1877. They were so successful at removing snags that, by 1876, the Montana removed only 37 snags in the entire stretch between St. Paul and the Des Moines Rapids (Anfinson, 2003, p. 40-43). Although the dredging and snag removal allowed steamboats to travel the river more safely, the bulk of the changes made were temporary. If maintenance efforts ceased, the river would quickly return to its natural state, full of snags, sand bars and leaning trees. To make more drastic, permanent channel modifications, an entirely new program with significant increases in funding was necessary (Anfinson, 2003, p. 50).

Congress authorized the 4½-foot channel project on June 18, 1878 (Anfinson, 2003, p. 79). In support of the project, an extensive survey, often referred to as Farquhar's survey after the Rock Island District commander, Major Francis Farquhar, was conducted between 1878 and 1879 (Anfinson, 2003, p. 82-83). Figure 2.1 shows an example of Farquhar's 1879 survey of the Mississippi River near La Crosse, WI.

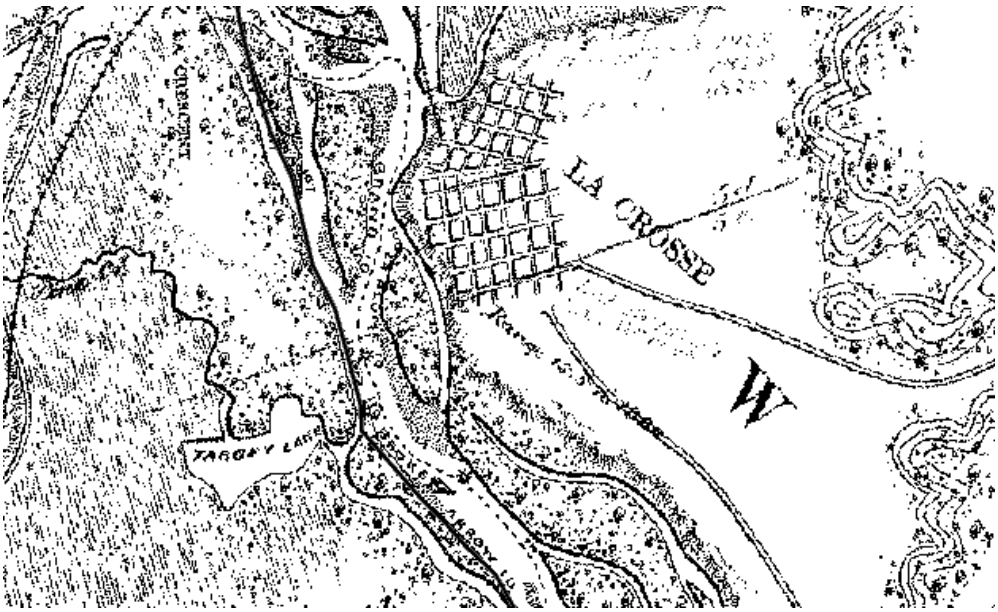

Figure 2.1: Farquhar survey map near La Crosse, WI.

Source: U.S. Geological Survey Upper Midwest Environmental Sciences Center. *Upper Mississippi River Historic Data Viewer.* http://umesc-gisdb03.er.usgs.gov/umr_historic_data/viewer.aspx (accessed 2012).

Captain Alexander Mackenzie assumed command of the Rock Island District in 1879. Under his watch, the Corps reduced the channel's width to 800 feet between Winona and La Crosse through the use of wing dams and closing dams. They built 336 miles of wing dams and closing dams, and laid over 197 miles of shoreline protection by 1905. They also built six reservoirs from which water could be released at low flows to help boost water depths on the river (Anfinson, 2003, p. 85-90).

Tough economic conditions around the turn of the century led to increasing pressure from cities on the river for further changes to the Upper Mississippi. They successfully lobbied Congress to authorize a survey for construction of a 6-foot channel in 1905. The completed survey report, submitted in June of 1906, argued that the project objectives could be accomplished by building more wing dams and closing dams, and raising or extending existing structures (Anfinson, 2003, p. 125-126). Congress would go on to authorize construction of the 6-foot project in March of 1907 (Anfinson, 2003, p. 140). The Corps worked to accomplish their mission of a 6-foot channel through the use of wing dams and closing dams, but still came up short in certain reaches of the river.

By 1918, no packetboats or barges carried freight between St. Louis and St. Paul and only local traffic used the river (Anfinson, 2003, p. 188). A unified group of farmers, industry, and politicians led by the Twin Cities real estate industry again pushed for the river's revival. After re-establishing commerce on the river through an agreement between the government run Inland Waterways Corporation (IWC) and a private company, the Barge Line Company, supporters turned their lobbying efforts to Washington D.C. After they failed to convince the Chief of Engineers, the House Rivers and Harbors Committee, and President Herbert Hoover to include the project in the 1930 River and Harbors Act based on a preliminary survey, they finally convinced the Senate to include it in their version of the bill. The Rivers and Harbors Act of 1930 was signed on July 3, 1930, providing authorization for the 9-foot project and initial funding of $7.5

million (Anfinson, 2003, p. 231-237,244). The authorization of the 9-foot channel would have long reaching effects on the hydrology and habitat of the Mississippi River.

2.2 Impacts of the Navigation Projects

Impacts to riverine habitat as a result of the construction of the locks and dams, as well as other navigation improvements such as river training structures and dredging, are extensive. Chen and Simons (1986) documented changes in hydrologic, hydraulic, and geomorphic characteristics and related those changes to navigational development and maintenance activities in the UMRS. They found that low dikes, built mostly during the 4½and 6-foot projects, had little impact on flood stages and did not change the position of the river appreciably. They did find, however, that surface area of the Upper Mississippi generally decreased, while island area increased, as a result of low dikes. Additionally, they found river bed elevation degraded about 0.5 meters (1.6 feet) in major portions of Pool 4 and in Pools 5 through 9. They found the bed in pools 24, 25 and 26 aggraded slightly, however.

Post lock and dam construction, Chen and Simons (1986) found that flood stages actually decreased slightly, probably due to a decrease in overbank vegetation that occurred when the floodplain was permanently inundated. Additionally, they found that river position didn't change appreciably, although river surface areas above the locks and dams generally increased and surface areas below the locks and dams decreased, probably due to sedimentation. Island areas decreased immediately upstream of the locks and dams and increased downstream. Also, due to the inundation, many natural levees became submerged, causing a system wide increase in the total number of islands.

The islands created immediately after lock and dam construction didn't last, however. Wind and wave induced island erosion caused a drastic decline in island areas in the lower part of many Upper Mississippi pools. In Pool 8, Fischer and Claflin (1995) reported the 1939 to 1989 reduction in area of islands in the lower part of the pool to be 79%. Islands are important to the riverine lake habitat for a few reasons. They provide

habitat for deer, raccoons, mink and river otters, and serve as nesting areas for turtles, ducks, and other birds. Additionally, islands protect aquatic vegetation by deflecting river currents and breaking up waves as they roll across the large impounded areas above the locks and dams (Janvrin et al., [no date]).

Sediment deposition in backwater regions is a major problem, as well. One such example, Pool 19 upstream of Keokuk Iowa, has seen a reduced volume of 58.4% when compared with its original impounded volume. A typical succession is from open water, to submerged macrophyte beds, to emergent macrophyte beds, and ultimately terrestrial area (Bhowmik and Adams, 1989).

2.3 Upper Mississippi River System Ecosystem Restoration

Multiple programs exist to rehabilitate or restore habitat in the UMRS. In the Water Resources Development Act of 1986, Congress established the Environmental Management Program (EMP). Later acts amended the program, including the 1999 WRDA, which extended the program without a termination date and required a report to Congress every 6 years. Through fiscal year 2012, a total of $441,933,000 has been allocated to the program system wide, allowing for construction of 26 projects in the St. Paul District (USACE – SP, 2012b). Additionally, the Navigation and Ecosystem Sustainability Program (NESP) was authorized as part of the Water Resources Act of 2007. No funding has been allocated for construction of any projects designed under the NESP through fiscal year 2013, however (USACE – SP, [no date, b]).

Three common techniques for habitat rehabilitation are to introduce flow to counteract oxygen depletion in backwaters or side-channel isolation, isolate backwaters to reduce sedimentation inputs, and construct islands to reduce wave energy and sediment resuspension (Theiling 1995). Some of these techniques have been applied specifically to Pool 8. A significant island building rehabilitation project has taken place in Pool 8, of which three phases including 25 islands have been constructed thus far (USACE – SP, 2012a). Phase II included rock sills as part of the Stoddard island complex. The rock

sills were designed to be overtopped during high water events but provide for minimal overtopping during October to March. A notch in the northernmost rock sill was designed to promote scour between the islands and to allow for oxygenated water exchange at low flows in the winter and summer months (Janvrin et al., [no date]).

2.4 Other Numerical Modeling Studies and Reference Condition Analysis in Pool 8

Numerous numerical hydraulic modeling studies have been conducted in Pool 8. Additionally, research defining various reference conditions has been performed, including work in the area of Pool 8.

The U.S. Army Corps of Engineers used a two-dimensional hydraulic model in the planning of Phase II of the Pool 8 Islands HREP. The model was used to evaluate the effect of island layout on promoting scour in interior channels and to predict under ice velocities in an effort to create overwintering habitat for centarchids (Janvrin et al., [no date]).

Similarly, as part of the 2000 Cumulative Effects Study prepared by WEST Consultants for the U.S. Army Corps of Engineers – Rock Island District, hydrodynamic model results were used to define typical hydraulic characteristics associated with UMRS aquatic classes. Those aquatic classes – defined as main channels, secondary channels, contiguous backwaters, and isolated backwaters in the study – were further used to identify habitat areas associated with defined ecological guilds (WEST Consultants, 2000).

IIHR – Hydroscience and Engineering has performed two studies specific to Pool 8. Smith (2011) used a pool scale two-dimensional model to generate a library of steady state flow simulations for input into an ecological model being developed at the University of Illinois. The study also demonstrated various model products that could be of use to biologists as an additional planning tool for restoration activities. Schubert

(2009) created a three-dimensional CFD model to model nutrient processing in Round Lake, located within Pool 8.

The U.S. Army Corps of Engineers used a two-dimensional hydrodynamic model to assess the impact of adjusting discharge through the Reno Spillway and Hastings Spillway in the Lock and Dam No. 8 embankments. River managers were concerned about the hydraulic head that exists at times between the main channel of the Mississippi River and the area known as Reno Bottoms. The study included an approximate simulation of historic conditions by removing the dam embankment from the model and making use of historic bathymetry information near the dam, as well as historic topographic information, to ensure that elevations near the dam were reasonable (USACE – SP, [no date, a]).

Theiling and Nestler (2010) and Nestler et al. (2010) presented a numerical framework for reference condition analysis and applied the framework to hydrologic variables in the UMR. They indicate that the framework can also be applied to other EECs, which could have utility for hydraulic condition comparisons presented in this study.

CHAPTER 3: NUMERICAL MODEL

3.1 Types of Numerical Models

Hydraulic models can be classified by how they simplify the governing equations of fluid flow in time and space and the assumptions associated with those simplifications (Toombes and Chanson, 2011). Generally, numerical models for simulation of river hydraulics can be lumped into three broad categories: one-dimensional (1-D), two-dimensional (2-D), and three dimensional (3-D). The increasing complexity of the flow field that must be modeled leads to the necessity of higher order modeling schemes. Along with making less simplifying assumptions, higher order modeling schemes generally require more time for model set-up and take more computation time to run.

The most simplified representation of fluid flows is accomplished with 1-D models, which assume, as the name indicates, that flow is largely unidirectional. As a result, there is no direct modeling of changes in flow distribution, cross section shape, or flow direction (Toombes and Chanson, 2011). The river and floodplain are represented by a series of cross sections oriented perpendicular to the flow, with a cross section-averaged velocity and water depth computed at each cross-sectional "slice" (Bates and De Roo, 2000). Those cross sections can then be linearly interpolated and combined with a DEM to generate a representative inundated area or depth grid, thus making 1-D modeling most efficient for large scale flood inundation studies. Because of the ecological focus of this study and with the associated interest of flow fields around floodplain structure, one-dimensional models do not provide the desired level of detail.

While 1-D models are typically used for modeling well defined and constant flow paths, 2-D models are commonly used for modeling floodplains or coastal and marine situations where the flow path is poorly defined. Most 2-D models are based on the depth-averaged Navier-Stokes equations, known as the 2-D Saint-Venant equations or the shallow water equations. The 2-D Saint-Venant equations are based on the assumption

that the horizontal length scale is significantly greater than the vertical length scale, which implies (assumes) that vertical velocities are negligible, vertical pressure gradients are hydrostatic, and horizontal pressure gradients are due to displacement of the free surface. 2-D models calculate velocities and depths across a grid or mesh that represents the topography of the study area (Toombes and Chanson, 2011). Along with increased computational time and costs required to set up the model, 2-D models require digital elevation data with complete coverage of the study area, whereas 1-D models can be created from elevation data gathered with traditional cross section survey methods. However, the increasing abundance of available continuous digital elevation data combined with decreasing costs of high performance computing allow for easier adoption of 2-D modeling for a wider variety of applications (Bates and De Roo, 2000).

3-D hydraulic models can vary widely in terms of complexity and capability, such as quasi-3-D approaches that can derive a third velocity component from the continuity equation after solving the Saint-Venant equations, to direct numerical simulations where turbulence is resolved at the fundamental level. For river hydraulics, 3-D models are most often used for detail around hydraulic structures where vertical velocities and acceleration are important, or for applications where eddies and recirculation drive residence times critical for biogeochemical processes and applications.

3.2 Sedimentation and River Hydraulics – Two Dimensional model (SRH-2D)

The numerical hydrodynamic modeling for this study was performed using SRH-2D, which was developed by the U.S. Bureau of Reclamation (USBR) for 2-D modeling of river systems. The current version of the model released to the public includes only the flow module, which solves the 2-D depth-averaged Saint-Venant equations using the finite volume method. Future releases of the model will include modules related to sediment, temperature, and vegetation modeling. Temporal discretization is performed implicitly, leading to a stable solution through a wider range of time steps, but requiring

more computational time than explicit methods. For spatial discretization, SRH-2D uses an unstructured hybrid mesh of quadrilateral or triangular mesh cells stored in the generic 2-D mesh format (.2DM). The ability to use both quadrilateral and triangular elements allows for greater flexibility when representing different features in the floodplain. For example, channels and levees may be represented with quadrilateral elements arranged in a structured fashion, while floodplain elements with a more irregular planform can be represented with triangular elements (USBR, 2008).

3.3 Governing Equations

The 2D Saint-Venant equations solved in SRH-2D are derived from the full 3-D Navier-Stokes equations for mass and momentum conservation in fluid flows, which are shown in equations (3.1) through (3.4). In the following equations ρ is water density; t is time; x, y, and z are Cartesian coordinates; u, v, and w are velocity components in the x, y, and z directions, respectively; g is the gravitational acceleration; p is pressure; and τ is viscous stress (White, 2011).

$$\frac{\partial \rho}{\partial t} + \frac{\partial}{\partial x}(\rho u) + \frac{\partial}{\partial y}(\rho v) + \frac{\partial}{\partial z}(\rho w) = 0 \tag{3.1}$$

$$\rho\left(\frac{\partial u}{\partial t} + u\frac{\partial u}{\partial x} + v\frac{\partial u}{\partial y} + w\frac{\partial u}{\partial z}\right) = \rho g_x - \frac{\partial p}{\partial x} + \frac{\partial \tau_{xx}}{\partial x} + \frac{\partial \tau_{yx}}{\partial y} + \frac{\partial \tau_{zx}}{\partial z} \tag{3.2}$$

$$\rho\left(\frac{\partial v}{\partial t} + u\frac{\partial v}{\partial x} + v\frac{\partial v}{\partial y} + w\frac{\partial v}{\partial z}\right) = \rho g_y - \frac{\partial p}{\partial y} + \frac{\partial \tau_{xy}}{\partial x} + \frac{\partial \tau_{yy}}{\partial y} + \frac{\partial \tau_{zy}}{\partial z} \tag{3.3}$$

$$\rho\left(\frac{\partial w}{\partial t} + u\frac{\partial w}{\partial x} + v\frac{\partial w}{\partial y} + w\frac{\partial w}{\partial z}\right) = \rho g_z - \frac{\partial p}{\partial z} + \frac{\partial \tau_{xz}}{\partial x} + \frac{\partial \tau_{yz}}{\partial y} + \frac{\partial \tau_{zz}}{\partial z} \tag{3.4}$$

Water is generally considered incompressible for most engineering problems, causing the density terms to drop out of the continuity equation. Furthermore, most river hydraulics problems can be further simplified by assuming a hydrostatic pressure distribution as a result of negligible vertical motion of water particles. When the 3D equations shown in equations (3.1) through (3.4) are vertically averaged, the 2-D Saint-

Venant equations, or shallow water equations, are derived. Equation (3.5) is the continuity equation and equations (3.6) and (3.7) are the momentum equations.

$$\frac{\partial h}{\partial t} + \frac{\partial hU}{\partial x} + \frac{\partial hV}{\partial y} = 0 \tag{3.5}$$

$$\frac{\partial hU}{\partial t} + \frac{\partial hUU}{\partial x} + \frac{\partial hVU}{\partial y} = \frac{\partial hT_{xx}}{\partial x} + \frac{\partial hT_{xy}}{\partial y} - gh\frac{\partial z}{\partial x} - \frac{\tau_{bx}}{\rho} \tag{3.6}$$

$$\frac{\partial hV}{\partial t} + \frac{\partial hUV}{\partial x} + \frac{\partial hVV}{\partial y} = \frac{\partial hT_{xy}}{\partial x} + \frac{\partial hT_{yy}}{\partial y} - gh\frac{\partial z}{\partial y} - \frac{\tau_{by}}{\rho} \tag{3.7}$$

In the above equations, h is the water depth; t is time; x and y are Cartesian coordinates; U and V are depth-averaged velocities in the x and y directions, respectively; T_{xx}, T_{xy}, and T_{yy} are depth-averaged stresses due to turbulence and dispersion; g is gravitational acceleration; z is the water surface elevation calculated by adding the bed elevation and water depth; τ_{bx} and τ_{by} are bed shear stresses; and ρ is the density of water (Lai, 2010).

Effective stresses are calculated using the Boussinesq equations as shown in equations (3.8) through (3.10). In the following equations, ν is the viscosity of water, and ν_t is the eddy viscosity, calculated with a turbulence model (Lai, 2010).

$$T_{xx} = 2(\nu + \nu_t)\frac{\partial U}{\partial x} \tag{3.8}$$

$$T_{yy} = 2(\nu + \nu_t)\frac{\partial V}{\partial y} \tag{3.9}$$

$$T_{xy} = (\nu + \nu_t)\left(\frac{\partial U}{\partial y} + \frac{\partial V}{\partial x}\right) \tag{3.10}$$

SRH-2D allows the modeler to choose between two turbulence models: a parabolic model shown in equation (3.11) and the two-equation k-ε model. The parabolic model was used for the current study. In equation (3.11), α is a model coefficient ranging from 0.3 to 1.0, and V_* is bed frictional velocity.

$$\nu_t = \alpha V_* h \tag{3.11}$$

The USBR suggests that the parabolic model works best for most field applications and notes that it requires less computing time. It is also suggests that final results may not be

sensitive to the model constant, α (USBR, 2008). This was confirmed by Smith (2011) through the performance of a sensitivity analysis using a model of similar scale to the current study. Smith (2011) found mean differences in water surface elevation between the default coefficient of 0.7 and coefficients ranging from 0.3 to 1.0 to be equal to or less than 0.00538 m (0.00164 ft) along a profile line extracted along the main channel of the Mississippi River.

Bed shear stress is calculated using equations (3.12) and (3.13), where *n* is Manning's coefficient (Lai, 2010). Manning's coefficient takes into account both bed roughness and form roughness and is the main method for calibration of the model. It is a spatially distributed constant.

$$\tau_{bx} = \rho\left(\frac{gn^2}{h^{1/3}}\right)U\sqrt{U^2+V^2} \tag{3.12}$$

$$\tau_{by} = \rho\left(\frac{gn^2}{h^{1/3}}\right)V\sqrt{U^2+V^2} \tag{3.13}$$

3.4 Numerical Discretization and Solution Process

In order to solve the 2-D Saint-Venant equations, which are partial differential equations with no analytical solution, both the spatial and temporal domain must be discretized, or broken up into smaller domains that can be reasonably approximated using numerical methods. SRH-2D solves the Saint-Venant equations using the segregated finite volume approach, with temporal discretization using the Euler implicit method (Lai, 2010).

For the spatial discretization, dependent variables are stored at the cell centers and the governing equations are integrated over the cell area using the Gauss integral. Cell face fluxes are calculated using a central difference scheme for the diffusive terms and a damped second-order central difference scheme for the convective terms to prevent oscillations in the solution (Lai, 2010).

Generally, temporal discretization can be either explicit, or implicit in nature. In explicit methods, the unknown variable at time t_n depends only on variables at t_{n-1}, while an unknown variable at t_n in implicit methods depends on neighboring cell values at t_n as well as values at t_{n-1}. Consequently, explicit methods result in equations that can be solved for one unknown variable while implicit methods require solving a system of equations, usually with large matrices (Anderson, 1995).

Each method has advantages and disadvantages. Explicit methods are easier to program and less computationally intensive. They are, however, conditionally stable when applied to the hyperbolic flow equations, meaning that grid size and timestep must be carefully chosen so that numerical errors aren't carried forward from previous calculations, eventually leading to a solution that diverges. Solution stability is given by the Courant number, as presented in equation (3.14), where Δx is the grid spacing, Δt is the time step, and c is a characteristic velocity. For a stable solution, the Courant number must be less than one.

$$C = c\frac{\Delta t}{\Delta x} \leq 1 \tag{3.14}$$

Implicit methods can be solved with larger timesteps and still remain stable. That can require less computational time for steady state problems as long as the additional time needed to solve the system of equations isn't greater than the gains made by using less timesteps. For unsteady problems, care must be taken to ensure that too large of a time step isn't chosen so that truncation error leads to incorrect results (Anderson, 1995).

As previously mentioned, SRH-2D solves the governing equations in a segregated manner. Within one iteration of the solution process, the momentum equations are solved first using the known values of water depth and eddy viscosity from the last time step, then the continuity equation is checked. If the velocities don't satisfy the continuity equation, an elevation correction equation is used to recalculate the water depth and then the velocities are recalculated. Finally, the scalar equations such as eddy viscosity and

bed shear stress are calculated. If an unsteady simulation is being performed, the process is then repeated within the same time step for the desired number of iterations (Lai, 2010).

CHAPTER 4: DIGITAL ELEVATION MODEL DEVELOPMENT

4.1 Source Data

As described in Section 2.1 , a variety of major historic river surveys were conducted. Most notable were the Warren Survey in the late 1860s and the Farquhar survey in the late 1870s. Neither survey contained the level of detail on the floodplain or the bathymetric data needed for a pool scale Digital Elevation Model (DEM). However, there is a detailed historic map created under the direction of the Mississippi River Commission (MRC) in the 1890s that has five foot contours on the floodplain and numerous bathymetric cross-sections in the channels. This map was created during the time of the 4½-foot project, but was not created as part of the navigation mission of the Corps. The river, as presented in this map, had already undergone initial modification through the construction of wing dams and closings dams. More discussion of the implications of these river training structures on the hydraulics within the river channel is provided in Chapter 7. The historic 1890 map did provide sufficient detail for construction of the DEM and the present hydrodynamic model.

The U.S. Geological Survey – Upper Midwest Environmental Sciences Center (USGS – UMESC) mosaicked and georeferenced the historic map plates into a MrSID compressed image that can be viewed in Environmental Systems Research Institute (ESRI) ArcGIS (ESRI, [no date]). MrSID is a set of software applications that compress large images and image databases and is patented by LizardTech (Los Alamos National Laboratory, [no date]; LizardTech, [no date]). The composite map representing Pool 8 was a mosaic of four individual MRC maps, numbers 170-173. The maps include the following data: Hydrology, Topology, Land Cover and Human Land Use information (USGS – UMESC, 2005).

4.2 Digitization Methodology

In general, pixel tracing software could not be used to automatically capture the contour lines directly from the map, due to "background noise" from other features present on the map. As a result, contours were traced by IIHR Research Computing Support staff into individual images corresponding to all of the contours of one elevation on the map. These images were then loaded into Softsoft Ltd.'s WinTopo Professional software, which generates vector files from raster files (SoftSoft Ltd, [no date]). Vectorisation is implemented in two steps using the WinTopo software. First, the image is "thinned," meaning lines in the raster are reduced from multiple pixels to a single pixel wide, creating a location for the vertex of the final polyline. Second, the vertices of the polyline are created at pixel locations and the polyline is smoothed and simplified according to user specified parameters. The Professional version of WinTopo provided two distinct advantages for this digitization. The first is an additional option for thinning and the second is the ability to batch process images into vector files. For this project, the "Best Combination" method was used for thinning, and smoothing and simplification of the final polyline used default parameters (SoftSoft Ltd, 2012).

Once the vector images were created in the geodatabase, an ESRI shapefile, they were imported into ArcMap and scaled visually to match the contours on the original map. The coordinate system was assigned and the contour elevations were added as an attribute to the polylines in the shapefile. Visual inspection and manual editing were required to correct areas where the thinning and pixel tracing process caused artifacts.

Cross-sectional bathymetry soundings were also shown on the maps. These points were digitized on the computer screen using ArcMap, by manually placing points at all of the sounding locations and entering a water depth corresponding to the original map data. The total number of points digitized was 4,430. The points were assigned a water surface elevation using stage information included on the historical maps. Because the original depth soundings took more than one day to survey, when the maps were

originally plotted, an average water surface elevation was calculated for each map and the depth soundings were adjusted to that average water surface. Lines of benchmarks, called "stone lines" on the historical maps, were located normal to the main channel at spacings of approximately three miles. Each map contained two or three stone lines. The average water surface elevation for each map was given at one stone line and the elevation change to the other stone lines on the map was also give. That allowed for calculation of the water surface elevation at two or three points on each map. For example, on Chart No. 171, the water surface elevation at stone line 214 is listed as 633.4 feet (193.06 meters) and the slope in feet from stone line 215 to 214 is given as 1.63 feet (0.50 meters). Since stone line 215 is upstream of 214, the elevation of the water surface at stone line 215 is 635.03 feet (193.56 meters).

Using that information, a continuous water surface was created in the form of a Triangulated Irregular Network (TIN) using the water level at each stone line as an isoline in the TIN. A significant assumption was made that the water surface in backwater areas and side channels did not vary with lateral distance from the main channel. As Figure 4.1 shows, the isolines for water surface were extended to the edge of the map area when the surface was generated. It was decided that with depth soundings recorded to the nearest foot, differences in water surface slope away from the main channel were negligible. To compute bed elevation at each sounding location, a raster image was created and the water surface elevations were extracted to each point. Those points were then available to generate the bathymetry surface.

4.2.1 Bathymetry Surface Generation

River channels, because of their anisotropic characteristics, often pose a unique challenge when trying to apply traditional interpolation methods. Those methods include inverse distance weighting, spline (tension and regularized), ordinary kriging (anisotropic and isotropic), natural neighbor, and TopoGrid (also known as Topo to Raster in the ESRI implementation as part of ArcGIS). Merwade et al. (2006) compared the methods

discussed above in both a Cartesian (x,y) and flow-oriented (s,n) coordinate system. A flow-oriented (s,n) coordinate system is implemented as shown in Figure 4.2.

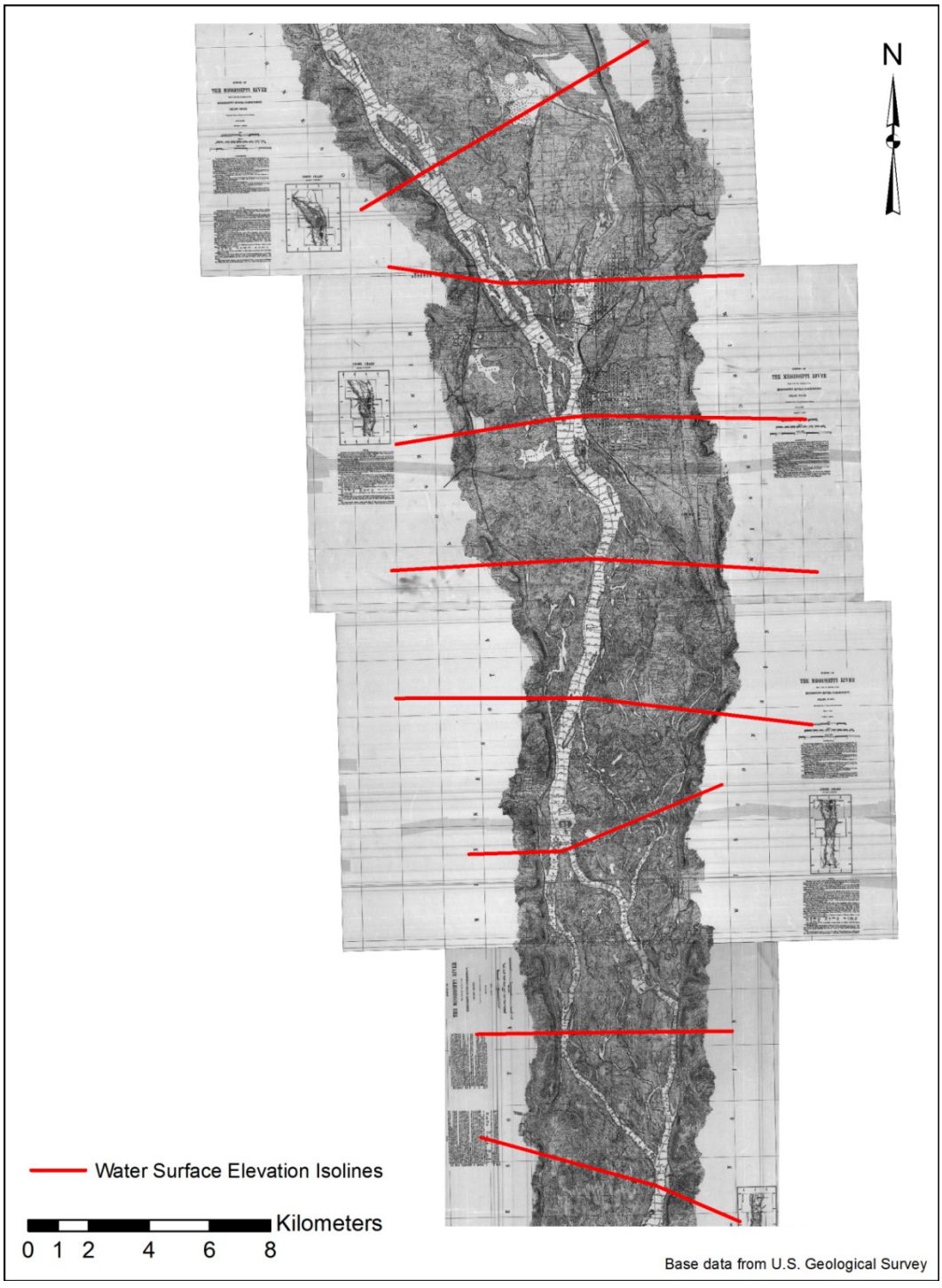

Figure 4.1: Water surface elevation isolines used to generate TIN of water surface.

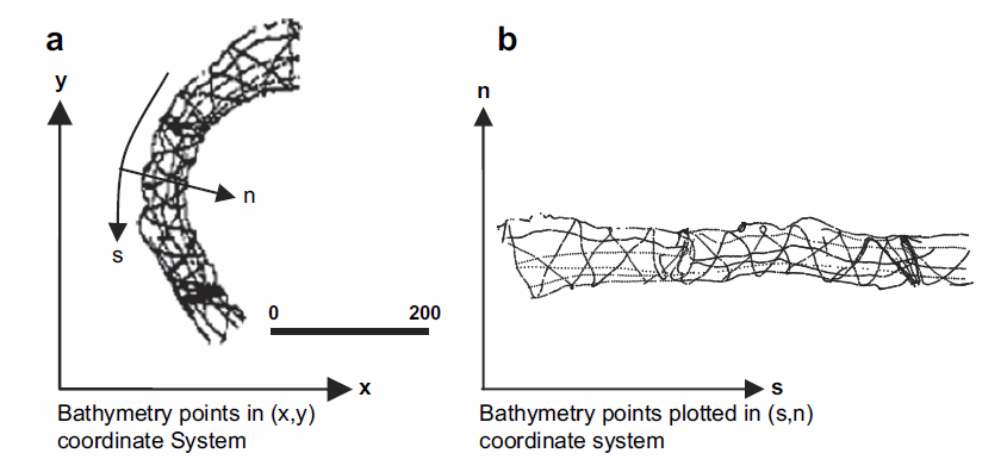

Figure 4.2: Coordinate transformation from Cartesian coordinates to a flow-oriented coordinate system.

Source: Merwade, V., A. Cook, and J. Coonrod. "GIS techniques for creating river terrain models for hydrodynamic modeling and flood inundation mapping." *Environmental Modeling & Software*, 2008: 1300-1311.

The s coordinate is the distance along the thalweg, which increases downstream from an arbitrary starting point. The n coordinate is the distance to the left or the right of the thalweg. When looking downstream, points to the right of the thalweg have positive n values and points to the left have negative n values. In the Merwade et al. 2006 study, it was determined that in a Cartesian coordinate system, isotropic kriging and TopoGrid performed best, but in a flow-oriented coordinate system, that anisotropic kriging, elliptical inverse distance weighting (EIDW), and TopoGrid were better.

It was found that none of the approaches (as outlined by Merwade et al. 2006) were the best for the final bathymetry in this study. In general, the results from use of the ArcGIS implementation of Topo to Raster were not acceptable due to gaps in the cross section spacing and lack of intermediate points between cross sections. This yielded large areas of inaccurate data that were generated by the algorithm. In addition, the search distance, which could not be changed, was too small, causing drastic changes in surface elevation near the points and large plateaus further from the points. Similar results were achieved when testing the available IDW and spline interpolation methods.

Finally, the EIDW algorithm is not available in ArcGIS, and, due to poor performance based on the other available methods (which were similar), the EIDW method was not investigated further.

As a result, the bathymetry was interpolated using an ArcMap extension called Bathymetry Interpolation, which was developed by Professor Venkatesh Merwade from Purdue University (Merwade, Cook and Coonrod, 2008). The bathymetry interpolation method was found to yield the most accurate and consistent results when constructing the bathymetry. The tool uses 3-D cross section polylines, a user defined 2-D channel centerline, and a polygon representing the upstream and downstream reach boundaries together with the channel bank as inputs. Vertices on the 3-D polyline, the channel centerline, and the bounding polygon are transformed from a Cartesian coordinate system to a flow-oriented coordinate system and linear interpolation is performed between the cross sections. The points are then transformed back into the Cartesian coordinate system and a network of 3-D profile and cross section lines is generated (Merwade, Cook and Coonrod, 2008).

The boundary polygon used for the interpolation was a simplified version of the open water land cover class polygon that was extracted from the land cover/use coverage obtained from UMESC (USGS – UMESC, 1999). The boundary polygon was edited to remove small bays and to add sand bars to the interpolation boundary in an effort to create the best representation of the river. The resulting extent of the boundary polygon for use of the interpolation tool is shown in Figure 4.3.

The boundary polygon was subsequently divided into numerous smaller polygons to give more control over the interpolation process. The channel centerline was drawn manually and also subdivided into sections corresponding to the smaller sized individual polygons. To generate the 3-D polylines for the cross section input for the interpolation tool, a spline raster was created for the whole domain using the digitized bathymetry points and points automatically generated along the lowest elevation contours. The

resulting raster dataset yielded accurate values along the cross section, because the points are spaced consistently and the point spacing along the cross section is small relative to distance between cross sections.

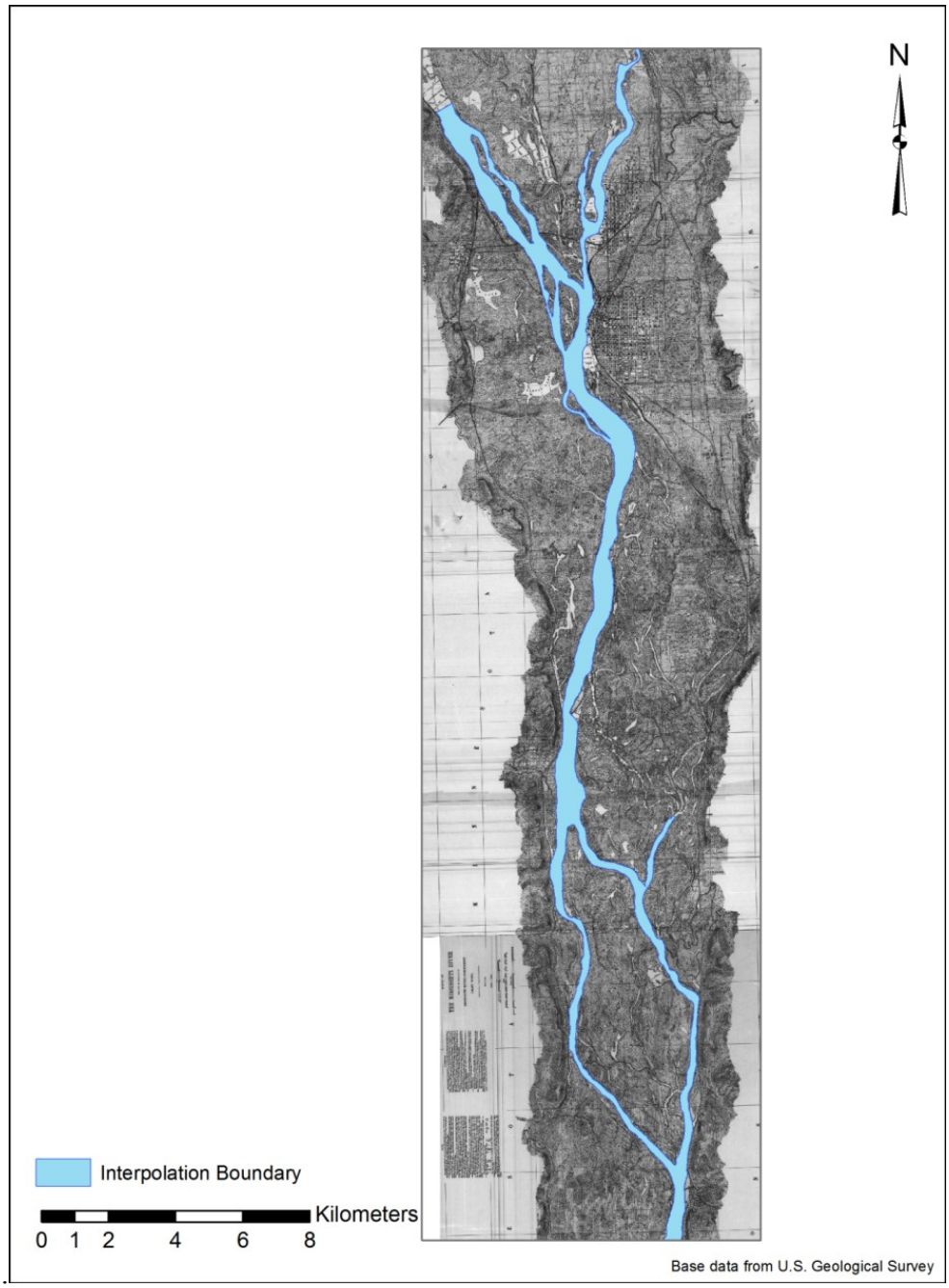

Figure 4.3: Boundary polygon (in blue) marking the outline of the main channel used for the bathymetry interpolation tool.

There are two types of spline interpolation methods available in ArcMap: Regularized Spline and Tension Spline. The Regularized Spline method creates a smooth, gradually changing surface, but one problem is that some of the points on the resulting surface may lie outside the original data range. In contrast, the final surface generated using the Tension Spline method does not vary outside of the sample data, so it was chosen as the best method for this study. It is important that the user can define the number of points the weighting of those points used in the interpolation. Fortunately, both methods (Regularized and Tension) allow for point selection and weighting. Finally, when using a Tension Spline, the point weight also affects the "stiffness" of the created surface. ESRI states that typical values for the weight coefficient used for tension splines are 0, 1, 5, and 10 (ESRI, 2007). The default number of points for interpolation in ArcMap is 12. In order to test the best number of points and weight coefficient to use in generating the final surface a sensitivity analysis of these parameters was tested. The sensitivity analysis tested both 6 and 12 points in addition to weighting coefficients of 0, 1, 5, and 10. It was found that for this application, the shape of the resulting cross sections was not sensitive to the number of points or the weighting of these points. Figure 4.4 illustrates the various sensitivity tests, with the resulting curves closely matched. The parameters chosen for the final surface are a weight of one with six points used for interpolation.

Once the generation of the 3-D mesh for the individual polygons was completed, the polygons were merged together so that a TIN could be generated. The interpolation tool allowed for seamless combination of smaller sections of the main channel by using the final cross section of an upstream reach as the first cross section of the downstream reach. With the side channels, it was often necessary to perform manual editing of the mesh to prevent artificial high areas where side channel contacted the main channel. This was due to the main channel polygon being carried through the side channel unless there

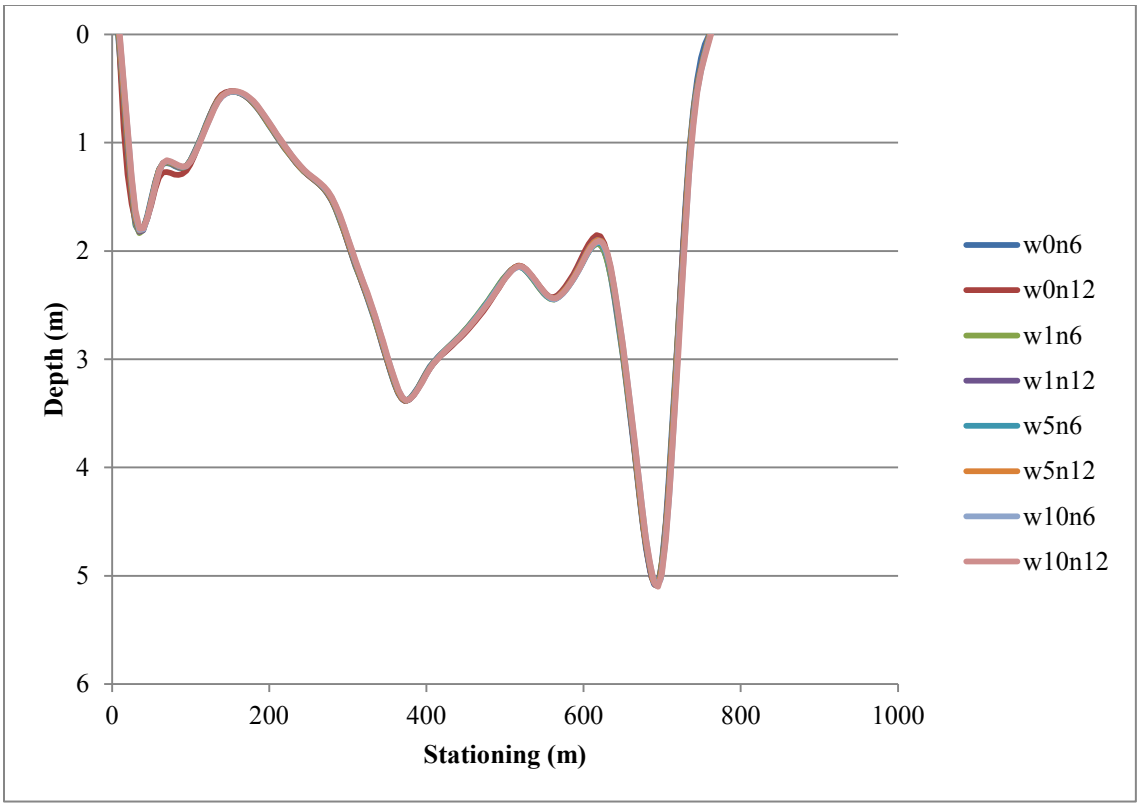

Figure 4.4: Spline interpolation sensitivity results from testing the number of interpolation points used (6 or 12) at various weight coefficients (0, 1, 5, and 10). Results illustrate insensitivity to weight and number of points used for the interpolation. In the legend, "w" indicates the weight and "n" indicates the number of points.

was a main channel cross section located at the opening to the side channel. A section of the historical 1890 Pool 8 contour map illustrating the 3-D bathymetric mesh and the resulting triangulated irregular network (TIN) surface for a side and main channel is shown in Fig. 4.5.

4.2.2 Floodplain Surface Generation

The creation of the floodplain surface DEM was next in the process. The available floodplain elevation data was from contour lines from the historic 1890 map. Floodplain surface interpolation was performed using the Topo to Raster tool in ArcGIS. Topo to Raster is an implementation of ANUDEM (Australian National University Digital Elevation Model) a software program developed by Michael Hutchison that generates

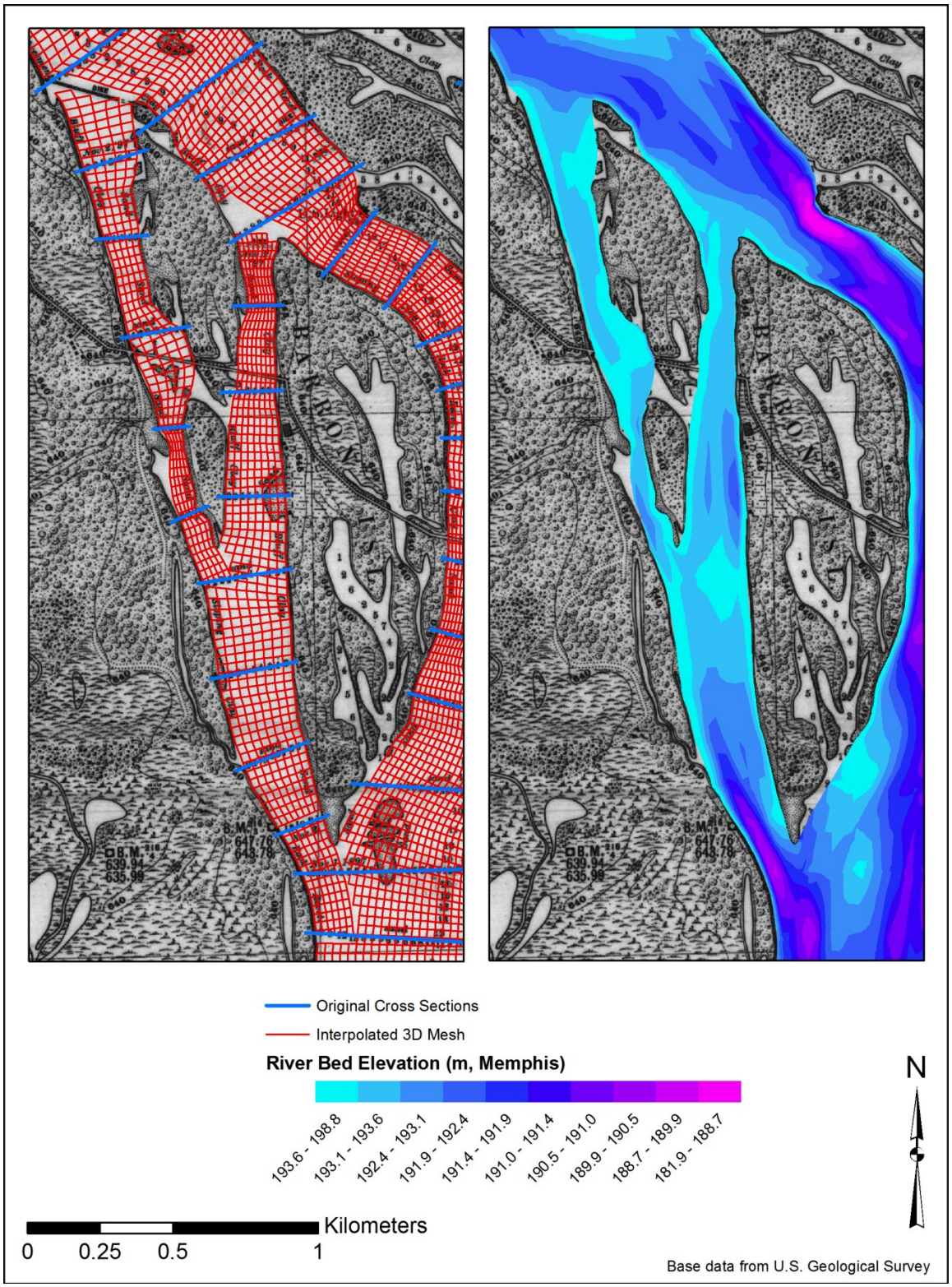

Figure 4.5: Section of the historical 1890 Pool 8 contour map illustrating the creation of the 3-D bathymetric mesh (on left) and resulting triangulated irregular network (TIN) surface (on right). Note the seamless integration of the side channel to main channel on the TIN surface.

DEMs from arbitrarily large topographic data sets (ESRI, 2009). The ANUDEM program is basically a discretized thin plate spline technique that uses a modified roughness penalty to allow the DEM produced to follow abrupt changes in terrain such as ridges and streams. ESRI states that Topo to Raster is the only ArcGIS interpolator specifically designed to work intelligently with contour inputs (ESRI, 2009). One big advantage of Topo to Raster is the drainage enforcement algorithm, which allows one to input stream network polylines and sink points into the tool. That allows for removal of unnatural sinks in the DEM and prevention of 'dams' in the DEM where known stream locations are. Experimentation with generating a TIN from the contour data indicated that the spline interpolation method provided by Topo to Raster would be the best option for DEM creation for this study. A TIN has no curvature between contours and is subject to both plateaus on ridges and incorrect drainage attributes. The drainage enforcement algorithm in Topo to Raster represents the small side channels and tributaries.

The following data sets were input into the tool: contour polylines with an elevation attribute, sink points with no elevation, a polyline stream network, bathymetry points with an elevation attribute, and a boundary polygon representing the limits of interpolation for the final DEM. A user specified raster cell size must be provided. For this study, five meters (16.4 ft) was chosen because the tool has a maximum number of cells in the final raster and using a smaller cell size would crash the tool.

The tool also allows the user to specify a maximum and minimum elevation to be used in the interpolation scheme. This feature was used to help correct unrealistic depressions in areas where steep bluffs meet the relatively flat floodplain. Spline algorithms try to fit a smooth line through two points with the minimum amount of curvature necessary, and this characteristic can cause unrealistic deep depressions at intersection of bluff and floodplain. Figure 4.6 illustrates one example of how one of these depressions was adjusted using the minimum elevation function in the tool. The

final result shown in Figure 4.6 still shows a depression, but one that is more realistic (one meter (3.3 ft) instead of three meters (9.8 ft)).

Because the contours on the floodplain were spaced at intervals of 1.5 meters (5 feet), a minimum elevation for interpolation was set 1.5 meters (5 feet) below the lowest contour shown on the map. This resulted in 1.5 meters (5 feet) of possible maximum error, with the rationale being that if there was an actual elevation lower than that, another contour would have been shown on the map in these locations. In the study area, the Mississippi River flows from north to south, so that higher elevations exist at the top of the map and lower elevations exist on the bottom portion of the map. As a result, the study area was divided up into three sections in the north-south direction, with minimum interpolation values of 190.5 meters (625 feet), 192 meters (630 feet), and 193.5 meters (635 feet) for each section. These three individual raster images were then mosaicked using the BLEND method in ArcGIS, which blends the overlapping values using a weighting factor based on the distance they are from the edge of the raster (ESRI, 2010).

The drainage enforcement option used was the ENFORCE_WITH_SINK method, which attempted to remove spurious sinks, but left those identified as real sinks by the user (ESRI, 2011). An iterative finite difference scheme is used for interpolation, starting with a coarse grid and refining the grid until the user specified size is reached (Hutchinson, 1989). In the ArcGIS implementation, the user is allowed to select the maximum number of iterations. The default was used because it was determined by visual inspection of contours generated from the DEM that there was no discernible difference in the final DEM when using a higher number of iterations. The discretization error factor adjusts the amount of smoothing when converting the input data to a raster. A range of 0.5 to 2 is the normal adjustment range (ESRI 2011). By comparing contours generated from the raster to contours on the source maps, it was determined that a value of 0.5 provided the best representation of the source data.

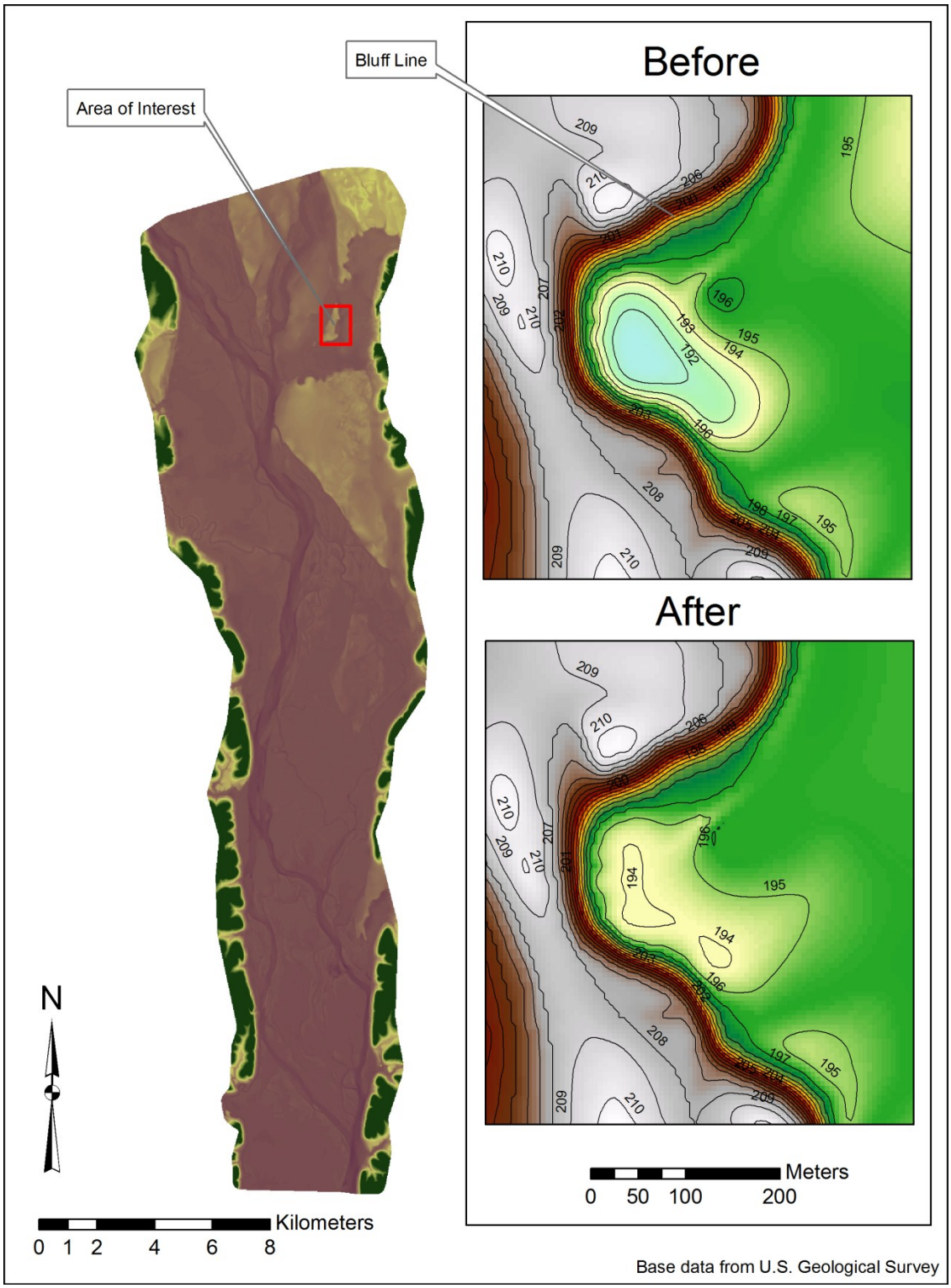

Figure 4.6: Map of Pool 8 with the area of interest highlighted showing correction of deep depressions by the software near the intersection of the bluff and floodplain. Note deep depressions (3 m) before correction versus shallower depression after correction (1 m).

Default values in the program were used for the remaining parameters: roughness penalty, tolerance one, and tolerance two, as there was no need to adjust these. Detailed explanations of how these parameters work are available in ESRI (2011).

4.2.3 Floodplain and Channel Merging

In summary, the floodplain DEM and bathymetry data were merged to create a seamless DEM representing the study area. Extensive manual editing was performed, especially where the main channel branched into side channels to accurately create the surface. The bathymetry interpolation tool interpolated the bank line through the side channels unless there was a cross section at the location of the split. There were also side channel areas that included bathymetry soundings but were not included in the main channel bathymetry interpolation process. When the drainage enforcement algorithm was used in those areas it resulted in an unrealistically deep channel, so they were recreated using the bathymetry interpolation tool for better results. The final raster DEM is shown in Figure 4.7.

4.3 Quality Control

A discussion of the accuracy of the resulting DEM when compared with the original map data is warranted. In particular, this section will discuss quality control in identify potential elevation differences between the historical map and resulting DEM. In addition, the reader should keep in mind that the original 1890 map may have its own limitations on how the data was collected and the map was made. However, the beginning assumption is that the 1890 map is the best available in its day and that all interpretations remain true to the original map.

A few different methods were used for quantifying the ability of the raster DEM to represent the elevation data from the original map source. One method used is the Root Mean Square Error (RMSE). The USGS provides RMSE values for its DEM products as a descriptor of the vertical accuracy. RMSE is defined in equation (4.1) on page 38.

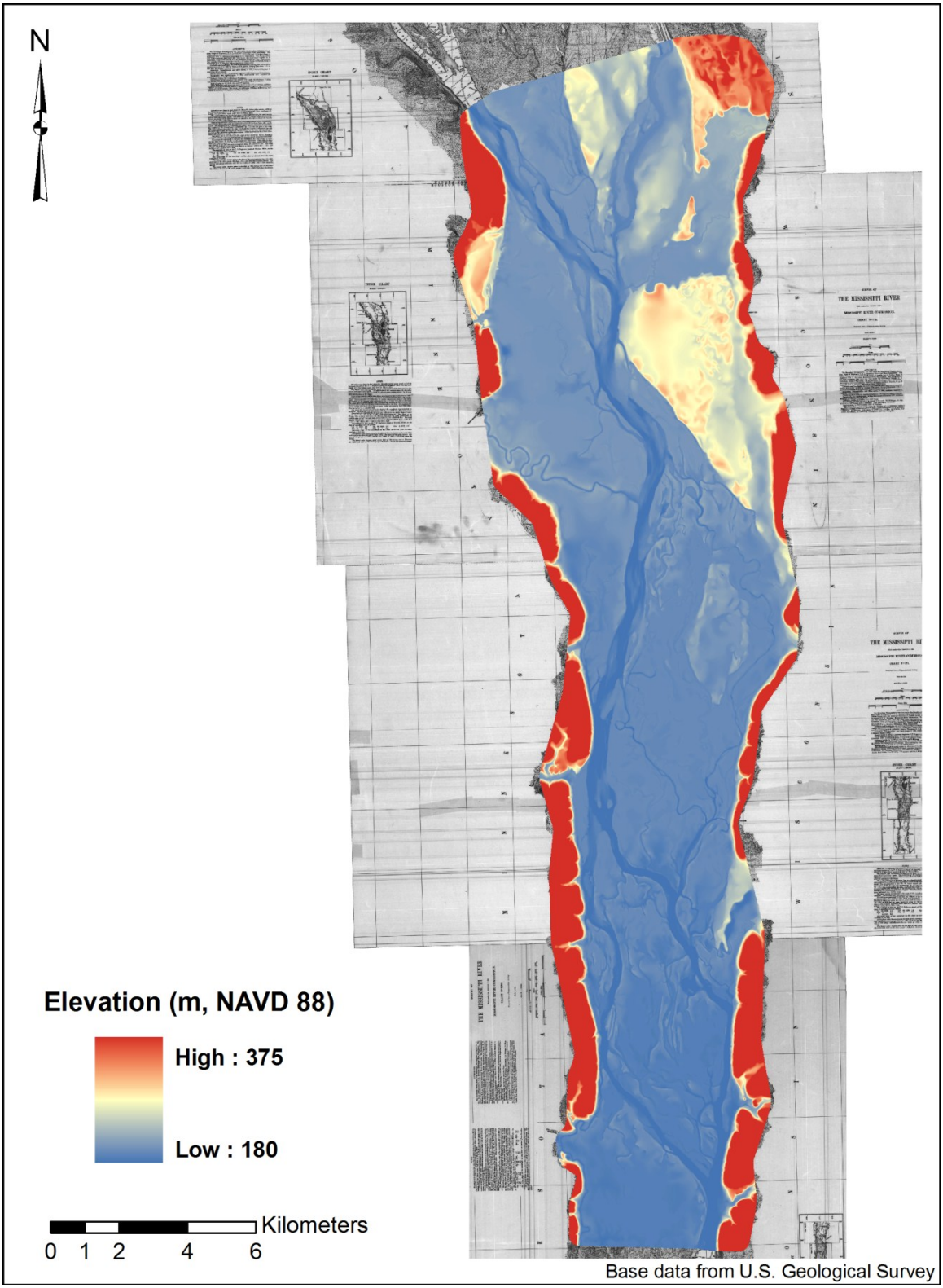

Figure 4.7: Final DEM constructed from the 1890 historical map for Pool 8 represented in raster form.

In Equation (4.1), z_i is the interpolated DEM elevation of a test point, z_t is the true elevation of a test point, and n is the number of sample points.

$$RMSE = \sqrt{\frac{\sum(z_i - z_t)^2}{n}} \tag{4.1}$$

The USGS lists acceptable test points in order of preference as field control, aerotriangulated test points, spot elevations, or points on contours from existing source maps with appropriate contour interval (USGS, 1998).

For this study, since the first two types of data weren't available, true elevation was taken to be a bathymetry sounding or a point falling directly on a contour line. Due to the limited amount of elevation data available compared to modern methods (such as LiDAR), all available contour and depth sounding data was used for the generation of the DEM rather than excluding some points from the interpolation process to later use as quality control points. This means that the quality control points had an influence on the DEM, but it was still determined to be more important that all available data was used for the DEM generation.

Different error measures can show trends in differences between the reference elevations and the elevations in the resulting raster DEM. As a result, the average absolute difference between the raster DEM and the reference data was also calculated as shown in equation (4.2). In equation (4.2), z_i is the interpolated DEM elevation of a test point, z_t is the true elevation of a test point, and n is the number of sample points.

$$Avgerage\ Absolute\ Difference = \frac{\sum|z_i - z_t|}{n} \tag{4.2}$$

Table 4.1 below summarizes the RMSE and absolute difference values for the bathymetry points and contour elevations less than 200 meters (656 ft). Maximum water surface elevations in the domain are highly unlikely to reach 200 meters (656 ft, reference the rating curves shown in Figure 5.4, page 55) so contours above that elevation

were not considered. The data for both the bathymetry points and the contour points combined wasn't shown because it is very similar to the contour only data. That's because the number of contour points is much greater than the number of bathymetry points. As expected, the contour points have a lower RMSE and absolute error because the spline interpolation method passes through the contours. Figure 4.8 and Figure 4.9 show the frequency of absolute errors and Figure 4.10 through Figure 4.12 show how the errors are spatially distributed in the study area.

Table 4.1: Errors Associated with DEM Interpolation for Contours Less Than 200 meters (656 ft).

Criteria	Bathymetry Points	Contour Points
RMSE (m)	0.40	0.26
Average Absolute Error (m)	0.21	0.08
Maximum Absolute Error (m)	4.29	5.97
Minimum Absolute Error (m)	0.00	0.00

As Figure 4.8 and Figure 4.9 show, many of the differences between the raster DEM and the reference data were less than 0.05 meters (0.16 ft), with most being less than 0.30 meters (1.0 ft). The spatial distribution plots show that the largest errors, most of which are not represented in Figure 4.9, are at the higher elevations well out of the floodplain. This is due to the steep gradients and may also be an artifact of the raster generation process. Due to the limitation in the number of grid cells that can be generated using Topo to Raster, the 5 meter grid cells may represent more than one contour in the steepest bluffs. While that has no bearing on the accuracy of the hydraulic study, it is worth noting in the assessment of the DEM quality as a standalone product.

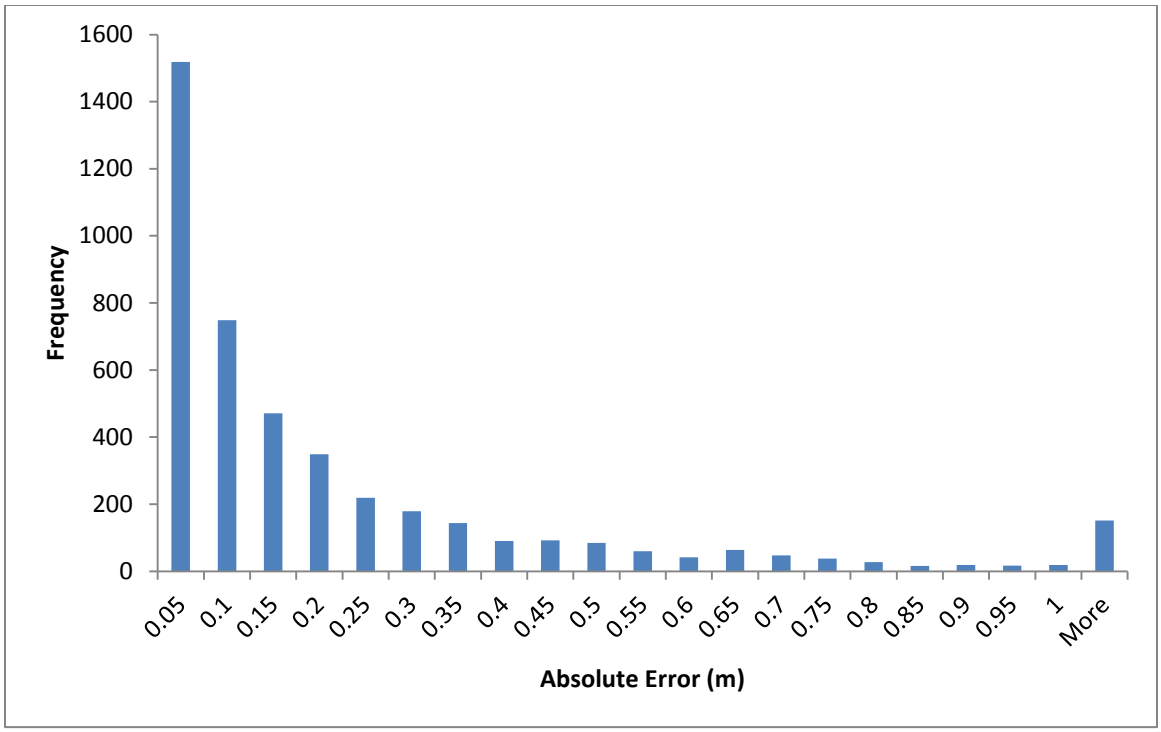

Figure 4.8: Histogram showing the frequency of differences between the reference bathymetry data and the raster DEM for all bathymetry points.

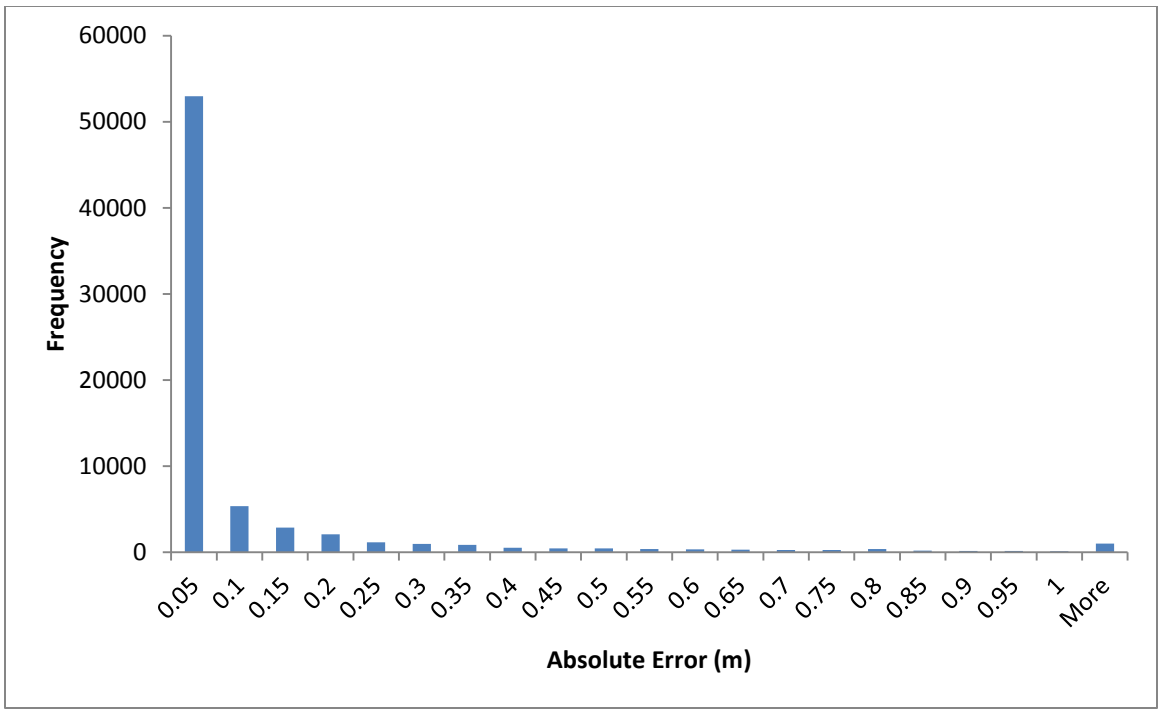

Figure 4.9: Histogram showing the frequency of differences between the reference contour data and the raster DEM at elevations less than 200 meters (656 ft).

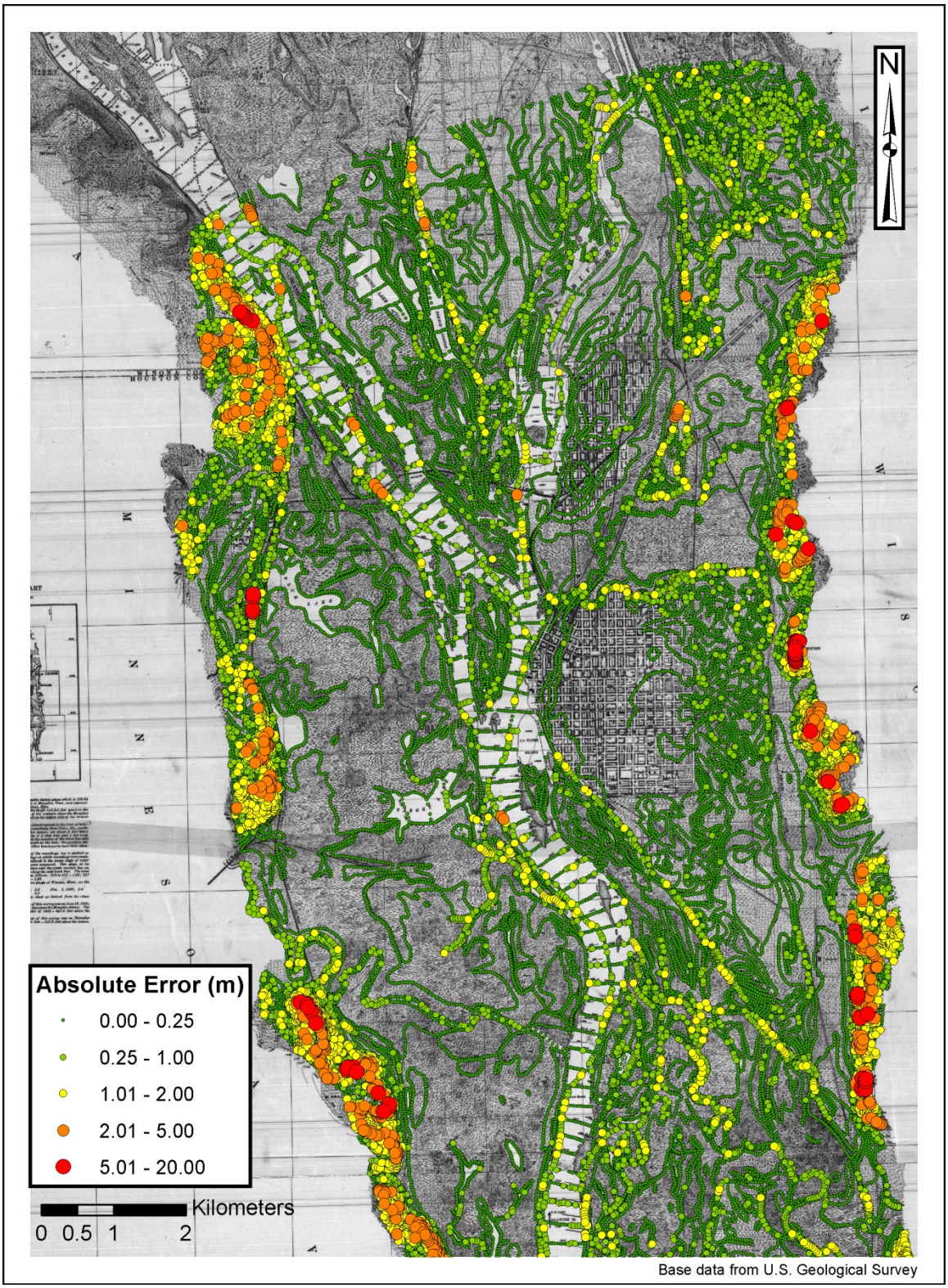

Figure 4.10: Spatial distribution of absolute error – 1 of 3.

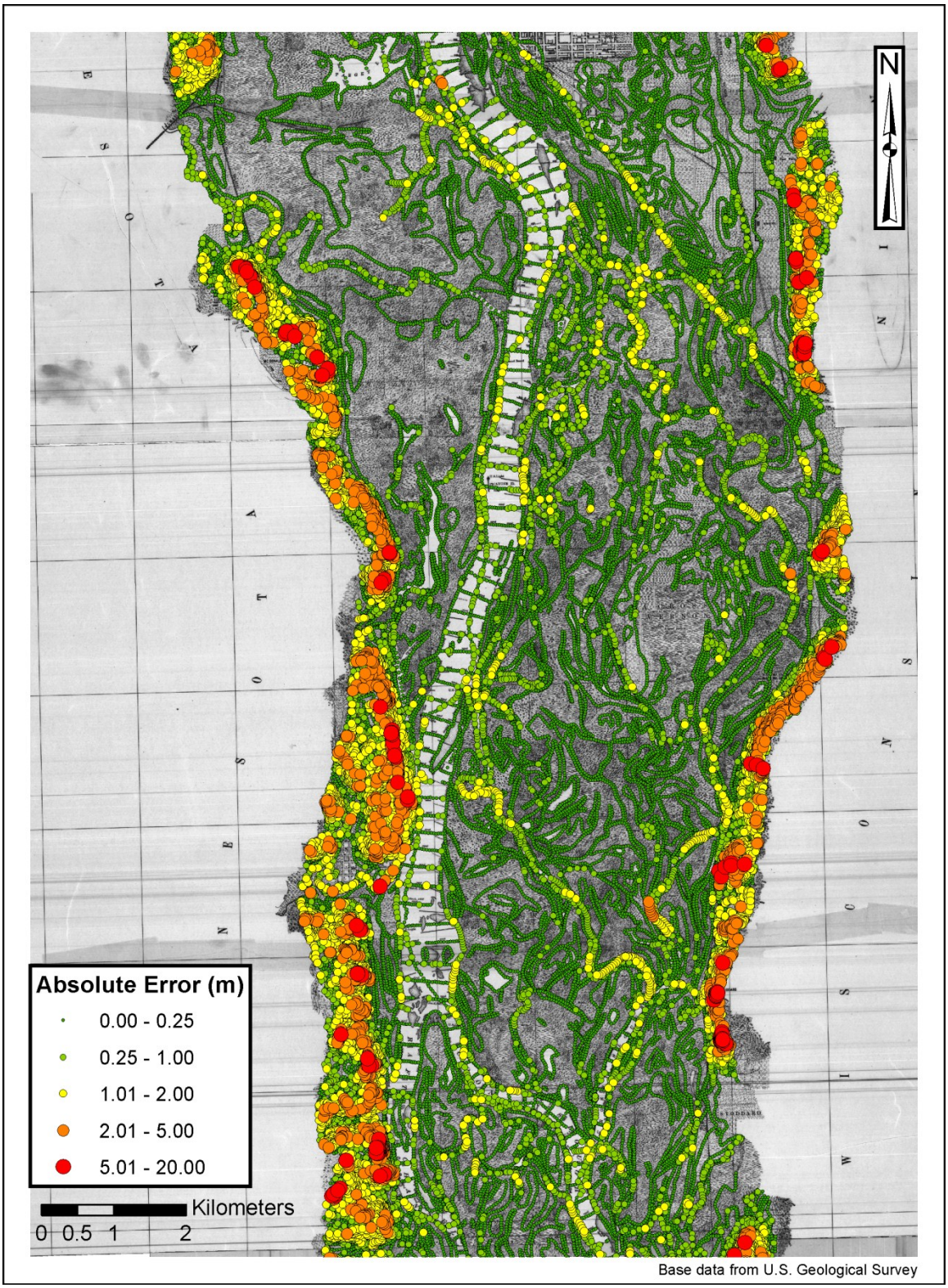

Figure 4.11: Spatial distribution of absolute error - 2 of 3.

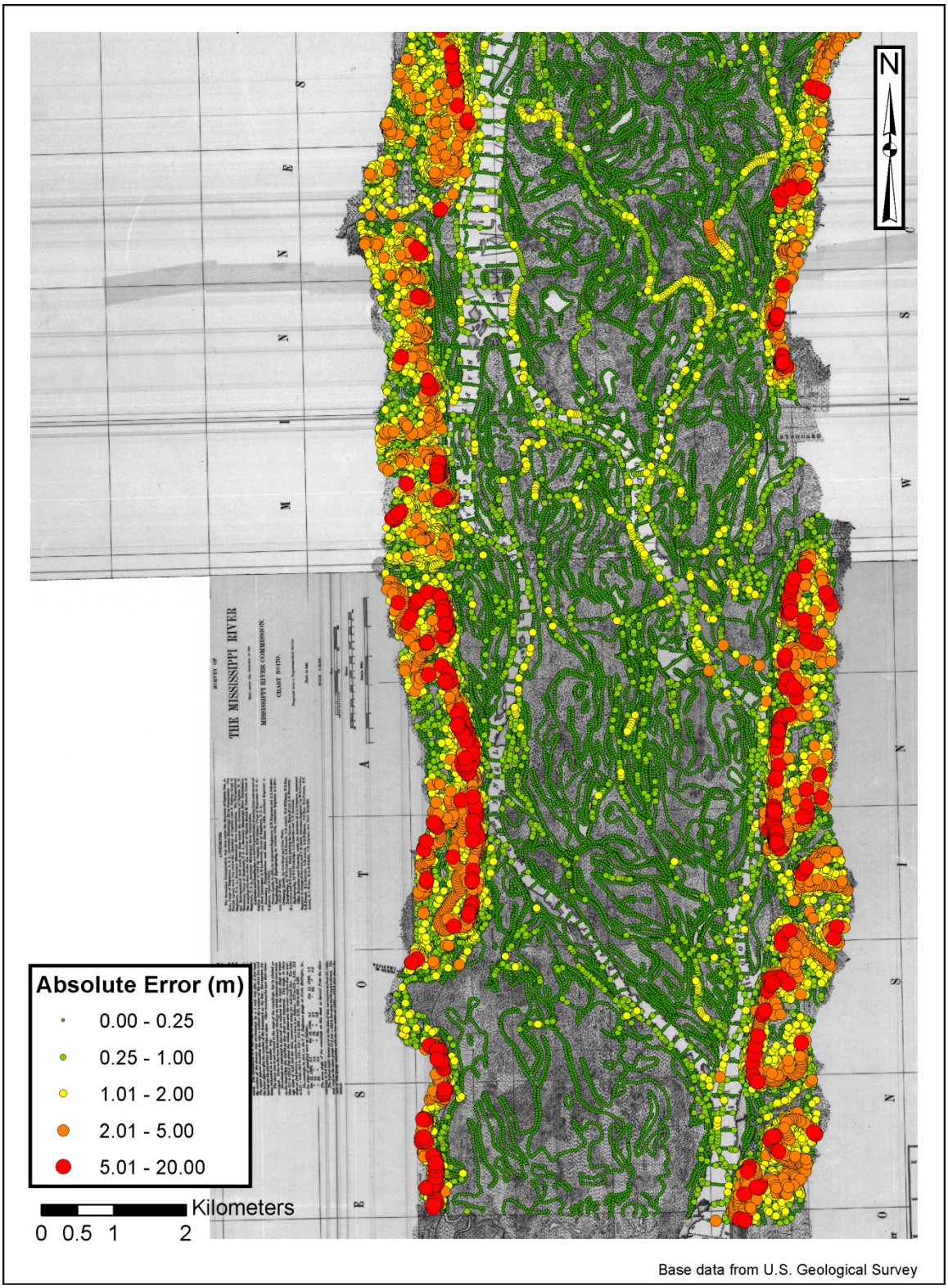

Figure 4.12: Spatial distribution of absolute error - 3 of 3.

4.4 Datum Conversion

There are four different vertical datums used for this study since the data sets span a range from the late 1890s to the present. These include the Memphis Datum, Mean Sea Level Datum – 1912 Adjustment (MSL 1912), National Geodetic Vertical Datum of 1929 (NGVD 29), and North American Vertical Datum of 1988 (NAVD 88). The historic MRC maps are in the Memphis Datum and the U.S. Army Corps of Engineers uses MSL 1912. Smith (2011) used NAVD 88 for modeling of current conditions, so all elevations were ultimately converted to NAVD 88 for easier comparison of historic and current conditions. NGVD 29 is used as an intermediate datum to convert between MSL 1912 and NAVD 88. Using information available on the U.S. Army Corps of Engineers St. Paul District's water control center website and the Corps' software program Corpscon (USACE – AGC, [no date]), a collection of raster images was created to perform datum conversions in ArcGIS or extract elevations at points of interest within the study area.

A summary of datum conversions for the study area are given in Table 4.2 (USACE, 1934). Conversions for both the Memphis Datum to MSL 1912 and MSL 1912 to NGVD 29 are given at discrete points along the river. Those points were then used to create isolines in ArcGIS, which were then used to generate TINs for each conversion step. Finally, the TINs were converted into raster images. The software program Corpscon was used to convert between NGVD 29 and NAVD 88. The domain was divided up into a series of points, each with elevation 100 meters (328 ft), spaced at 10 meter (32.8 ft) intervals in the Northing and Easting directions. Those points were then run through Corpscon. Finally, the original 100 meter (328 ft) elevation was subtracted to give a value for the datum conversion and a raster was created. With a conversion between each of the four datums in raster format, the raster images can then be added or subtracted as necessary using the Spatial Analyst extension in ArcGIS.

Table 4.2: Datum conversions to convert from Memphis Datum, MSL 1912, NGVD 29 and NAVD 88 datums for Lock and Dam 7 and Lock and Dam 8.

To convert from:	Add at Lock and Dam 7 (m):	Add at Lock and Dam 8 (m):
Memphis to MSL 1912	-2.13	-2.15
MSL 1912 to NGVD 29	-0.15	-0.16
NGVD 29 to NAVD 88	-0.03	-0.02

CHAPTER 5: HYDRODYNAMIC MODEL DEVELOPMENT – HISTORIC CONDITIONS

5.1 Mesh Creation

Mesh creation parameters for historic conditions were based off earlier mesh resolution data used in a study of current conditions for Pool 8 (Smith, 2011). The USGS – UMESC staff determined that a 30 meter nominal node spacing would be adequate to meet project goals of the Pool 8 2-D model for that study, and the author increased the node spacing at points farther from open water to a maximum of 90 meters (295 ft) (Smith, 2011). In an effort to develop a comparable model for historic reference conditions, the node spacing was held consistent. In certain areas, most notably the La Crosse River, Root River, and several small side channels in the middle part of the study reach, node spacing was decreased to approximately 15 meters (50 ft) to capture the channel with three nodes: one at each bank line and one in the middle of the channel. The final mesh had approximately 260,900 elements and 192,800 nodes.

Mesh resolution was controlled by drawing feature arcs, which are polylines with nodes at a given spacing. Feature arcs are used to delineate both material types (e.g. forest, grassland, or open water in this study) or to outline significant topographical features. One example of an important topographical feature to outline is the point where floodplain areas meet a bluff. That allows for controlled node spacing at the base of the bluff, preventing random node placement along the boundary and creating an unnatural representation of the steep break line caused by the bluff.

Feature arcs are connected to form polygons, which are used to specify a material type and meshing scheme. Two different meshing schemes were used to generate the mesh for this study: paving and patch. The paving method generates triangular elements and the patch method generates an unstructured polygonal mesh. Patch was used for the open water areas and paving was used primarily for the floodplain.

In the generic mesh format, both element types are stored in an unstructured manner. Elements are defined by an index number unique to that element, a type (triangular or quadrilateral), what node numbers make up the element, and the material type assigned to the element. Nodes are described by a unique index number and x, y, and z Cartesian coordinates. Nodestrings are also defined with a unique number and the node numbers that make up the nodestring. Nodestrings are used for assigning boundary conditions and acting as monitoring lines when placed within the domain (Aquaveo, 2009).

5.2 Land Cover

Land cover and land use data are important in constructing the hydrodynamic model, particularly for selection of material roughness values. The historic maps used for this study did include some land cover information that was digitized into a polygon shapefile by the USGS – UMESC and is shown in Figure 5.1 (USGS – UMESC, 1999). However, the original maps did not contain legends describing what the map symbols represent. While the UMESC staff was working on digitization of the MRC maps, they consulted a historian at the University of Wisconsin – Madison and located a legend for the land cover types. Subsequent discussions with other historians led to the classification and description of most of the land cover information contained on the maps (USGS – UMESC, 1999).

Seventeen land cover types were identified in the area which is now Pool 8. Those seventeen classes were then combined into eight broader classes by UMESC that were adequate for determining material roughness values for this study. Those eight classes are identified in Table 5.1 below, along with the percent coverage of the present day Pool 8 and a base Manning's n value before calibration.

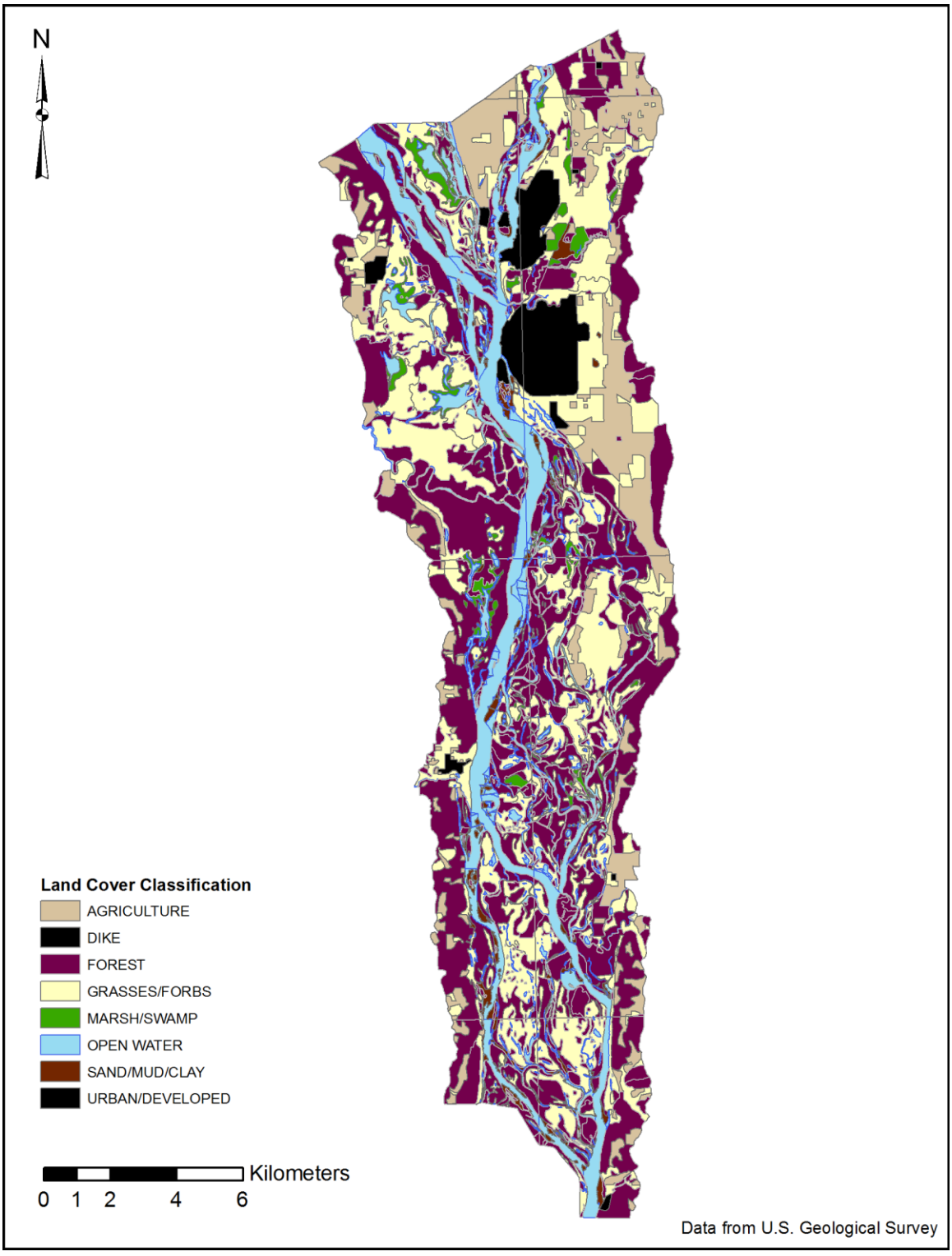

Figure 5.1: 1890s Historic Land Cover/Land Use shapefile.

Table 5.1: Land cover from the historic 1890 map for Pool 8 as defined by the USGS-UMESC and base Manning's n as assigned for this study.

MRC Land Cover Class	Description[a]	Percentage of Coverage	Base Manning's n value[b]
Agriculture	Areas farmed for crops.	11.61	0.035
Dike	Wing dams and closing dams.	0.03	Not used
Forest	Includes areas covered with trees and areas cleared for agriculture or river for riverboat fuel.	39.30	0.080
Grasses/Forbs	Includes areas of mixed grasses, forbs and brush.	26.85	0.035
Marsh/Swamp	Areas believed to include emergent vegetation. It is unknown if rooted floating aquatics and submergents are included.	1.92	0.035
Open Water	Areas identified as open water.	14.15	0.030
Sand/Mud/Clay	Believed to be areas of clay river bank, sand, and mud.	1.67	0.030
Urban/Developed	Urban areas.	4.47	0.100

[a] Source: USGS – UMESC. "1890s Land Cover/Use [Metadata]" *GIS Data - Pool 8 - Upper Mississippi River*. August 30, 1999. http://www.umesc.usgs.gov/rivers/upper_mississippi/reach_1/pool_8/p8_gis_data.html

[b] Source: Strum, T. W. Open Channel Hydraulics. New York, NY: McGraw-Hill, Inc., 2001.

5.3 Boundary Conditions and Model Parameters

5.3.1 Sources of Data

Downstream water surface elevations were determined from profiles found in the U.S. Army Corps of Engineers' 1971 Reservoir Regulation Manual (USACE – SP, 1971). A scanned version of Plate 11 from Appendix 8 of the manual was obtained via email (Janvrin, 2011-2012). Plate 11 includes historic open river profiles from which the elevations near present day Lock and Dam 8 were obtained.

Discharge data was gathered from five different gages maintained by the U.S. Geological Survey or U.S. Army Corps of Engineers. Table 5.2 summarizes the gage location, historical period of record used for the simulations, and managing agency.

Table 5.2: Stream gage location, period of record, and managing agency for Pool 8 of the Mississippi River.

Gage Location	Period of Record	Managing Agency
Black River at Galesville, WI	Oct. 1, 1909 – Oct. 21, 2008	USGS
La Crosse River at La Crosse, WI	Oct. 1, 1999 – Aug. 4, 2012	USGS
Root River at Houston, MN	Dec. 28, 1931 – Aug. 4, 2012	USGS
Lock and Dam 7	Jan. 1, 1959 – Dec. 31, 2011	USACE
Lock and Dam 8	Jan. 1, 1959 – Dec. 31, 2011	USACE

5.3.2 Discharge Scenarios

Discharge scenarios were calculated using an average mass conservation method developed by Young (2006) and used by Smith (2011) for a similar study of current conditions within Pool 8. Ten steady state discharge scenarios ranging from 283 to 2832 m^3/s (10,000 to 100,000 ft^3/s) in increments of 283 m^3/s (10,000 ft^3/s) were calculated

using stream flow data from five stream gages listed in Section 5.3.1 . This range covers flows that are exceeded less than 5% of the time to flows that are exceeded over 95% of the time. Figure 5.2 shows the flow duration curve at Lock and Dam 8 for the period of record from 1972 to 2000. This period of record was chosen for the flow duration curve to be consistent with reference discharges used by the U.S. Army Corps of Engineers, U.S. Geological Survey, and others in various hydrologic reports. For calculating the discharge scenarios, the entire period of record shown in Table 5.2 was used.

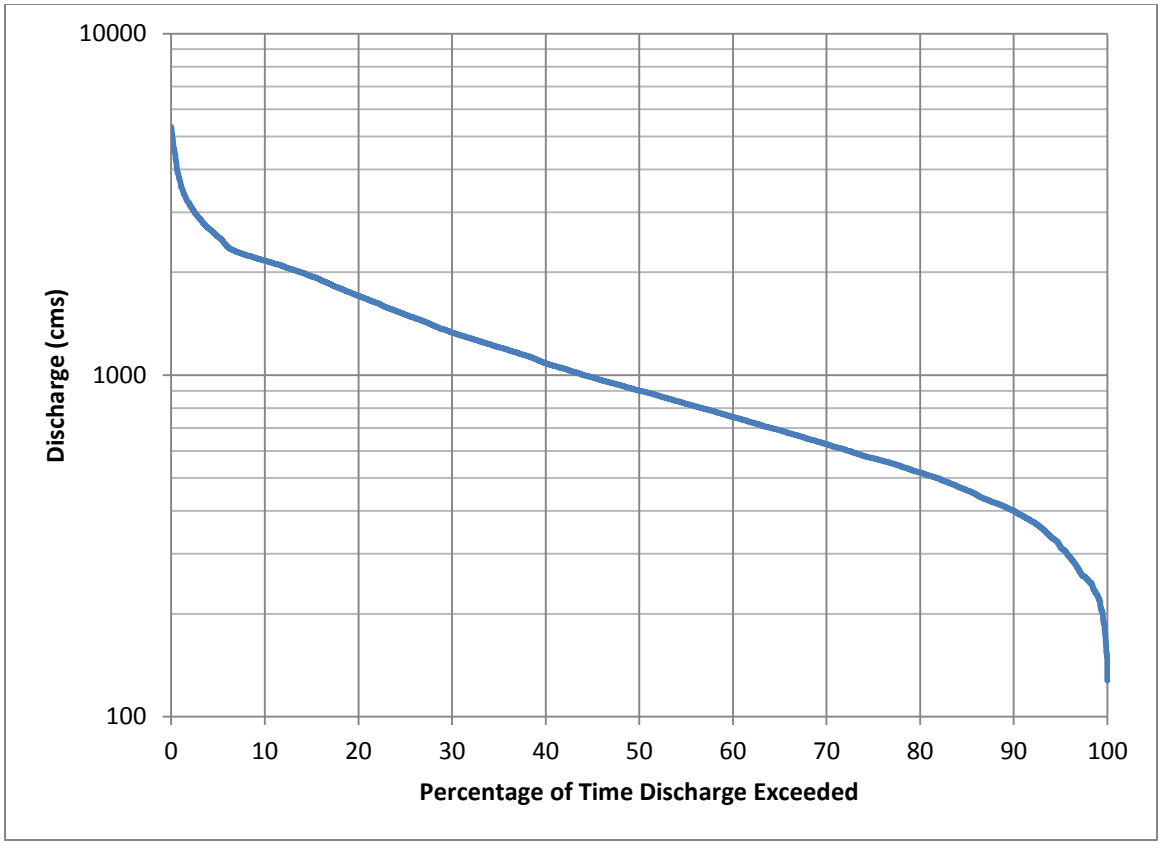

Figure 5.2: Flow duration curve at Lock and Dam 8 for the period of 1972 to 2000.

Data source: U.S. Army Corps of Engineers – St. Paul District. *Water Control Center.* (no date). http://www.mvp-wc.usace.army.mil/ (Accessed November 2012).

Discharges for the Mississippi River were calculated by subtracting the Black River from Lock and Dam 7 because, after impoundment, the Black River confluence is above Lock and Dam 7, but for the historic condition model the confluence of the two rivers is within the model domain. The data for all five stream gages was grouped by date, and then filtered to include the desired discharge through present day Lock and Dam 8 plus or minus five percent.

As an example of how the discharge scenarios were calculated, consider the 566 m^3/s (20,000 ft^3/s) scenario. All dates with discharges ranging from 538 m^3/s (-5%, 19,000 ft^3/s) to 594 m^3/s (+5%, 21,000 ft^3/s) through Lock and Dam 8 were selected. For those dates, the discharges at each stream gage were averaged for the total period of record at the gage. The average discharge for each inlet (Black River, La Crosse River, Root River, and Lock and Dam 7) was then divided by the total average inflow (sum of average discharges for the Black River, La Crosse River, Root River and Lock and Dam 7) to calculate a percentage of total inflow from each inlet to the model. In some cases, the total average inflow did not equal the total outflow measured at Lock and Dam 8 for these calculations. As a result, an additional step was made for these cases where model discharge at each inlet was calculated by multiplying the percentage of total inflow for each inlet by the average discharge at Lock and Dam 8. This ensured that the total mass of water entering the model was proportioned correctly to each inlet and equaled the total mass exiting the model.

5.3.3 Downstream Water Surface Elevations

Downstream water surface elevations were taken from the reservoir regulation manual profiles for each discharge scenario (USACE – SP, 1971). A minor adjustment was made (approximately 0.05 meters or 0.16 feet) to the water surface elevation to account for the distance between the most downstream point on the water surface profiles in the reservoir regulation manual and the actual location of the downstream boundary of the model. The water surface elevation at the exit of the model was extrapolated

approximately 760 meters (2,500 ft) using roughly that last 6 kilometers (3.7 miles) of the open river profiles, where the slope of the water surface was consistent. The elevation was then converted from the MSL 1912 vertical datum to NAVD 88 because all elevations in the computational mesh were NAVD 88.

5.4 Calibration/Validation Data

Three different sources of data were used for calibration and validation of the historic model. Open river profiles at a variety of discharges were obtained from the U.S. Army Corps of Engineer's Reservoir Regulation Manual and compared with historic high and low water surface profiles from the original 9-foot channel study (USACE – SP, 1971). In addition, the MRC maps used in development of the DEM contained water surface elevations and slopes from the dates that the bathymetric surveys were performed. Discharge data was not included on the MRC maps, but the slope of the water surface can still provide valuable information for calibration of the model.

Water surface profiles from the various historic sources were digitized using Plot Digitizer, a free software program distributed under the GNU General Public License, to develop a table of (River Mile, Elevation) coordinate pairs for each of the given discharges (Huwaldt, 2012). For the profiles from the reservoir regulation manual, those coordinate pairs were then assigned Cartesian coordinates in ArcGIS using two datasets – a sailing line for the Mississippi River navigation channel (USACE – SP, 2010) and a point shapefile containing river miles (USGS – UMESC, 1996). The sailing line is a polyline dataset representing the recommended navigation route for ships using the Mississippi River. It does not include river mile measurements, so the point shapefile was used to assign them. A PolylineM, which is ESRI's term for a polyline containing measured values, river miles in this case, was created by dividing up the polyline into segments representing one mile. The linear referencing capabilities of ArcGIS were then used to create a point shapefile with points at the proper spatial location that also contained attributes for river mile and water surface elevation. These point shapefiles

were used to extract simulated water surface elevations for comparison while calibrating and validating the model.

5.4.1 1971 USACE Reservoir Regulation Manual

Historic water surface profiles for a wide range of discharges shown Figure 5.3 were digitized from Appendix 8, Plate 11, of the U.S. Army Corps of Engineers Reservoir Regulation Manual (USACE – SP, 1971). The profiles of interest on Plate 11 are the open river profiles, which were noted as being derived from pre-canalization records on the plate.

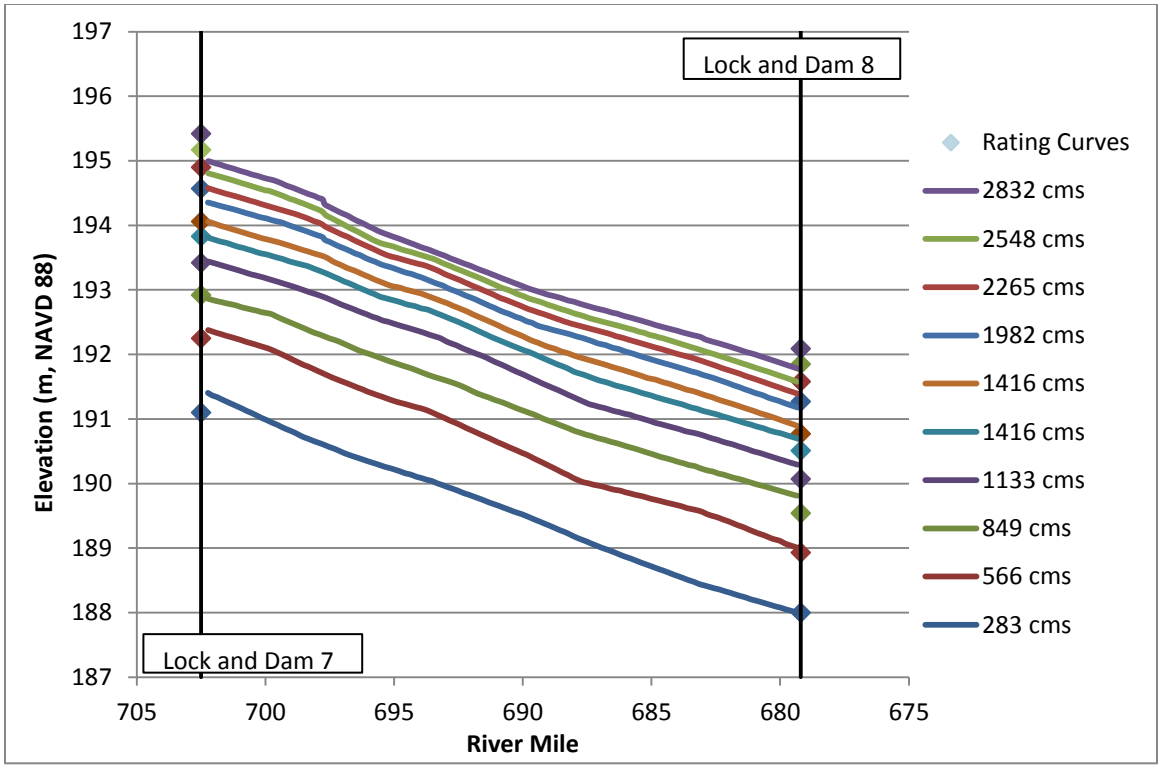

Figure 5.3: Open river profiles from 283 to 2832 m^3/s (10,000 to 100,000 ft^3/s).

After checking with various sources at the U.S. Army Corps of Engineers, it is believed the profiles were plotted using rating curves developed at the lock and dam sites, as well as other key locations as part of the original 9-foot channel project, with straight

profiles drawn in between (Landwehr, 2012). This assumption was checked by digitizing rating curves obtained from the original 9-foot project report submitted to Congress in 1931 by the U.S. Army Corps of Engineers (House 1931). These rating curves were compared with rating curves generated from the profiles in the reservoir regulation manual. Figure 5.4 and Figure 5.5 show the two rating curve comparisons for the Lock and Dam 7 and 8 locations, respectively.

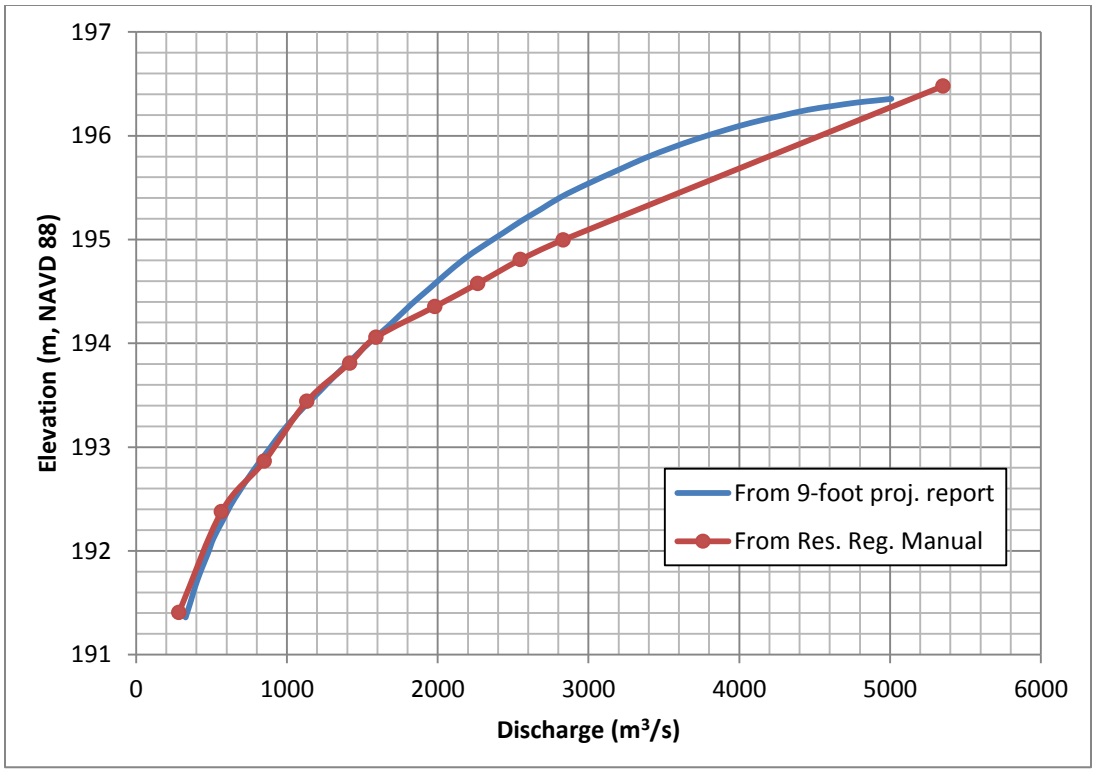

Figure 5.4: Stage-discharge relationship comparison at present day Lock and Dam 7.

The rating curves show that at both the Lock and Dam 7 and Lock and Dam 8 locations, the water surface elevation shown in the reservoir regulation manual is lower than the 9-foot project report at high discharges.

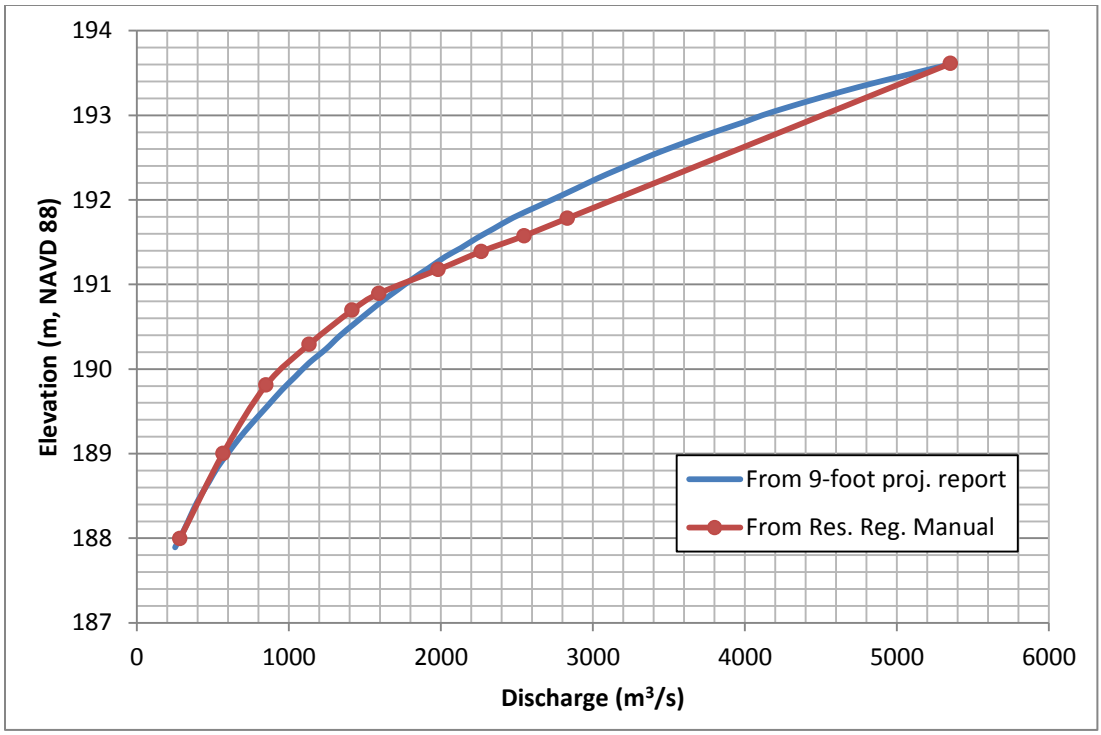

Figure 5.5: Stage-discharge relationship comparison at present day Lock and Dam 8.

5.4.2 1931 9-foot Channel Report

Two profile sheets from the 9-foot project report were also found during the search for historic data sources. The profile sheets include three historic high and low water profiles – the historic high water event recorded in 1880, and two low water events from 1864 and 1930. In order to compare the profiles with those obtained from the Reservoir Regulation Manual, they were digitized using Plot Digitizer (Huwaldt 2012). Because the horizontal scale on the profiles were miles below the Omaha Railway Bridge in St. Paul instead of river miles, the location of Lock and Dams 6 through 9 on the profile were assigned river miles 714.1, 702.5, 679.2, and 647.9, respectively. It was assumed that the vertical datum of Mean Sea Level shown on the profiles was the 1912 adjustment. These profiles are represented as dashed lines on Figure 5.6 and can be compared to equivalent profiles from the Reservoir Regulation Manual shown as solid lines of the same color.

In addition to the profile lines, the 9-foot report included preliminary design plan sheets at each lock and dam location. These plan sheets include estimated elevations and discharges for the historic flow events, which are summarized in Table 5.3. Note that higher discharges are estimated upstream for both the 1864 and 1930 low water events, with the relative magnitude of the events switching, as well. At present day Lock and Dam 7, the discharge for the 1864 event was higher, but at present day Lock and Dam 8, the discharge for the 1930 event was higher.

Table 5.3: Historic discharge events.

Event	Present Day Location	Water Surface Elevation (m, NAVD 88)	Discharge (m^3/s)
1864 – Low Water	Lock and Dam 7	191.73	405
	Lock and Dam 8	187.85	241
1880 – High Water	Lock and Dam 7	196.39	4998
	Lock and Dam 8	193.64	5352
1930 – Low Water	Lock and Dam 7	191.46	343
	Lock and Dam 8	188.08	297

There are discrepancies between the profiles shown in Figure 5.6, as well. The 1930 profiles seem more questionable, due to the inconsistencies both between the Reservoir Regulation Manual (red solid line) and the 9-foot project report (red dashed line), and between the plan and profile sheets in the 9-foot project report itself. There also seems to be inconsistencies with the water surface slope, such that there is actually an increase in water surface elevation near River Mile 697. This is where the two profile sheets in the 9-foot project report matched. The 1864 profile, shown as the blue dashed

line, seems to be most probable due to the fact that the plan sheet elevations (blue dots) and the profile are consistent, and there is no increase in water surface near River Mile 697.

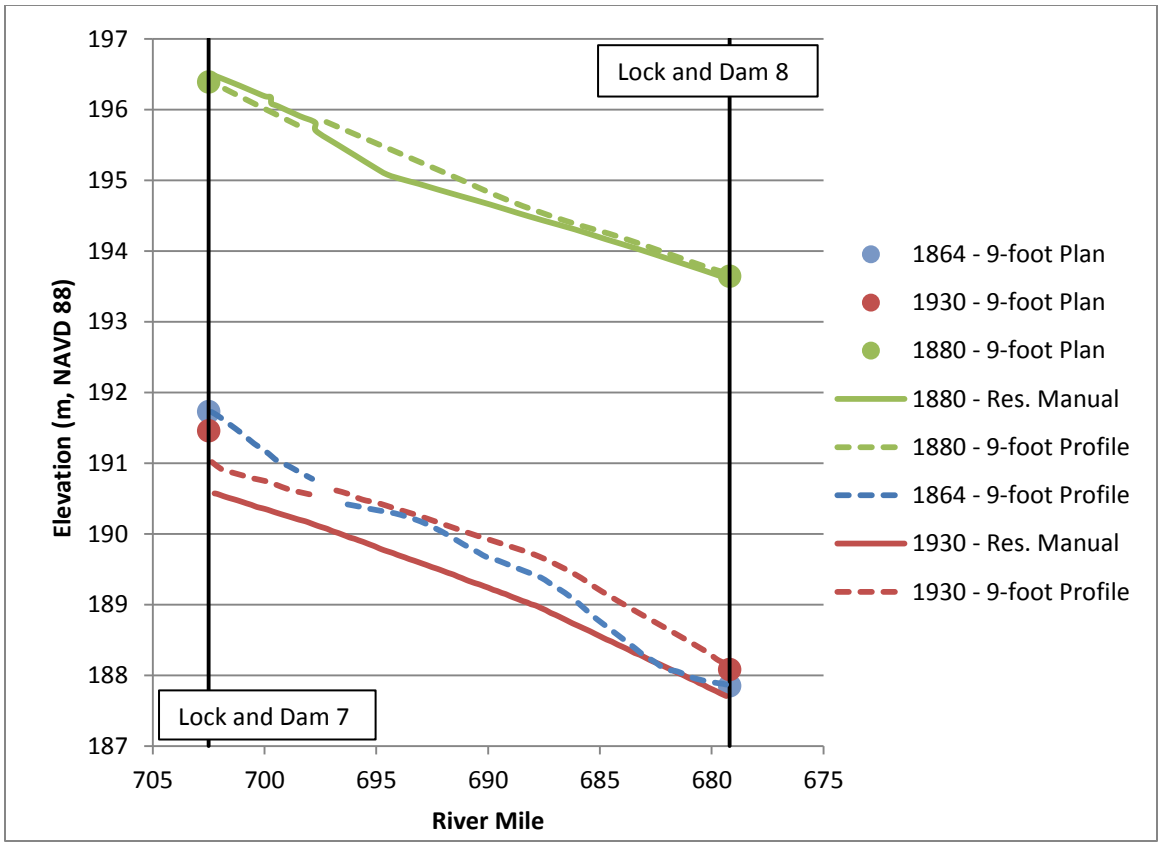

Figure 5.6: Comparison of historic flow event profiles from multiple sources.

5.4.3 1897 Mississippi River Commission Survey

When the bathymetry soundings were gathered as part of the MRC surveys, water surface elevations for the days the bathymetric surveys were performed were recorded on the map plates. The water surface elevations were given at one stone line on each of the four maps in the mosaic, as was the change in elevation between each of the stone lines upstream and downstream. A point shapefile was created with one point in the main

channel at each stone line, and an elevation assigned from the information shown on the map. A river mile attribute was also added to each point using the PolylineM with river mile measurements. The stone line locations and water surface elevations were plotted as round points connected by black lines on Figure 5.7.

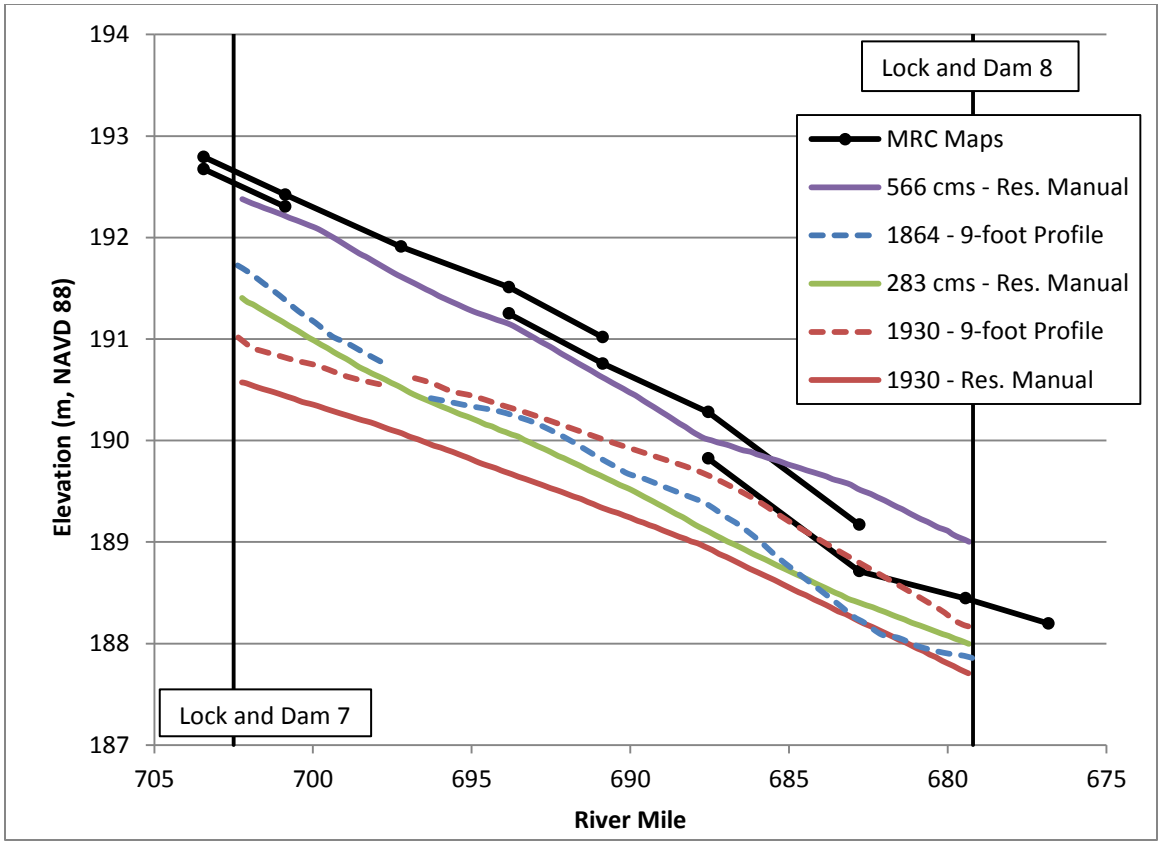

Figure 5.7: Comparison of MRC maps with other sources.

It's important to note that the MRC maps didn't contain actual profiles, just information to calculate discrete elevations at each stone line. Because real elevations were not listed on the maps for the river bed, elevations had to be calculated from the given water surface and recorded depth soundings. As a result, at lower discharges, while the river is contained within the main channel, the assumed slope of the water

surface can influence model results significantly more than if real elevations were available.

5.4.4 Differences in Historic Data

Figure 5.7 illustrates the differences in source data at low discharges. For example, the 1930 profiles, shown in red, are almost 0.5 meters (1.6 ft) different near present day Lock and Dam 7. Additionally, at the profile sheet match lines near River Mile 697, the water surface profile from the 9-foot report actually increases in the downstream direction for the 1930 profile, indicating a problem with the profile accuracy for the purposes of this study. Differences in slope indicate energy losses that are different for the same reach of the study area as well.

Differences between the profiles can be due to a few reasons. For one, significant changes to the channel were made between 1864 and 1930 with the construction of many wing and closing dams. It's not known what adjustments were made to the profiles to account for these changes, if any. Also, it's not known if the profiles were calculated or measured. If they were calculated or otherwise generated from maps, accuracy of the source mapping then becomes important as well. All of these difficulties are to be expected when trying to "go back in time" and recreate a historic condition. The value in gathering data from different sources is that it is possible to make an informed decision about model parameters, and realize that if the model is not reproducing data from a particular source entirely accurately, it doesn't necessarily mean the model is incorrect.

5.5 Historic Condition Model Calibration and Sensitivity Analysis of Roughness Coefficients

To compare simulated results to reference data, the point shapefiles generated from the Reservoir Regulation Manual profiles were used to extract modeled water surface elevations from a raster image generated using the model results. Those points can be graphed in Excel to compare measured water surface values with modeled water surface values.

Calibration using SRH-2D is accomplished by adjusting the material roughness values. This affects the bed shear stress, which is a sink term in the momentum equations (equations (3.6) and (3.7)). In some numerical models, calibration can be performed by adjusting the eddy viscosity. The USBR states in the SRH-2D manual that the eddy viscosity model coefficient shouldn't be used for calibration, however (USBR, 2008).

5.5.1 Calibration at Low Flows

Calibration of channel roughness was performed at low flows using the 283 m^3/s (10,000 ft^3/s) and 566 m^3/s (20,000 ft^3/s) profiles. As Section 5.4.4 explained, there is some uncertainty in the exact water surface profiles at low discharges. Initial calibration efforts attempted to match the 283 m^3/s (10,000 ft^3/s) and 566 m^3/s (20,000 ft^3/s) profiles directly, but that wasn't possible with realistic coefficients for bed roughness. At low flows, modeled water surface profiles at the upstream end of the study area were about 0.5 to 0.6 meters (1.6 to 2.0 ft) higher than the reference water surface profile and generally reflected the slopes of the profiles from the MRC maps (shown as black lines on Figure 5.7).

It was decided to calibrate the model at low flows to simulate water surface profiles parallel to the reference data. If a steady, uniform flow regime is assumed for the study reach that would cause the energy grade lines of the simulated and reference water profiles to be parallel as well, and thus total energy losses comparable in a given reach. The 1930 profiles were not used for reference due to inconsistencies between the reservoir regulation manual and the 9-foot channel report. Figure 5.8 shows both the uncalibrated and calibrated profiles for the two discharges when compared with the reservoir regulation manual. Although the calibrated profiles actually deviate farther from the reference data in terms of magnitude of upstream elevation than the uncalibrated profiles, the slopes match better throughout the study area. When compared with the 1864 low water profile from the 9-foot channel report, the modeled water surface slopes match very well and the magnitude of the differences is less (Figure 5.9). For the 283

m^3/s (10,000 ft^3/s) simulation, differences between the simulated profile and the reference profile ranged from less than 0.1 meters to 0.6 meters (0.3 to 2.0 ft). For the 1864 low water simulation, which used a discharge of 241 m^3/s (8,500 ft^3/s) as shown in Table 5.3, the maximum difference between the simulated and reference profiles was about 0.6 meters (2.0 ft) maximum, with differences in a majority of the reach less than 0.3 meters (1.0 ft).

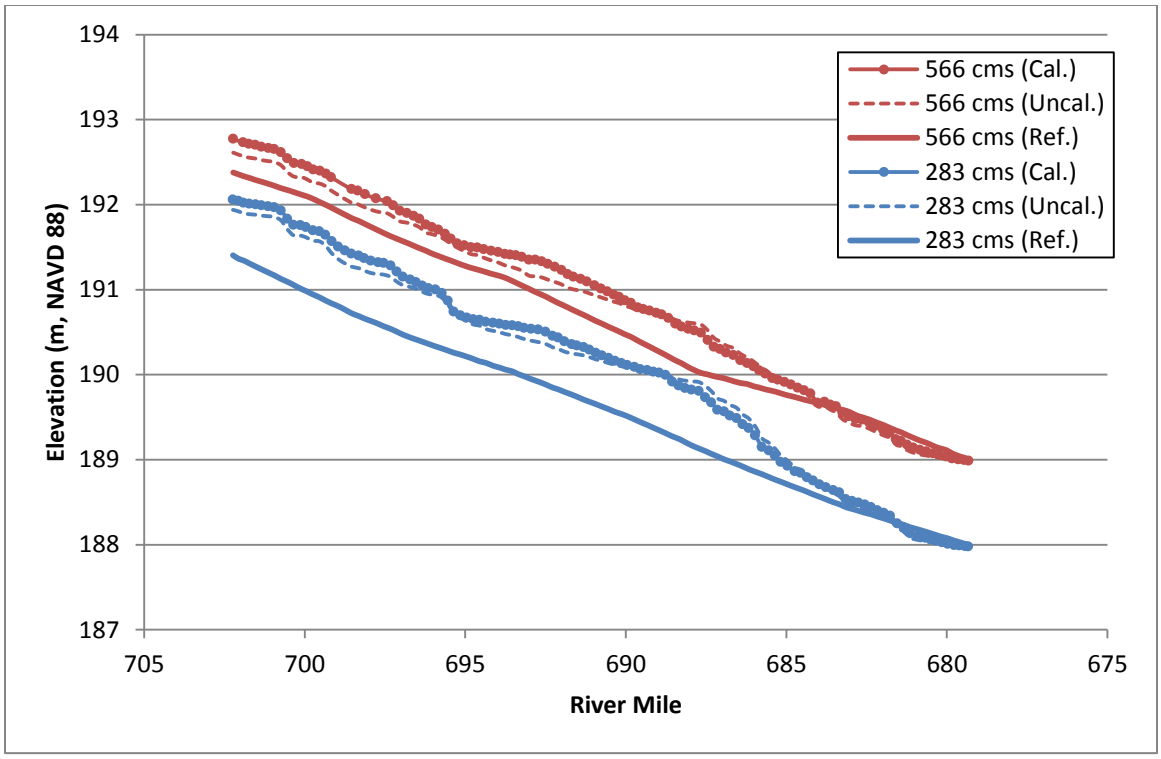

Figure 5.8: Uncalibrated and calibrated profiles compared to reservoir regulation manual.

5.5.2 Calibration at High Flows

Once the best achievable calibration for channel roughness was found for low flows, simulations were performed at 1133 m^3/s(40,000 ft^3/s) and 2265 m^3/s (80,000 ft^3/s) and compared with the profiles from the reservoir regulation manual (USACE - SP 1971). Base floodplain roughness coefficients, shown in Table 5.1, were compared

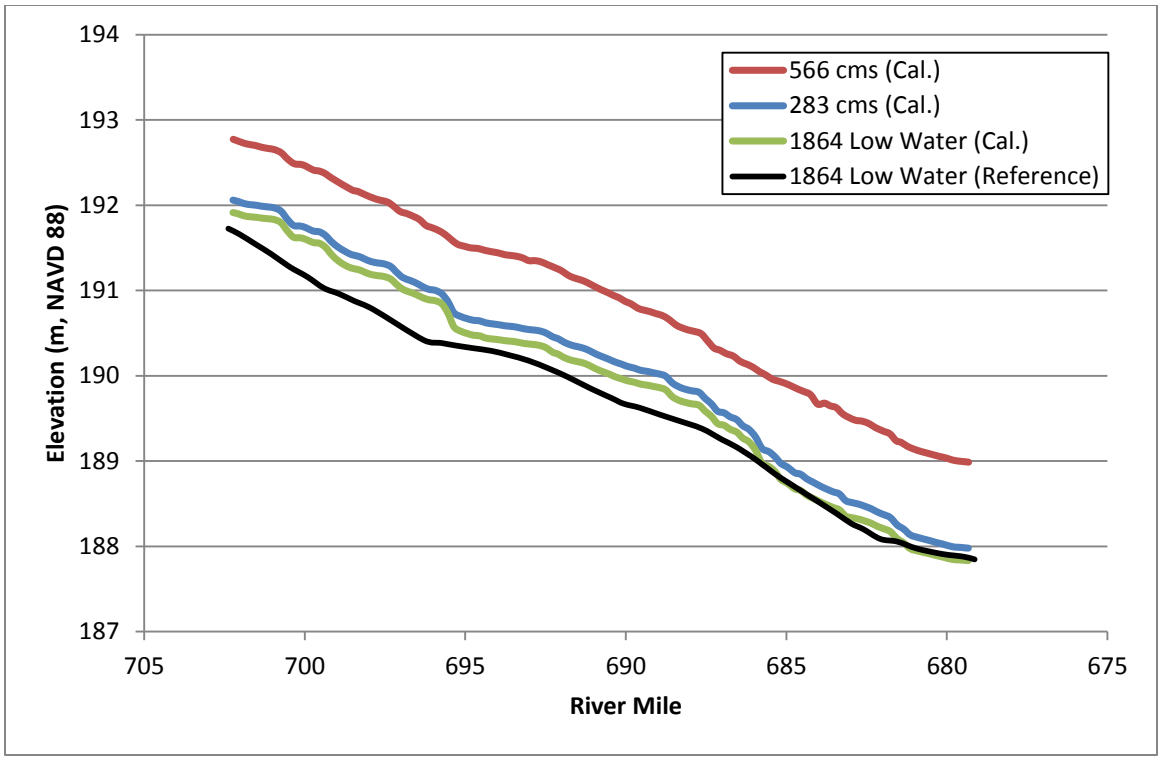

Figure 5.9: Calibrated profiles compared to 1864 low water profile.

with values adjusted positively and negatively 20% and 40% to evaluate model sensitivity of floodplain roughness. The water surface profiles for the reference data, base roughness scenarios, and the positive and negative 40% scenarios are shown in Figure 5.10 on page 64. Figure 5.10 shows that the hydrodynamic model is generally insensitive to roughness coefficients at high flows, as represented by the fact that water surface slopes are consistent for a wide range of roughness coefficients.

Due to the insensitivity of the model to roughness coefficients, it was decided to use the base roughness coefficients for the final simulations. Figure 5.11 on page 65 shows how modeled water surface profiles compare to reference data from the reservoir regulation manual for a range of discharges from 283 to 2549 m^3/s (10,000 to 90,000 ft^3/s). It demonstrates that as discharges increase, the model predicts lower water surface elevations than the reference profiles. This is consistent with Figure 5.10, which shows

that the profiles are generally higher than the reference data at 1133 m^3/s (40,000 ft^3/s) but are equal or lower to the reference data at 2265 m^3/s (80,000 ft^3/s). The difference in water surface elevations could be due to the rating curves used to plot the reference data. The final Manning's roughness coefficients are shown in Table 5.4.

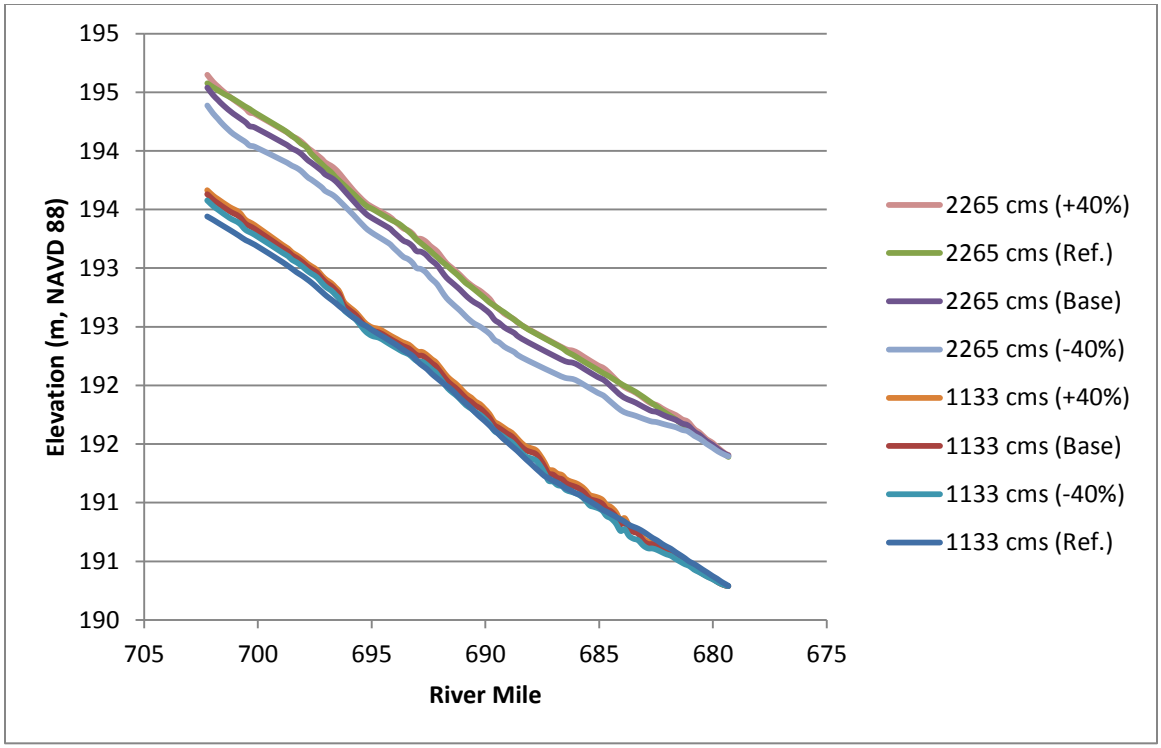

Figure 5.10: Uncalibrated (base) and calibrated profiles at high discharges.

5.5.3 Investigation of Model Sensitivity to Downstream Water Surface Elevation

The sensitivity of the model to the downstream water surface elevation was tested to determine the effect on the entire study reach. Simulations were performed with the downstream water surface elevation equal to the value shown in the reservoir regulation manual, and with the elevation increased and decreased by 20 centimeters (0.7 ft). As

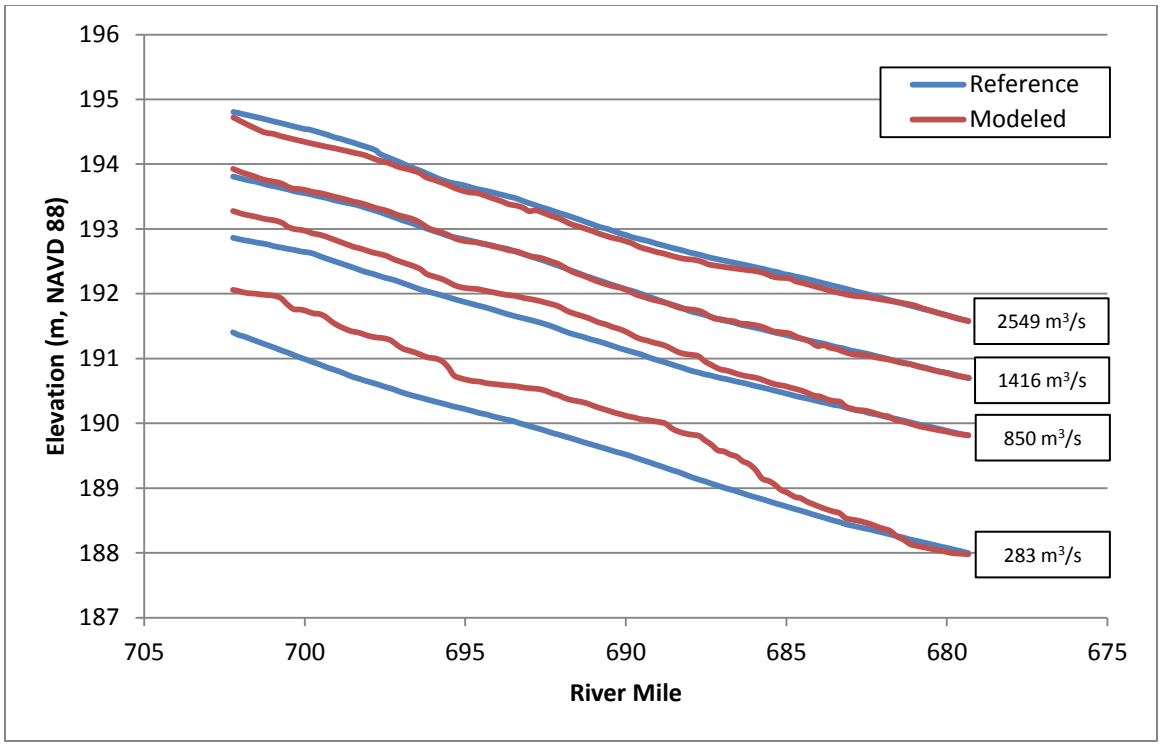

Figure 5.11: Comparison of modeled water surface to reference data for discharges of 283 m^3/s through 2549 m^3/s (10,000 ft^3/s through 90,000 ft^3/s).

Table 5.4: Historic condition model final roughness coefficients

Material	Roughness Coefficient
Open Water	0.024 – 0.040
Marsh/Swamp	0.035
Agriculture	0.035
Forest	0.080
Grasses/Forbs	0.035
Sand/Mud/Clay	0.030
Urban/Developed	0.100

illustrated in Figure 5.12, the change in elevation only affected the model from the downstream boundary upstream to approximately River Mile 687. Upstream from that location, the same normal depth was reached for all simulations. This indicates that the modeled water surface elevation that is higher than the reference water surface elevation above river mile 687 at low flows was not caused by an incorrect downstream boundary condition. At discharges of 850 m^3/s (30,000 ft^3/s) or less, the downstream water surface elevation could be increased to reduce the slope near River Mile 687, but that would contradict the rating curves (Figure 5.5) and slope of the water surface indicated on the MRC maps (black line on Figure 5.7).

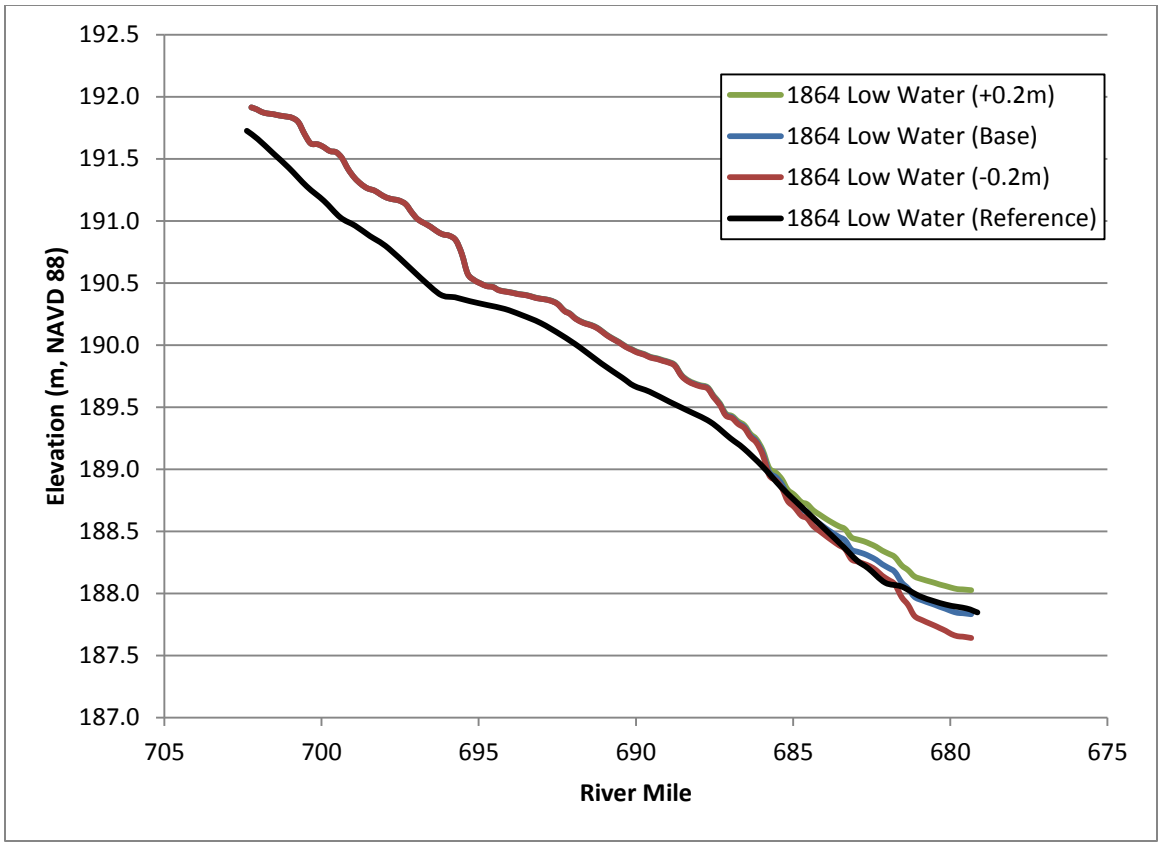

Figure 5.12: Comparison of downstream water surface elevations showing sensitivity of model to boundary condition at 241 m^3/s (8,500 ft^3/s).

5.6 Investigation of Model Sensitivity to Channel Topography

After calibrating the roughness coefficients to best match the water surface slopes in the reference data, model sensitivity to changes in bed topography was investigated to determine if minor topography changes would significantly influence model results at low discharges. This investigation included local adjustments to areas that appear to be constrictions to the flow when viewing the plan form of the river, changes to bed elevations in three major secondary channels (shown in Figure 5.13) that could affect discharge distribution between the main channel and secondary channels, and changes to the main channel bathymetry around wing dams that may have concentrated flows in a narrower channel, thus increasing water surface elevations.

5.6.1 Widening of Narrow Areas in the Main Channel to Investigate the Effect of Constrictions

The first change that was investigated was adjusting mesh node elevations to widen the channel in areas that appeared constricted when viewing the plan form of the river. These areas also showed higher velocities as a result of the channel narrowing. The goal of widening the channel in these areas was to determine if a constriction of the channel was causing an increase in water surface elevation that would affect upstream water surface elevations, as well. The main areas that were widened were near river mile 683 and 684 (reference Figure 1.3, page 8). The effect on water surface elevations as a result of widening the channel was relatively small for the whole reach. The slope of the water surface immediately upstream of the topography change decreased, indicating that velocities decreased due to increases in cross sectional area. Due to the decreased velocities, bed shear stress decreased and thus energy dissipation decreased and the slope of the water surface flattened. However, further upstream from the constriction, the bed topography was held constant, meaning that normal depth was once again reached and there was no influence from backwater effects due to the downstream widening of the

channel. The fact that backwater effects were minimal and changes to the water surface slope undesirable upstream of the large, arbitrary change to the channel cross section led to the conclusion that major cross sectional modifications were not justified to adjust modeled water surface profiles to more closely match reference profiles.

5.6.2 Deepening of Main Channel to Investigate the Effect of Wing Dams

The historic MRC map used as the elevation source for the hydrodynamic model showed over 70 wing dams and closing dams upstream of River Mile 687. When simulation results for water depth for the 283 m^3/s (10,000 ft^3/s) simulation were examined, a few large areas of shallow depth, also in the areas where wing dams are shown on the MRC maps, became apparent. To investigate whether or not the difference between the simulated profiles and the reference profiles was due to the effect of wing dams in the simulated results, the DEM was modified to deepen the channel in the area of the wing dams.

There was not an exact amount of material 'removed' in the wing dam areas when the channel was deepened. Rather, the plan form view of water depths from the model simulations was examined along with the DEM. The bed topography in areas that were shown as having wing dams on the MRC maps and shallower depths in the model results was lowered to match levels upstream, downstream, and closer to the main channel. That resulted in lowering of bed elevations in approximately the one to two meter range. The red profile line in Figure 5.14 shows the effect of removing the major areas of wing dams upstream of River Mile 687.

Removing the areas of higher bed topography around the wing dams resulted in a reduction in the water surface elevation of approximately 0.2 meters (0.7 ft) through much of the domain upstream of River Mile 687. This is due to the deeper channel, which spreads out the discharge over a larger cross sectional area, thus reducing the water surface elevation. Although the elevation of the water surface profile matches the

reference profile (1864 low water shown as the black line) better in some areas, the slope of the modeled water surface throughout the domain does not match the reference profile as well as the unaltered profile (shown as green dots). Due to the fact that the there was no way to know exactly how much bed aggradation between the wing dams occurred, or the elevations of the wing dams themselves to determine their effects on the hydraulics of the reach, the bed topography changes were not incorporated into the final hydrodynamic model.

5.6.3 Deepening of Secondary Channels to Investigate the Effect of Discharge Distribution

The modeled water surface profiles begin to deviate most from the reference water surface profiles shown in the reservoir regulation manual (USACE - SP 1971) near River Mile 687, where a major secondary channel known as the Raft Channel splits off from the main channel. The bed elevation in the Raft Channel was lowered 0.6 meters (2.0 ft) to investigate the effect that lowering the bed had on conveyance through the Raft Channel and the main channel, and thus the effect on the water surface profile in the main channel.

The bed modifications were made for two reasons. The first reason is that the historic map showed a closing dam at the opening of the Raft Channel, which would have blocked some of the discharge that was naturally conveyed through it, and concentrated that flow in the main channel. Although the closing dam was not directly captured in the raster DEM, if water surface levels were lower in the Raft Channel due to less water being conveyed through it, and the water surface level was assumed to be the same as in the main channel, that could cause the real elevations assigned to be higher than what they were in reality. That is due to the fact that real bed elevations were assigned based on water surface elevations given on the maps (as described in Section 4.2), and if the water surface level was assumed to be higher, when the water depths shown on the map for the Raft Channel were subtracted from the higher water surface elevation, the bed

elevation would be higher as well. The second reason bed topography changes in the Raft Channel were tested is that there could have been bed aggradation due to decreased velocities downstream of the closing dam. These same factors apply to the two major secondary channels in the upstream part of the pool indicated by the yellow circles in Figure 5.13.

The bed topography changes in the secondary channels were incorporated into the DEM containing the topography changes around the wing dams described in Section 5.6.2 . The water surface profile for a discharge of 283 m^3/s (10,000 ft^3/s) that resulted from lowering the bed 0.6 meters (2.0 ft) in the three major secondary channels is shown in Figure 5.14 (page 72) as the blue line. In additional to the wing dam changes, this profile line includes changes to both the Raft Channel and the two secondary channels in the upstream part of the pool. Separate simulations were performed with changes made to either the upstream secondary channels or the Raft Channel, and those simulations revealed that the effect of the two changes were independent, meaning water surface profiles for the two different scenarios converged near River Mile 695. The model result from a single simulation combining both changes is presented here for clarity.

Table 5.5 on page 72 shows how discharge distribution between the main channel and the Raft Channel changes with the two different changes to the bed topography. Lowering the bed topography of the Raft Channel 0.6 meters (2 ft) had the largest effect on discharge distribution, causing one third of the total discharge to be conveyed in the Raft Channel. While measured values are not available to compare with the simulated values for discharge distribution, these results are important to confirm that the lower water surface level in the main channel is in fact caused by lower discharge in the main channel and higher discharge in the Raft Channel.

In much the same way as the wing dam changes, the changes to the secondary channel resulted in water surface elevations that more closely reflected the reference data, but the slopes of the water surface did not match as well. Additionally, the change in bed

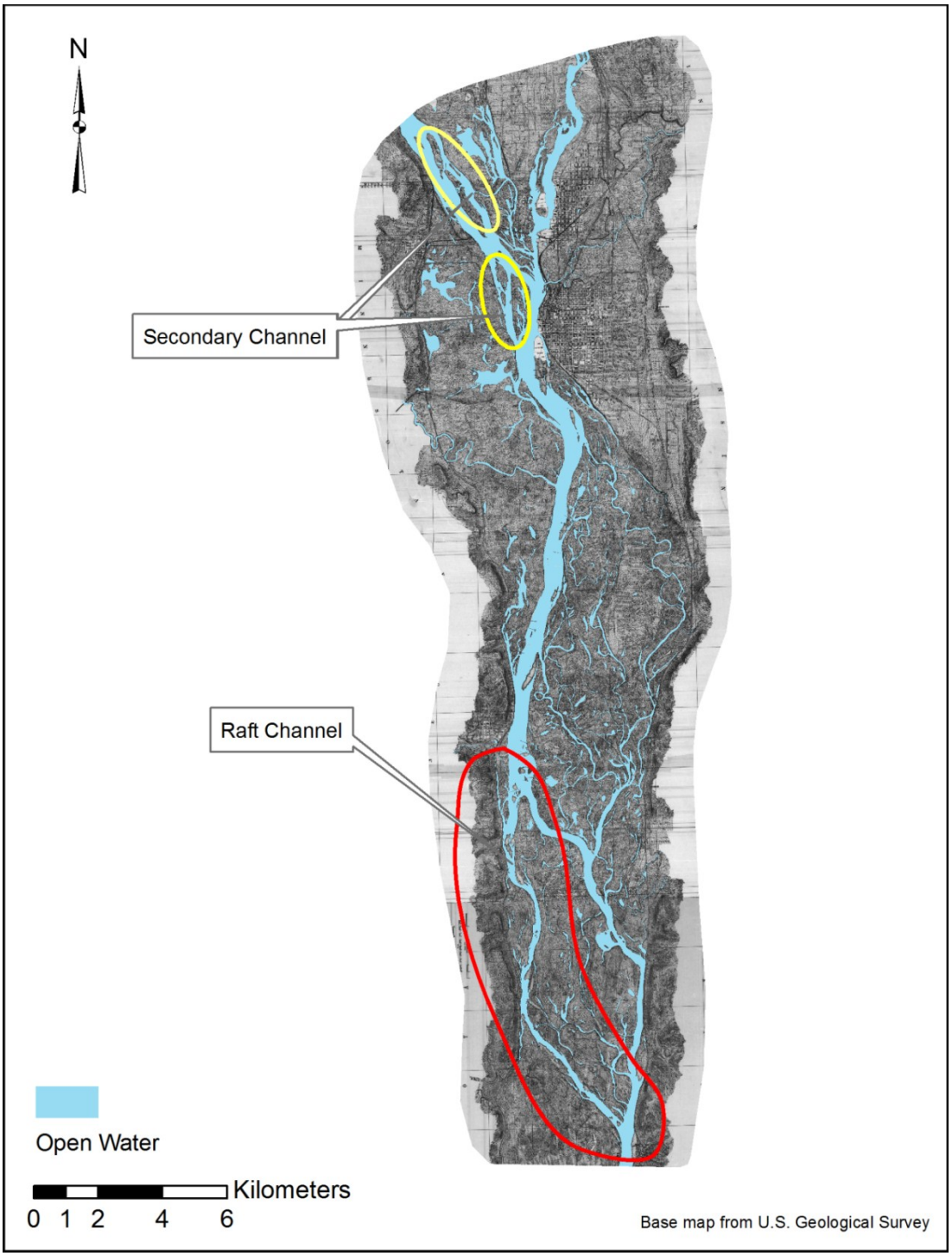

Figure 5.13: Illustration of secondary channels and Raft Channel that were modified to test model sensitivity to bed topography.

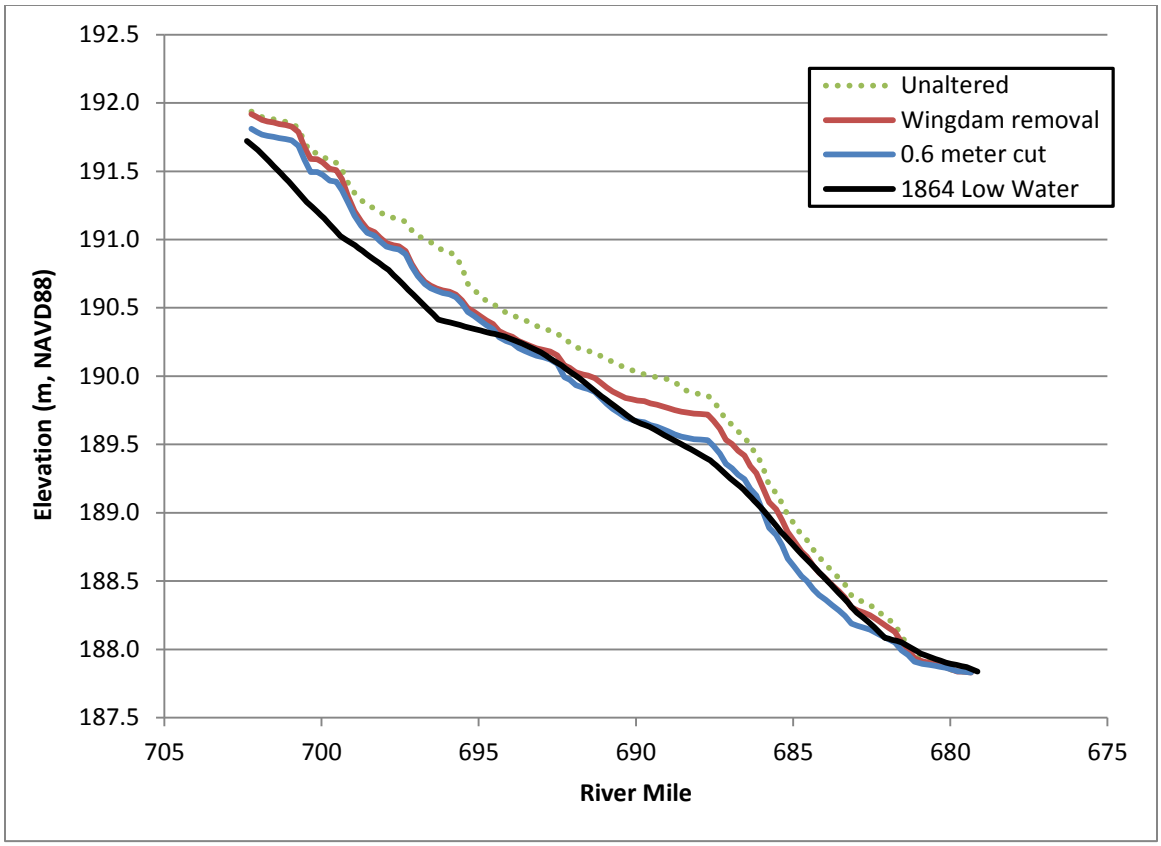

Figure 5.14: Water surface profiles showing model sensitivity to channel topography.

Table 5.5: Discharge distribution between the main channel and Raft Channel at 283 m^3/s (10,000 ft^3/s)

	Main Channel		Raft Channel	
	Discharge (m^3/s)	**Percentage**	**Discharge (m^3/s)**	**Percentage**
Unaltered	248	92	23	8
Wingdam removal	219	81	52	19
0.6 meter cut	180	66	91	34

elevation of 0.6 meters (2.0 ft) was relatively large when compared to common water depths of 0.3 to 1.8 meters (1.0 to 5.9 ft) shown on the reference MRC maps. The maximum change in water surface elevation as a result of these bed topography changes is about 0.2 meters (0.7 ft) near River Mile 687. This relatively large change in bed elevation for minimal change in water surface elevation led to the conclusion that these changes were not justified to reconcile differences between modeled water surface profiles and reference water surface profiles.

The changes showed what affects that broad bed topography changes made to discharge distribution and water surface slopes throughout the model. In addition, the model could provide differences on velocity affects. These are the benefits of hydraulic modeling. It is now possible to make many different changes to investigate different scenarios with minimal effort. After these changes were made and the results analyzed, it added more confidence that the model wasn't significantly affected by minor topography errors.

5.7 Additional Modeling Challenges and Parameters

Monitoring lines were utilized to ensure that the model reached a steady state prior to ending the simulation. In some cases (at discharges less than approximately 10 m^3/s or 350 ft^3/s) in the La Crosse and Root Rivers, there was some flow stagnation near the model boundary, thus preventing the contribution from those tributaries from reaching the downstream exit to the model. This is due to the small slopes present in the tributary channel, which caused the gravitational force to balance with the inertial forces in the momentum equation. This issue was solved for the La Crosse River by specifying an initial water surface elevation in the tributary channel for the first 700 meters (2,300 ft). This length was chosen to allow for a constant water surface to be input such that the flow would still be contained within the banks of the tributary. The water surface elevation had no physical significance, but it was essentially utilized to provide an initial 'slug' of water to drive the flow downstream at low flows. For the Root River, the

channel bathymetry was modified to provide a gently sloping bed that was consistent from the edge of the model domain to the river's confluence with the Mississippi River. This was needed because simply specifying an initial water surface elevation at the Root River did not provide enough inertial force to drive the flow at the lowest discharges.

Appendix C of the SRH-2D user's manual lists a number of parameters that can be changed during code execution to control the solution. These parameters include time step, total simulation time, output file interval, damping coefficient for the convective term, number of iterations per time step, relaxation factors for the continuity and momentum equations, and the coefficient for the parabolic turbulence model (USBR, 2008). Relaxation factors, coefficients for the turbulence model, and the damping term were not modified from default model values for this study. As discussed in Section 3.3 , the current condition Pool 8 model (Smith, 2011) of similar scale and boundary conditions was not found to be sensitive to the turbulence model coefficient and there were no convergence issues that would have required adjusting the other parameters.

5.8 Conclusions about Model Development, Calibration, and Sensitivity Analysis

The hydrodynamic model was calibrated to provide the best representation of pre-impoundment conditions for the available data. By matching water surface slopes throughout the domain to the reference water surface slopes, energy losses shown in the reference data were properly simulated by the model. Both low flows, which represented primarily one dimensional flow in the main channel, and high flows, which represented more complex two-dimensional flows, were shown to reproduce energy losses correctly.

Model sensitivity to changes in bed topography was also tested. The results indicated that major changes in bed topography were required to influence water surface elevations and discharge distribution between the side channels and main channel. The relative insensitivity of the model to the bed topography, combined with the raster DEM

accurately being able to reproduce the reference data (as shown in Section 4.3) shows that uncertainties in the hydraulic model due to bed topography are small.

CHAPTER 6: HYDRODYNAMIC MODEL DEVELOPMENT – CURRENT CONDITIONS

A hydrodynamic model that is able to simulate current flow conditions in Pool 8 was constructed by Smith (2011). The goal of that study was to develop a two-dimensional hydrodynamic model that could be used for current and future management of the river (Smith 2011). Similar to the current study, Smith generated a finite volume mesh in Aquaveo SMS and used SRH-2D to solve the 2D Saint-Venant equations. The model used a seamless DEM developed by the USGS – UMESC for elevation data.

6.1 Current Study Mesh Refinement

For the current study, the old Pool 8 mesh (Smith 2011) was refined in a few areas to better capture small scale features in the floodplain. In particular, most work was done in the La Crosse River and Root River areas. The Root River has tall but relatively narrow natural levees that were not captured in a few spots in the original mesh used for the 2011 study. Those areas were refined so that the river is contained within its banks (reflecting the narrow levees) rather than spilling out into the floodplain at low flows.

In addition, the seamless DEM does not include bathymetry data for the La Crosse River. As a result, the old mesh had elevations for the channel that were actually water surface elevations from when the LiDAR surveys were conducted. To allow for more natural flow through the lowland areas of the La Crosse River floodplain, elevations were manually assigned to the mesh points representing the center of the channel to allow for more conveyance in the channel itself. Elevations were picked at a few key points between where the La Crosse River enters the model domain and the tributary's confluence with the Mississippi River to ensure that they were corresponding with the adjacent bank elevations and to make sure that they were lower than the surrounding floodplain elevations. A simple straight interpolation process was then performed between the key points to update the mesh for the La Crosse River.

In addition, one area of future interest for the current condition model may be the hydrodynamics in the lower part of Pool 8, where wave induced erosion of old islands has occurred after impoundment and subsequent restoration initiatives are replacing the eroded islands. Due to the broad focus of the original study, the old mesh did not include sufficient detail in these areas to best capture the restored islands. Therefore, the mesh was further refined in the areas around the islands to ensure that the island features were captured in detail if future work in this area is needed. Additionally, as part of the mesh refinement around the islands in the lower part of the pool and tributary channels, a finer DEM was used than in the initial study of current conditions. The current study uses the DEM at its original 2 meter (6.6 ft) resolution instead of resampling the raster image to 10 meters (32.8 ft).

6.2 Boundary Conditions, Roughness Coefficients and Validation Data

Due to the minor mesh refinements made, and use of a 2 meter DEM instead of a 10 meter DEM, the validation and calibration simulations were re-run. The calibration data was a water surface elevation profile extracted from a LiDAR dataset flown by Sanborn Map Company for the USGS, and the validation data was from a Real Time Kinematic (RTK) Global Navigation Satellite System (GNSS) survey conducted by the USGS (Smith 2011). Boundary conditions were calculated using gage and discharge data from November 7, 2007 for the calibration simulation and June 4, 2010 for the validation simulation. The U.S. Army Corps of Engineers publishes log data every four hours for the locks and dams and the control points in the pool. The log data includes discharge through the main dam gates, spillways, or culverts through the dam embankment, as well as pool and tail water elevations at the dams and control points. The gage readings taken at 8 a.m. were used for both simulations because the gage data obtained for the tributaries was recorded at 8 a.m., as well. The total discharge at Lock and Dam 8 for both dates of interest was higher than the sum of the input from Lock and Dam 7 and the tributaries, so

all inputs were increased an equal percentage (approximately 5% for the calibration simulation and 3% for the validation simulation) for continuity. This difference is most likely due to additional surface runoff or groundwater contributions in the domain.

The model parameters used for the new simulations are shown in Table 6.1 and the resulting calibration and validation statistics are shown in Table 6.2. Negative differences indicate modeled results lower than measured values. Figure 6.1 compares the calibration data with the modeled water surface and Figure 6.2 compares the validation data with the modeled water surface. The model showed excellent agreement with the field data at the roughness coefficients used for the original study (Figure 6.1and Figure 6.2), so it was determined that minor changes made to the model did not necessitate re-calibration. As was noted in the original study, a barge interrupted data collection for the validation water surface profile. Therefore, the author hypothesized that the disruption, along with decreasing discharges throughout the day may have contributed to the difference between the simulated and measured water surface. However, these differences are small (centimeter scale).

With the model's ability to accurately represent known discharge events confirmed, steady state simulations were run for discharge scenarios ranging from 283 m^3/s to 2832 m^3/s (10,000 ft^3/s to 100,000 ft^3/s) in increments of 283 m^3/s (10,000 ft^3/s). Three discharges of interest were examined more closely for the comparisons made in Chapter 7. They are 850 m^3/s (30,000 ft^3/s, exceeded approximately 50% of the time), 1416 m^3/s (50,000 ft^3/s, exceed approximately 25% of the time), and 2549 m^3/s (90,000 ft^3/s, exceeded approximately 5% of the time).

Table 6.1: Current condition calibration and validation simulation parameters.

Calibration Flow Conditions		**Validation Flow Conditions**	
Inlet	**Discharge (m^3/s)**	**Inlet**	**Discharge (m^3/s)**
Lock and Dam 7	1127.0	Lock and Dam 7	770.2
French Island Spillway	8.6	French Island Spillway	2.8
Onalaska Dam	51.0	Onalaska Dam	21.9
Lacrosse River	8.9	Lacrosse River	8.6
Root River	33.4	Root River	20.5
Exit	**Discharge (m^3/s)**	**Exit**	**Discharge (m^3/s)**
Reno Spillway	0	Reno Spillway	0
Hastings Spillway	0	Hastings Spillway	0
Exit	**Elevation (m)**	**Exit**	**Elevation (m)**
Lock and Dam 8	191.87	Lock and Dam 8	191.85

Table 6.2: Current condition calibration and validation statistics.

Calibration Statistics (m)		**Validation Statistics (m)**	
Mean Difference	0.00	Mean Difference	0.03
Largest Negative Difference	- 0.31	Largest Negative Difference	- 0.14
Largest Positive Difference	0.36	Largest Positive Difference	0.13
Standard Deviation	0.08	Standard Deviation	0.02

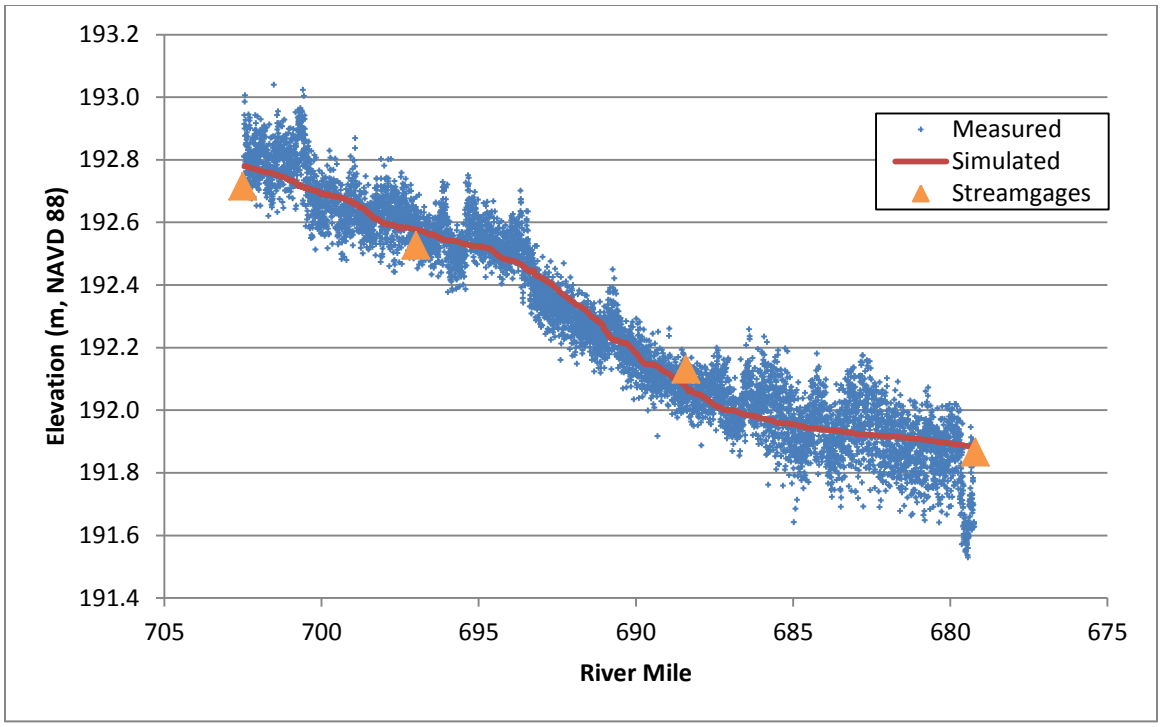

Figure 6.1: Water surface profile for the current condition model calibration simulation (using the refined mesh) compared to measured data for Pool 8.

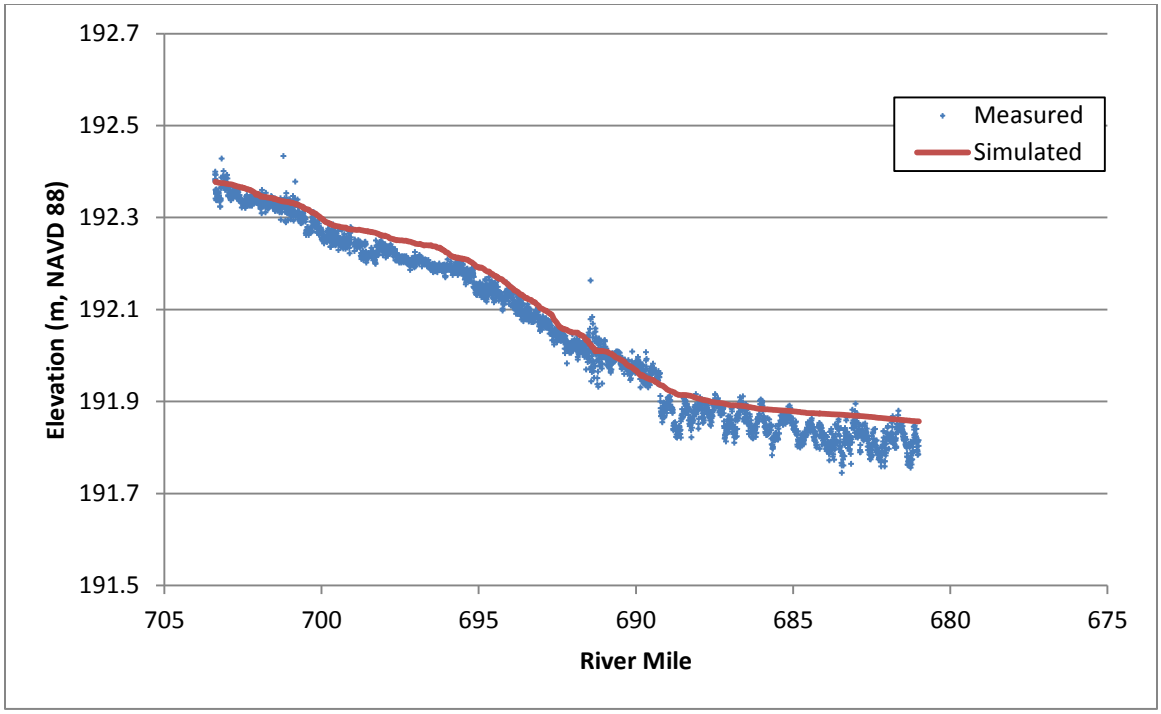

Figure 6.2: Water surface profile for the current model validation simulation (using the refined mesh) compared to measured data for Pool 8.

CHAPTER 7: MODEL APPLICATIONS

7.1 Discharge Distribution throughout the Floodplain

Discharge distribution was calculated at three cross sections in both the current and historic condition models. The cross sections were located at approximately River Miles 694, 690, and 682. Monitoring lines, a feature of the SRH-2D numerical code used for this study, were utilized to calculate the discharge through the channel and floodplain areas. A simple division was made in the model domain to better examine channel versus floodplain areas. In particular, when dividing the domain into channel and floodplain areas, an effort was made to keep lengths of the monitoring lines consistent between the current condition simulations and the historic condition simulations and begin and end the monitoring lines at local maximum elevations that most clearly differentiate the floodplain and channel areas.

Figure 7.1 through Figure 7.3 illustrate the percent of total discharge in the different zones of the floodplain. At the two most upstream cross sections (River Mile 694 and River Mile 690) discharge distribution trends were similar for both historic and current conditions, with the most flow concentrated in the main channel for both cases. However, discharges in the left floodplain area at River Mile 694 were higher in the current condition model, even though the area is not directly impacted by the higher, constant water levels of the impounded area. When examining the plan form view of the river and model results, it becomes evident that the side channels are carrying more discharge under current conditions. This is most likely due to the added connectivity of the main channel to the backwater areas lower in the pool. This added connectivity increases discharge in the side channels further upstream as the water is conveyed to the inundated area. The same can be said for River Mile 690. River Mile 690 is on the upstream end of the inundated area, so more of the conveyance in the left floodplain area is due more directly to the inundation than at River Mile 694.

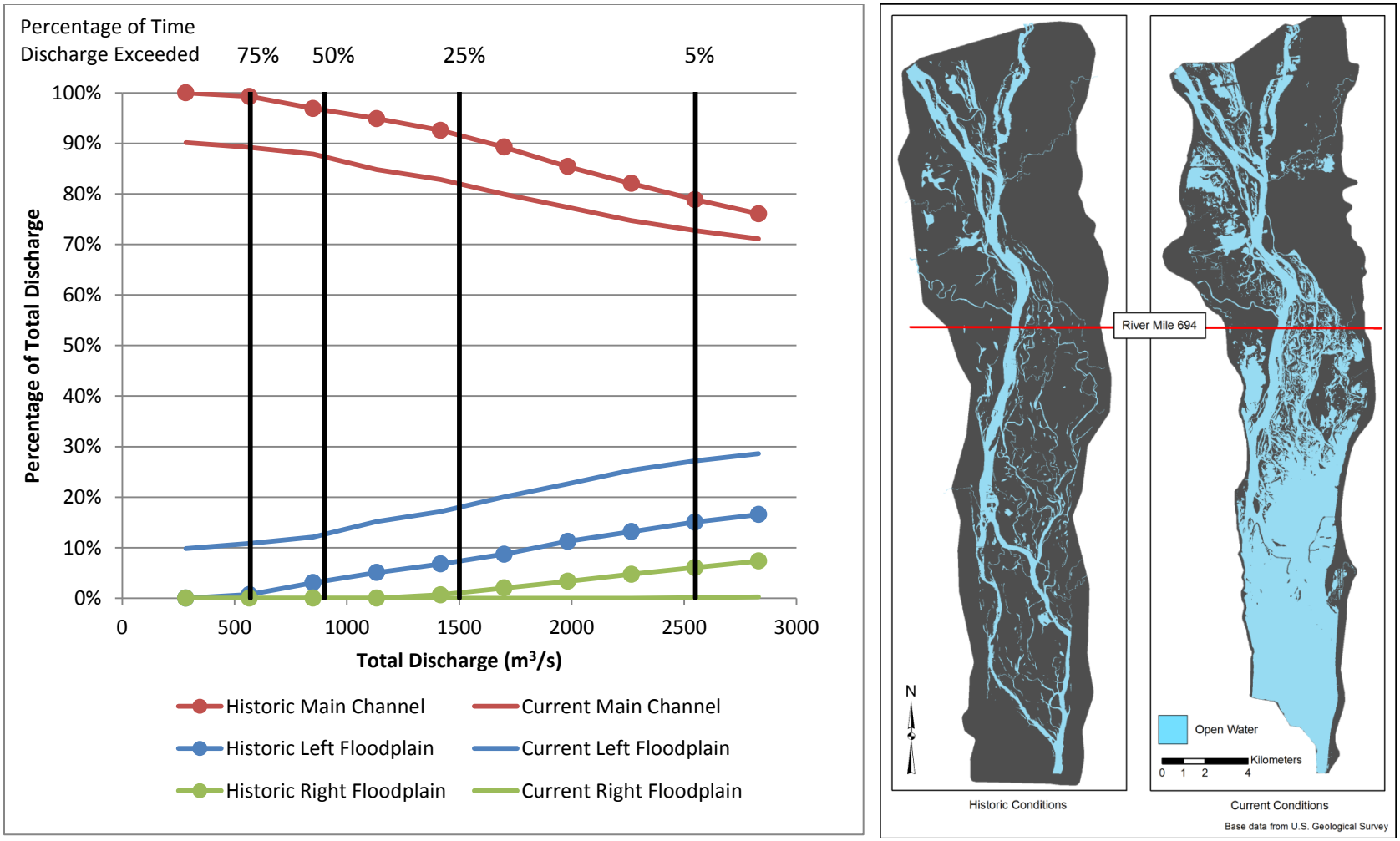

Figure 7.1: Flow distribution within the floodplain at River Mile 694.

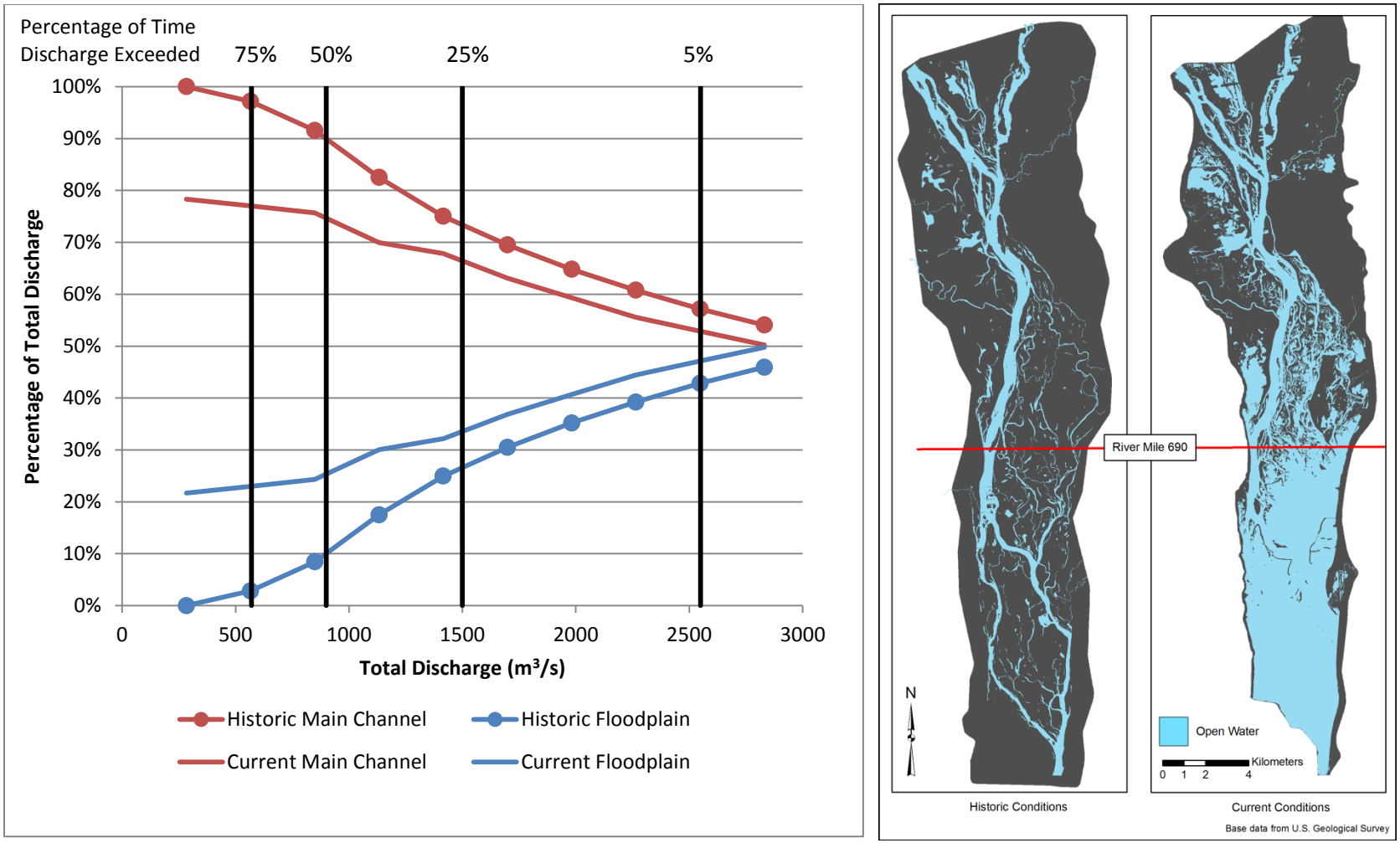

Figure 7.2: Flow distribution within the floodplain at River Mile 690.

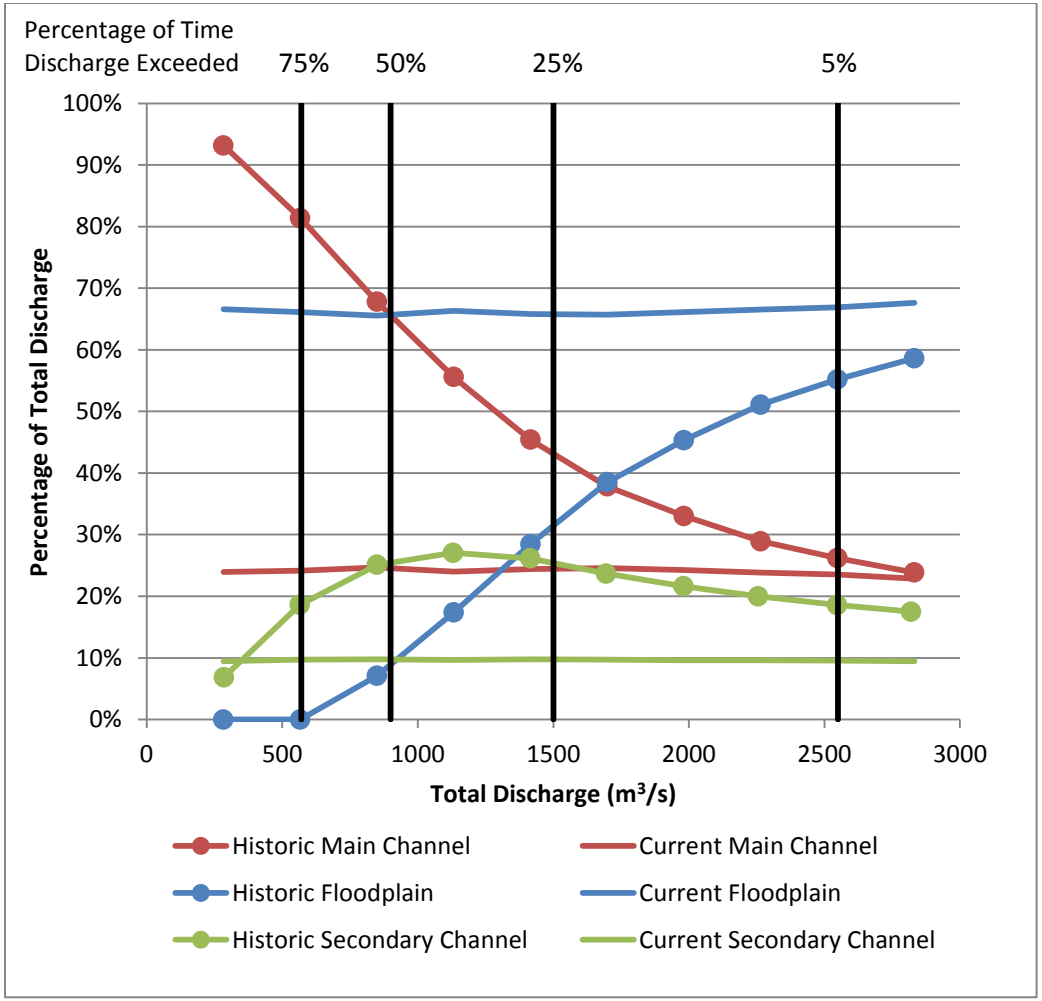

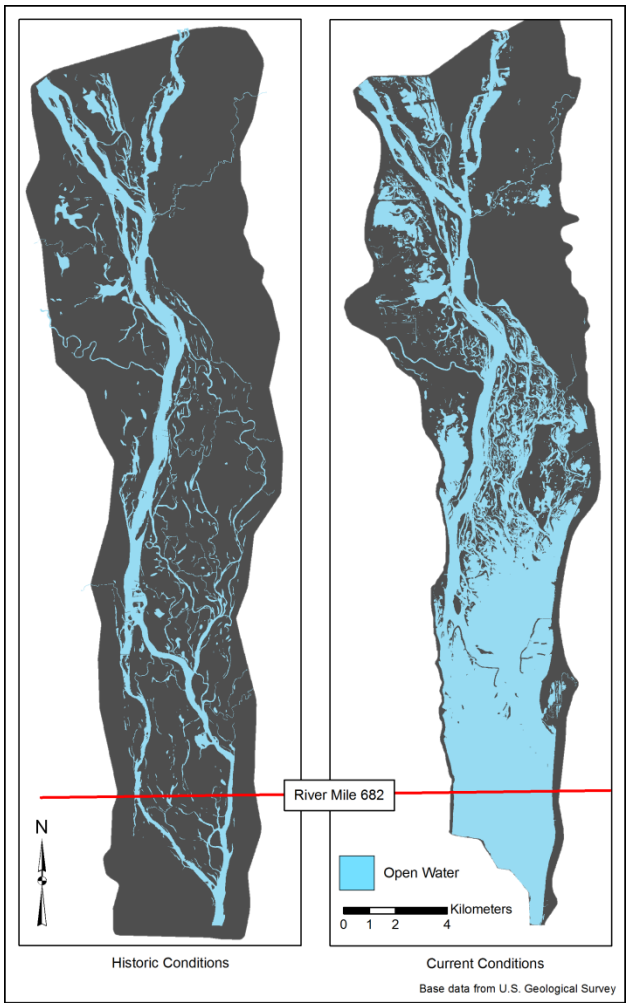

Figure 7.3: Flow distribution within the floodplain at River Mile 682.

At River Mile 682, the effects of impoundment from the locks and dams are most evident. The current condition model shows very little fluctuation in discharge distribution across the range of discharges modeled when compared to historic conditions. That is due to the stable water levels maintained in the lower part of the pool. In contrast, the historic condition model shows a much more dynamic interaction between the main channel and floodplain. At total discharges less than 2265 m^3/s (80,000 ft^3/s), a majority of the discharge is conveyed in the main and secondary channels, and only above 2265 m^3/s (80,000 ft^3/s) does the majority of the flow shift to the floodplain.

These results show the important implications for habitat and the biota that inhabits the floodplain areas. In a broad sense, with a redistribution of discharge comes a redistribution of the river's energy from the main channel onto the floodplain. What was historically a faster flowing main channel containing most of the energy is now a broad, slow-moving slack water lake with the energy distributed throughout the floodplain. Also noteworthy is that the part of the reach that historically showed the most dynamic shifts in discharge distribution is also the part that now has the least redistribution of flow as a function of discharge. There is less diversity of flow over the temporal and spatial scale post-impoundment. These observations highlight the importance of re-creating the natural dynamics of the floodplain/channel interactions in the lower part of the pools.

7.2 Classification and Spatial Comparison of Velocities

Modeled velocities were classified and compared using methods similar to those used in the 2000 Cumulative Effects (CE) Study for the UMRS, assembled by WEST Consultants for the U.S. Army Corps of Engineers. The velocities were classified into three bins: low (0.15 m/s (0.5 ft/s) and less), medium (0.15 to 0.45 m/s (0.5 to 1.5 ft/s)), and high (0.45 m/s (1.5 ft/s) and higher) on the basis of biological significance to several fish species (WEST Consultants, 2000). A similar binning process was performed on the

historic and current condition model results for the present study and the results are presented graphically in Figure 7.4 through Figure 7.6.

The upper part of the model showed the least amount of change from historic to current conditions. Other than higher velocities in the main channel under historic conditions, velocities in the backwater areas were similar, primarily falling into the low or medium range. At 2549 m^3/s (90,000 ft^3/s), the historic condition model indicates more areas of higher velocity on the right floodplain than under current conditions due to more discharge being conveyed in that area under historic conditions.

In the middle part of the pool, velocities in the side channels are higher under current conditions than historic conditions, with many areas falling into the medium range at 850 m^3/s (30,000 ft^3/s). At the higher discharges of 1416 m^3/s and 2549 m^3/s (50,000 ft^3/s and 90,000 ft^3/s), the trend of higher velocities also holds true. Some velocities even fall into the high velocity bin under current conditions at 2549 m^3/s (90,000 ft^3/s, Figure 7.6), while most velocities were in the medium bin under historic conditions. The higher velocities in the side channels coincide with the observation made in Section 7.1 that more discharge is being conveyed in the floodplain areas under current conditions at River Miles 694 and 690 than was historically.

The most noticeable difference in velocities for all discharges is in the lower part of the pool. Under historic conditions, many areas of the Raft Channel have medium to high velocities for a discharge of 850 m^3/s (30,000 ft^3/s). Under current conditions, velocities in the Raft Channel are much lower, not exceeding 0.45 m/s (1.5 ft/s), even for a discharge of 2549 m^3/s (90,000 ft^3/s). At 2549 m^3/s (90,000 ft^3/s), most of the velocities in the inundated area are in the 0.15 to 0.45 m/s (0.5 to 1.5 ft/s) range for current conditions. The only areas of low velocity are found downstream of the islands built as part of Phase I and Phase II of the Pool 8 Islands HREP [island locations shown in (Janvrin et al., [no date])]. Under historic conditions, the natural levees that these island building projects worked to re-create provided the areas of low velocities.

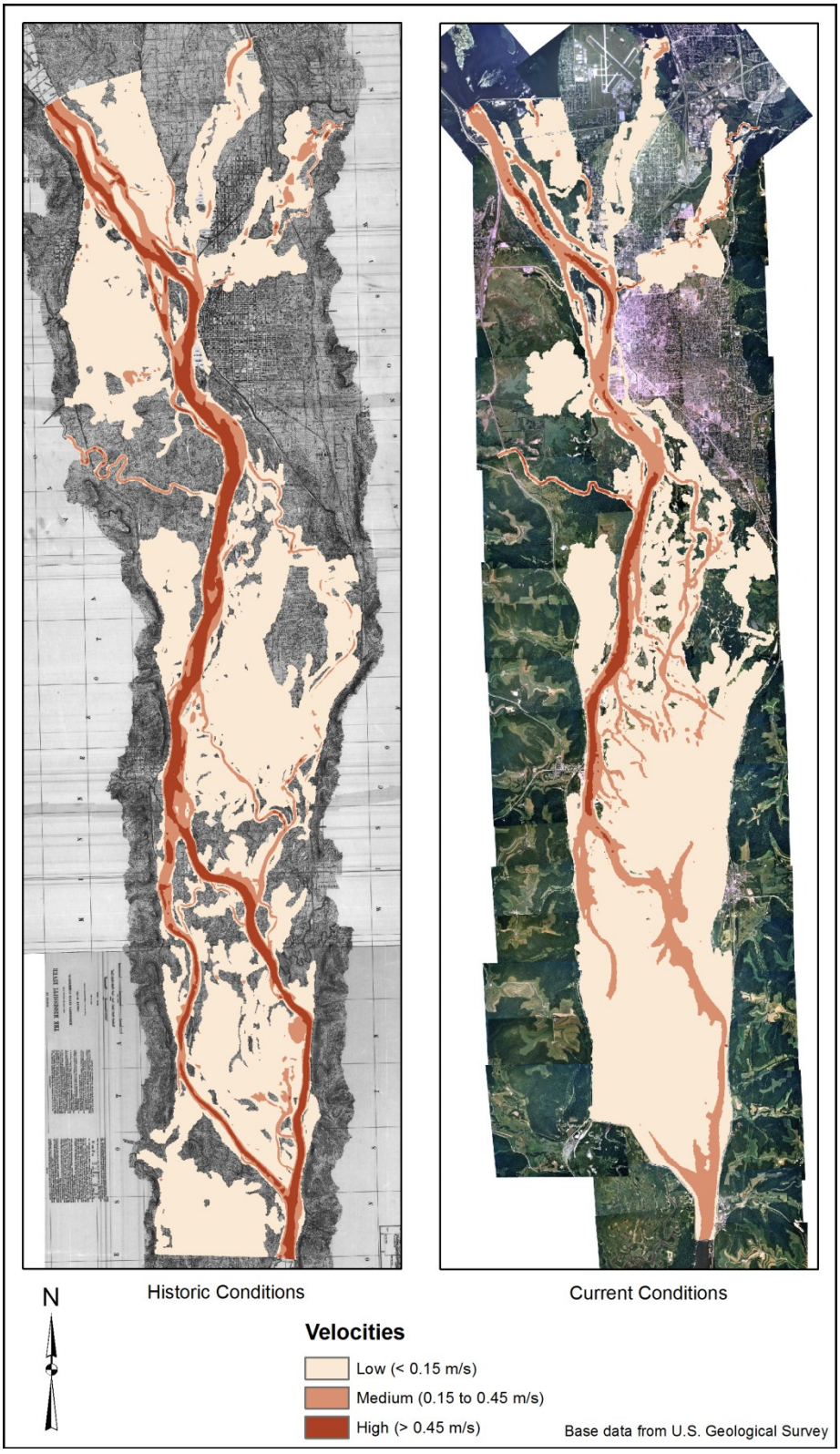

Figure 7.4: Velocity classification of historic and current condition simulations at 850 m^3/s (30,000 ft^3/s) discharge.

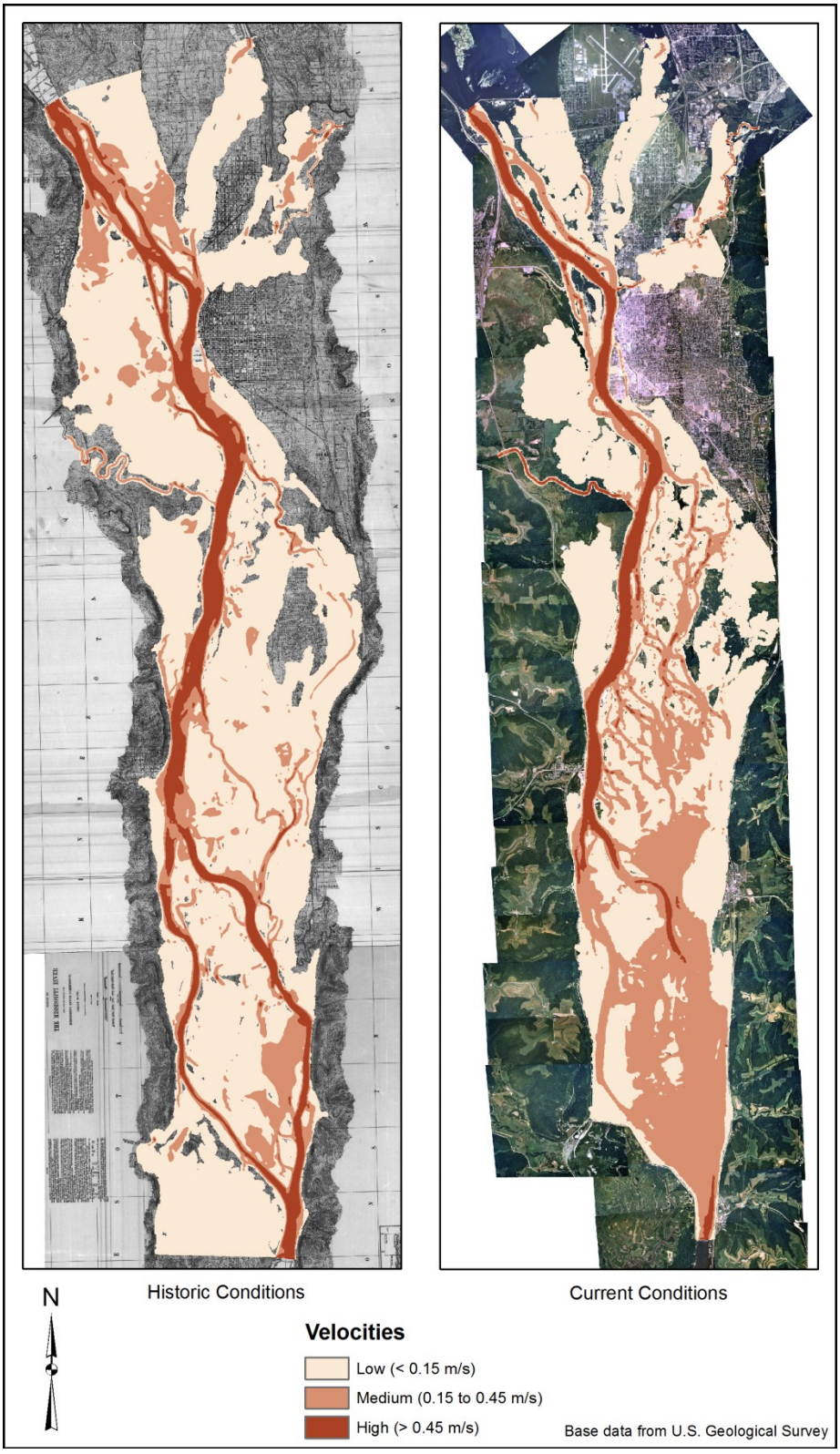

Figure 7.5: Velocity classification of historic and current condition simulations at 1416 m^3/s (50,000 ft^3/s) discharge.

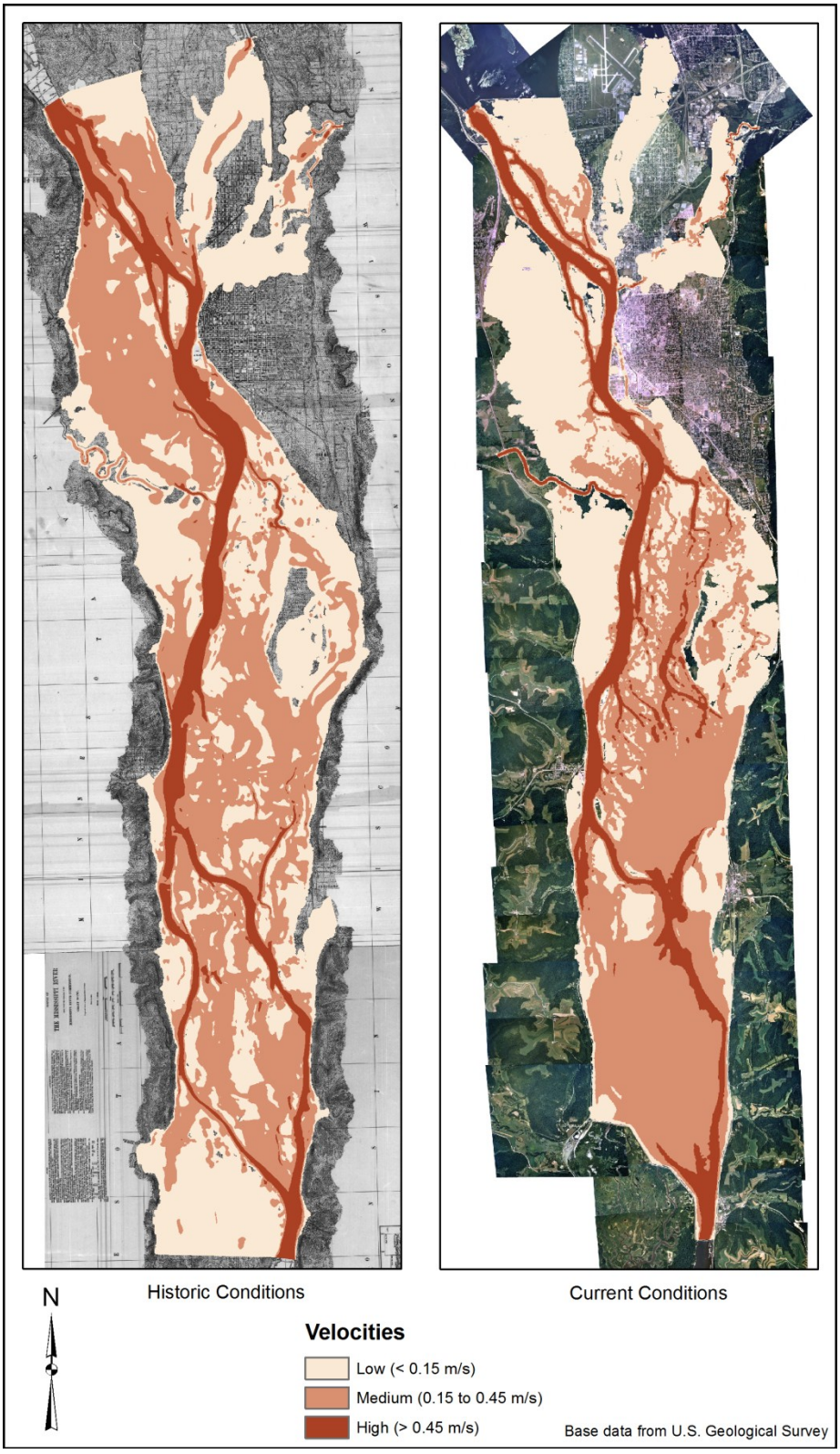

Figure 7.6: Velocity classification of current and historic condition simulations at 2549 m^3/s (90,000 ft^3/s) discharge.

7.3 Velocity Classification by Aquatic Area Methodology

Model results for depth and velocity magnitude were also classified by aquatic area class and compared using histograms. In the CE Study, a modified version of an unpublished method developed by the U.S. Army Corps of Engineer's Waterways Experiment Station was used to classify open water areas into main channel, secondary channel, contiguous backwater, and isolated backwater areas so that an analysis of velocities in each aquatic area could be performed (WEST Consultants, 2000).

For this study, the 1989 Land Cover/Land Use (LCU) shapefile for Pool 8 was used as the basis for the aquatic areas under current hydrodynamic conditions. Table 2-1 in Volume 2 of the CE Study showed how the LTRM classifications in the 1989 LCU data compare to the classifications used in the CE Study (WEST Consultants, 2000). Using Table 2-1 and the 1989 LCU data, a shapefile of main channel, secondary channel, and contiguous backwater areas was created for current conditions.

A shapefile for pre-impoundment conditions was created in a similar fashion using an 1890 LCU shapefile. Land cover classes in the for historic conditions were not as specific as those used for the current condition model due to the data being historic in nature, so more manual editing was performed to get a consistent coverage to compare with current conditions. In general, the main channel was defined as the channel that conveys a majority of the discharge. Secondary channels were defined as having a minimum top width of 50 meters (164 ft) on the map (assumed to be normal flow conditions) with an inlet and exit to the main channel. Contiguous backwaters were defined as having a direct connection to the main channel at normal flows, but a narrower width than secondary channels and/or a lack of a defined flow path with both an inlet and an outlet to the main channel like secondary channels. Minor tributaries (La Crosse and Root River) were not included in the analysis because accurate bed topography data was not available for those areas, so there is more uncertainty in model results. This is consistent with the CE Study analysis, as well.

Areas classified as open water, sand/mud/clay, marsh/swamp, and dike were all used as a basis for the aquatic area classification (reference Table 5.1 for land cover class descriptions) for the historic model. The sand/mud/clay land cover class was used because many of the contiguous backwater areas in the lower part of the pool included this land cover classification for the channel areas. The dike land cover class, in this application, is referring to wing dams and closing dams. Using these land cover classes and manual editing according to the classification criteria defined above, a shapefile containing main channel, secondary channel, and contiguous backwaters was created for historic conditions.

For the CE Study, the pools were also delineated into upper and lower regions based on a qualitative observation that the plan form characteristics of the lower 1/3 of each pool were influenced more by the impoundment from the dams than the upper 2/3 of each pool (WEST Consultants, 2000). A similar division was made to the current condition model domain for this study, and then the historic condition model results were divided at the same location for an equivalent upper-lower pool comparison.

Figure 7.7 through Figure 7.9 are depth and velocity histograms comparing current and historic conditions for main channel, secondary channel, and contiguous backwater areas at 850 m^3/s (30,000 ft^3/s) discharge. This discharge was chosen because it is exceeded 50% of the time for this reach. The histograms were created by calculating the percentage of computational nodes within the given aquatic area class of interest. A percentage of the total nodes in each aquatic area class was calculated rather than using the number of nodes, because the number of nodes in each aquatic area class was different between historic and current conditions. For example, reference Figure 7.7, which shows a much larger open water area for current conditions due to inclusion of the inundated area to the main channel aquatic class. Due to the uniform spacing of the computational nodes throughout the channel and floodplain, it can be assumed for analysis that each node represents the same amount of aquatic area.

The most noticeable difference in both depths and velocities is in the main channels, as illustrated by Figure 7.7. In the upper part of the pool, a shift to higher water depths is observed, most likely due to dredging. Average depths shifted from 2.8 meters (9.2 ft) under historic conditions to 4.6 meters (15 ft) under current conditions. In the lower part of the pool, a high percentage of the depths shifted to the one to three meter (3.3 to 9.8 ft) range, from an average depth of 3.3 meters (10.8 ft). This does not necessarily indicate that deeper areas became shallower due to bed aggradation or lower water levels, but rather it reflects the addition of the inundated floodplain to the main channel aquatic area in the calculations. In the upper part of the pool, the percentage of low velocities increased slightly (lowering average velocities from 0.5 m/s to 0.4 m/s (1.6 ft/s to 1.3 ft/s)), due primarily to the deeper depths in the channel. The percentage of lower velocities in the lower part of the pool increased drastically, however. The average velocity shifted from 0.6 m/s (2.0 ft/s) under historic conditions to 0.1 m/s (0.3 ft/s) under current conditions. An interesting trend in the depth and velocity histogram results for the main channel is observed in Figure 7.7. For both depth and velocity in the upper and lower parts of the pool, the distributions under historic conditions resembled a normal distribution. Under current conditions, the data becomes skewed, especially in the lower part of the pool.

In the secondary channels (Figure 7.8), depths generally increased slightly and velocities decreased in the upper part of the pool. A decrease in depths in the 0.5 to 2 meter (1.6 to 6.6 ft) range, and an increase in depths greater than 4 meters (13.1 ft) was shown by the model. The general plan form characteristics of the secondary channels, as defined for this study, were changed less in the upper part of the pool than the lower part. In the lower part of the pool, most of the secondary channel area was inundated with the construction of the locks and dams, as indicated by the minimal amount of open area shown in the lower part of the pool on Figure 7.8. This makes it difficult to make a definitive conclusion about differences in pre- and post-impoundment hydrodynamic

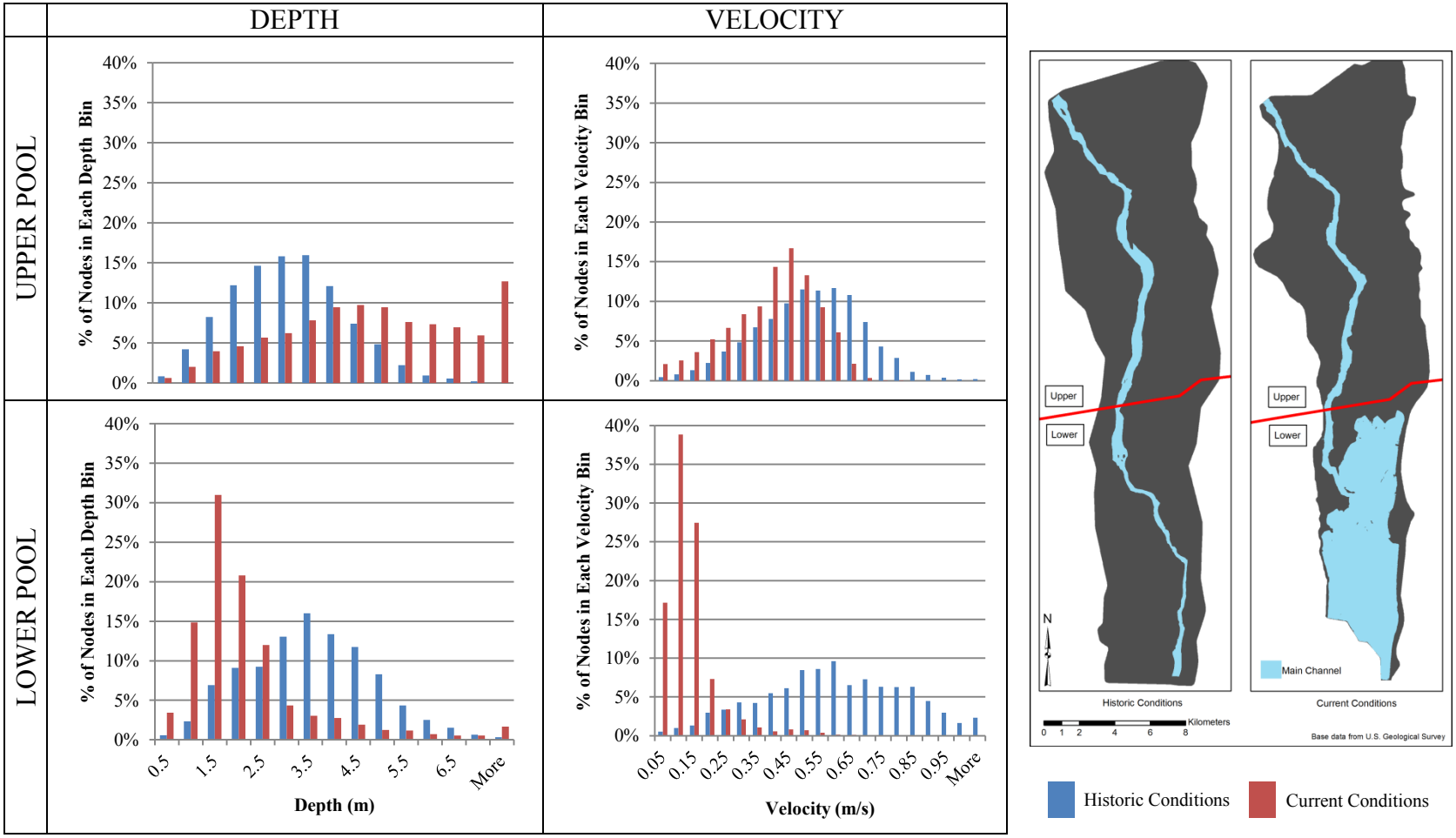

Figure 7.7: Depth and Velocity Histograms Comparing the Upper and Lower Main Channel Areas for Current and Historic Conditions at 850 m^3/s (30,000 ft^3/s) discharge.

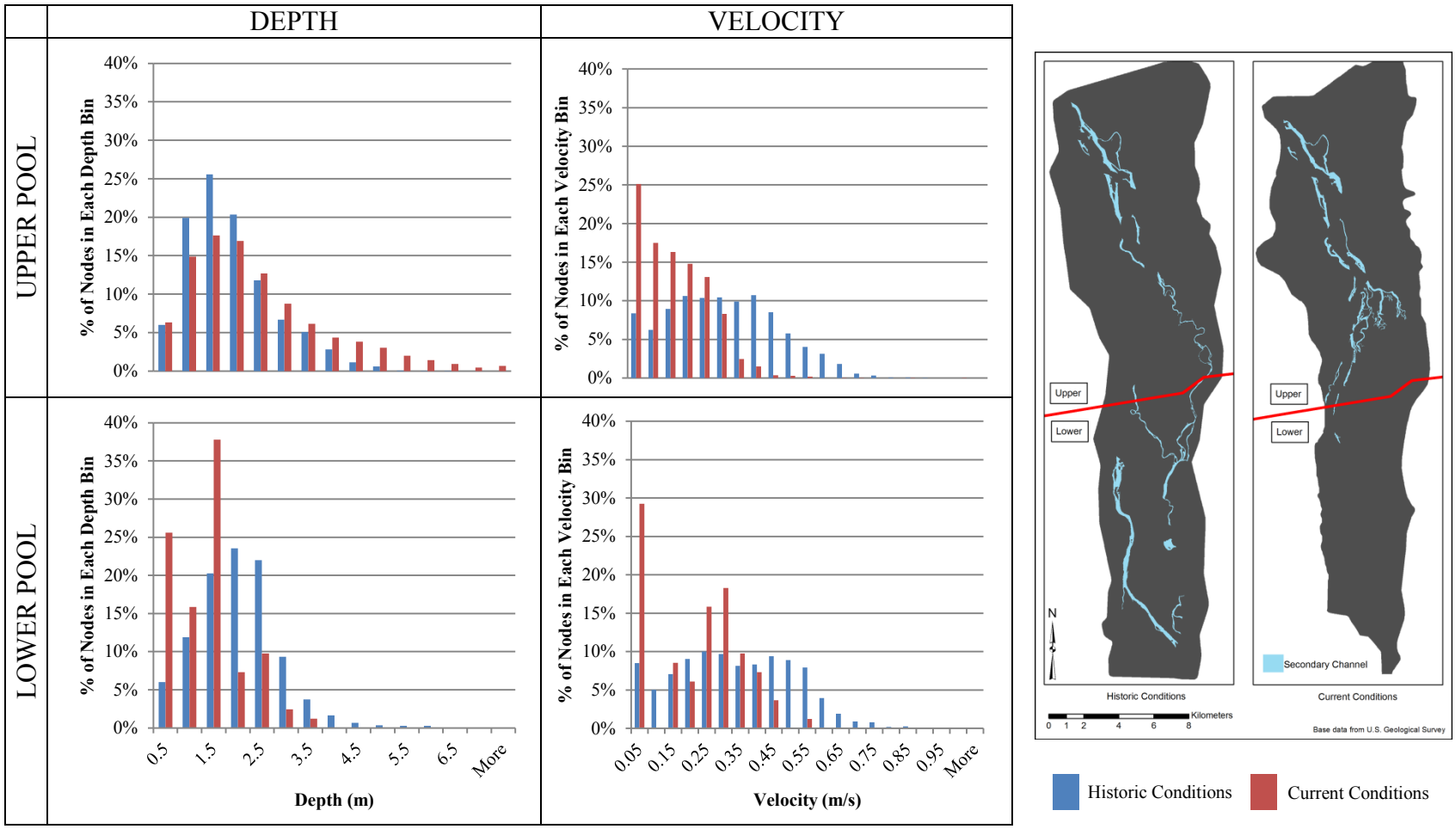

Figure 7.8: Depth and Velocity Histograms Comparing the Upper and Lower Secondary Channel Areas for Current and Historic Conditions at 850 m^3/s (30,000 ft^3/s) discharge.

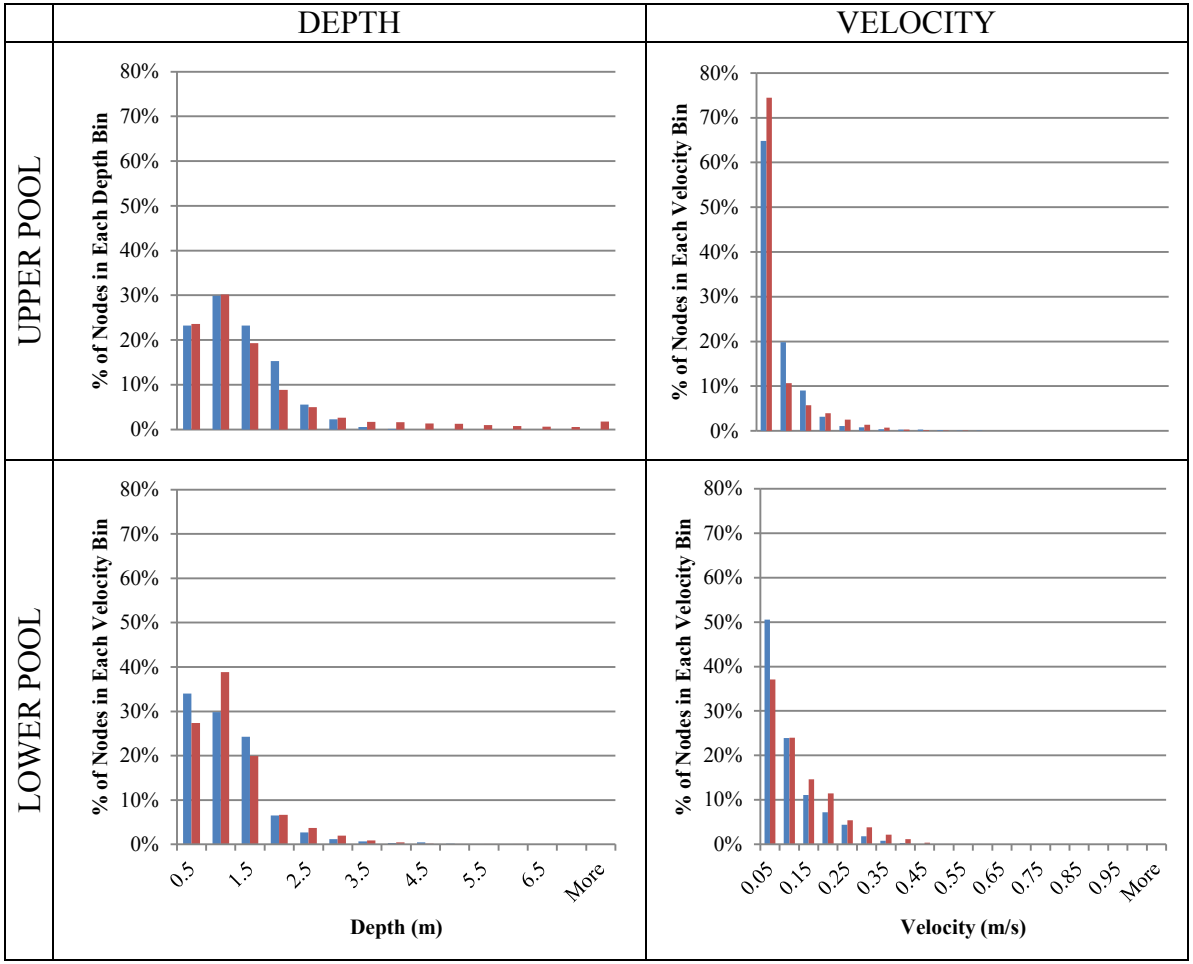

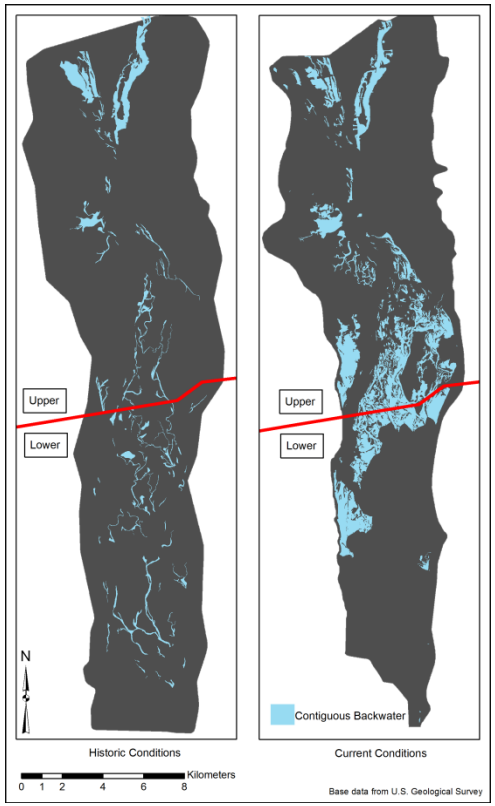

Figure 7.9: Depth and Velocity Histograms Comparing the Upper and Lower Contiguous Backwater Areas for Current and Historic Conditions at 850 m^3/s (30,000 ft^3/s)discharge.

conditions in the lower part of the pool due to a minimal number of computational nodes in secondary channel areas.

Differences between historic and current conditions in contiguous backwater areas were least apparent when compared with the changes seen in the main channel and secondary channel areas. Velocities remained low (most less than 0.25 m/s or 0.82 ft/s) and most depths remained less than 2.5 meters (8.2 ft). Although hydrodynamic conditions have not changed as drastically as other aquatic classes, the location of many of the backwater areas has shifted to being located upstream of the inundated area rather than scattered throughout the floodplain. The added connectivity in the lower part of the pool has permanently connected the old secondary channels to the main channel.

7.4 Sediment Diameter Mobilized and Areas of Incipient Motion

The current condition hydrodynamic model and the historic condition hydrodynamic model were used as tools to better understand what sizes of sediment may be mobilized based on bed shear stress and to identify potential areas of incipient motion for the average sediment size measured in the upper part of Pool 8. Bed shear stress is primarily a function of bed roughness, depth and velocity, as shown in Equations (3.12) and (3.13). It is proportional to depth and Manning's roughness coefficient and inversely proportional to depth, meaning it will be highest in shallow, high velocity areas with high roughness coefficients.

The estimation of sediment diameter mobilized based on Shield's parameter is shown in Figure 7.10 through Figure 7.12. These plots are generated using Equations (7.1) through (7.4). Equation (7.1) was developed by Brownlie (1981) to express Shield's parameter τ_c* in terms of the particle Reynolds number R_{ep}. It is a numerical fitting of the original Shield's curve to get an explicit relationship for Shield's parameter in terms of particle diameter, sediment specific gravity, and the viscosity of water. In Equation (7.2), g is gravitational acceleration, R is the submerged specific gravity of the

sediment, d is the sediment diameter in meters, and ν is the dynamic viscosity of water at 10° C. In Equation (7.3), ρ_s is the density of sediment and ρ is the density of water. In Equation (7.4), τ_{bc} is the critical bed shear stress, γ_s is the specific weight of sediment, and γ is the specific weight of water. The specific gravity of the sediment was assumed to be 2.65, a common assumption for sediment transport.

$$\tau_c^* = 0.22Re_p^{-0.6} + 0.06\exp(-17.77Re_p^{-0.6}) \tag{7.1}$$

$$Re_p = \frac{\sqrt{gRd}d}{\nu} \tag{7.2}$$

$$R = \frac{\rho_s - \rho}{\rho} \tag{7.3}$$

$$\tau_c^* = \frac{\tau_{bc}}{(\gamma_s - \gamma)d} \tag{7.4}$$

A direct calculation of sediment diameter mobilized using bed shear stress was not possible because both Equation (7.1) and (7.4) are functions of diameter. Using Equation (7.1), a range of particle Reynolds numbers and Shields parameter values were calculated for a range of sediment diameters from 0.01mm to 40mm to cover all of the bed shear stress values output by the model. A critical bed shear stress value was then calculated for each diameter of sediment by solving Equation (7.4) using the corresponding Shield's parameter calculated using Equation (7.1). With a sediment diameter and corresponding critical bed shear stress, the sediment diameter can be appended to the model results at each computational node using the lookup function in Microsoft Excel.

When a median sediment size (d_{50}) is assumed and Equation (7.4) is rearranged to solve for bed shear, bed shear can be plotted and the contour plots categorized to show where bed erosion may occur. Figure 5-6 in the 2000 Cumulative Effects Study (WEST, Consultants 2000) shows the d_{50} of bed material for many of the pools in the UMR. If one focuses on just geomorphic reach 3 (Pools 5 through 9), a trend is observed of

decreasing median sediment sizes in the downstream direction. Additionally, sorting within each pool is observed, with smaller median sediments sizes measured at the downstream end of the pools when compared with the upstream end. This makes sense with the slower velocities upstream of the lock and dams. The lighter sediment stays in suspension in the faster velocities immediately downstream of the lock and dams, and settles to the bed as velocities decrease in the inundated area of the lower pool. The d_{50} for the study area was selected to be 0.8 mm. Figure 5-6 shows a d_{50} of approximately 0.4 mm in the lower and middle parts of the pool, but it was decided that the 0.8 mm sediment size is more representative of the pool as a whole, because the upper parts of the pools maintain more of their natural character. In reality, the historic median sediment size is most likely between 0.4 and 0.8 mm because the sediment wouldn't be sorted due to the locks and dams. Figure 7.13 through Figure 7.15 show the plots of where incipient motion is expected to occur for a d_{50} of 0.8 mm when comparing historic conditions with current conditions.

When the plots are examined, it becomes apparent that under historic conditions, larger sediment sizes were likely to be mobilized for all three discharges examined due to the larger bed shear stresses throughout the reach. At higher discharges, higher floodplain roughness due to the large areas of forest, combined with faster velocities, causes higher bed shear stresses, which appear on the plots as areas where larger sediment sizes are mobilized. Under current conditions, the main areas of scour are located in the main channel, with minimal initiation of motion below where the Raft Channel and main channel diverge (reference Figure 7.13).

Examination of dredging records from the U.S. Army Corps of Engineers indicates that most dredging since 1981 has been performed between River Miles 687.5 and 690.8, where Figure 7.10 indicates that sediment sizes in the 1 to 1.5 millimeter range can no longer be mobilized under current conditions at 850 m^3/s (30,000 ft^3/s) (USACE – SP, 2011). This coincides with the general decrease in sediment size

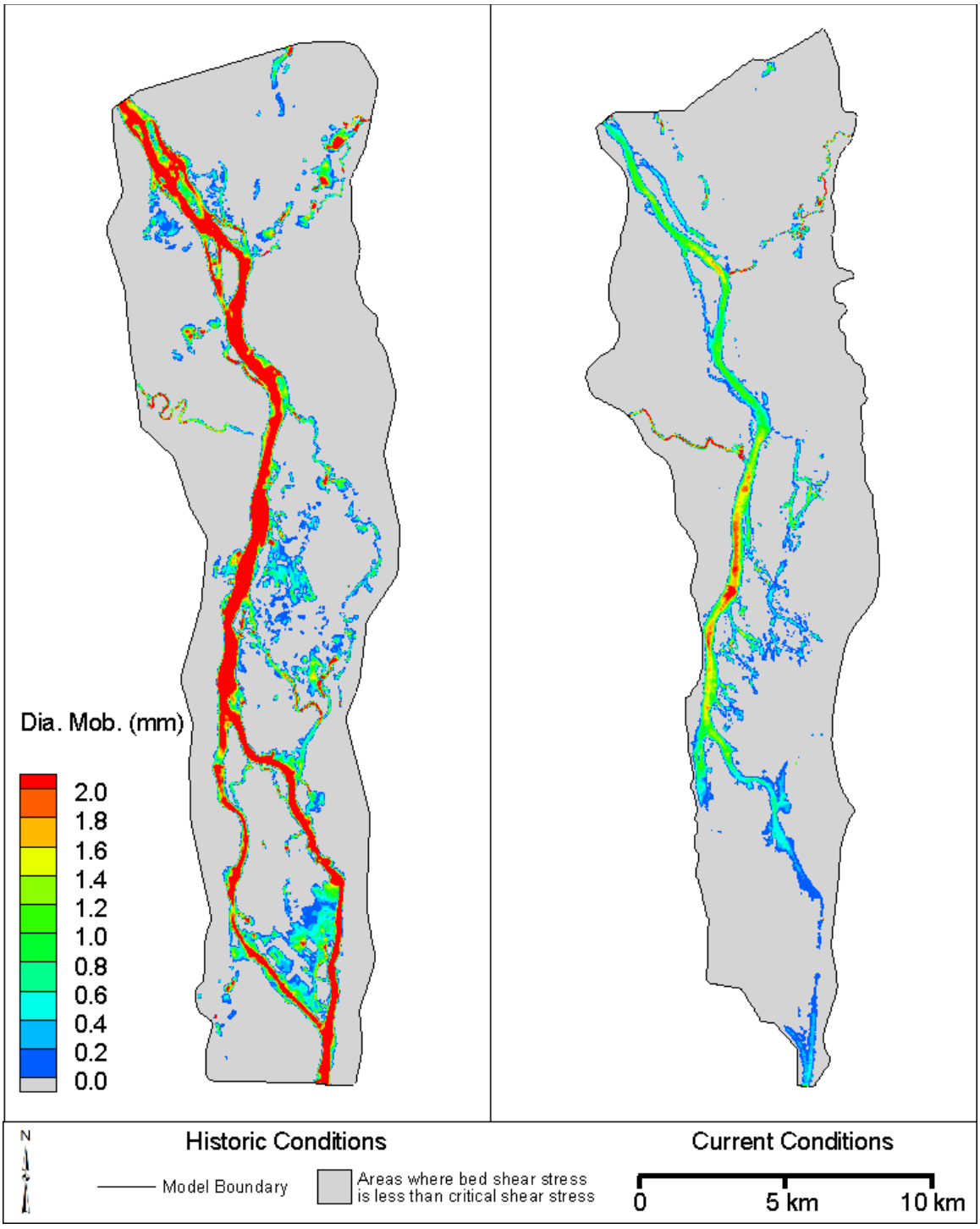

Figure 7.10: Comparison of sediment grain size (in millimeters) mobilized at 850 m^3/s (30,000 ft^3/s) under historic and current conditions. Areas shown in gray are areas with bed shear stresses less than critical shear stress.

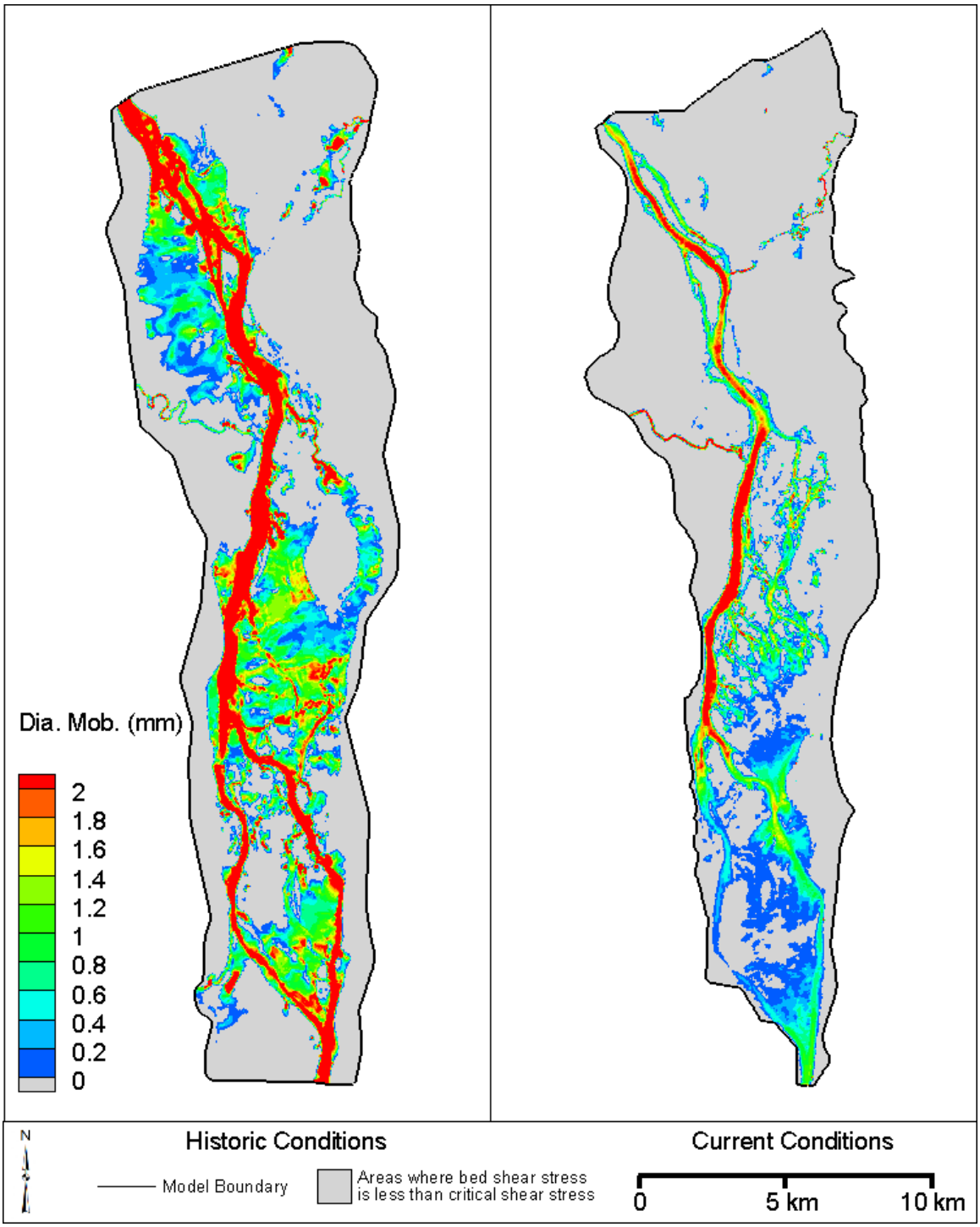

Figure 7.11: Comparison of sediment grain size (in millimeters) mobilized at 1416 m^3/s (50,000 ft^3/s) under historic and current conditions. Areas shown in gray are areas with bed shear stresses less than critical shear stress.

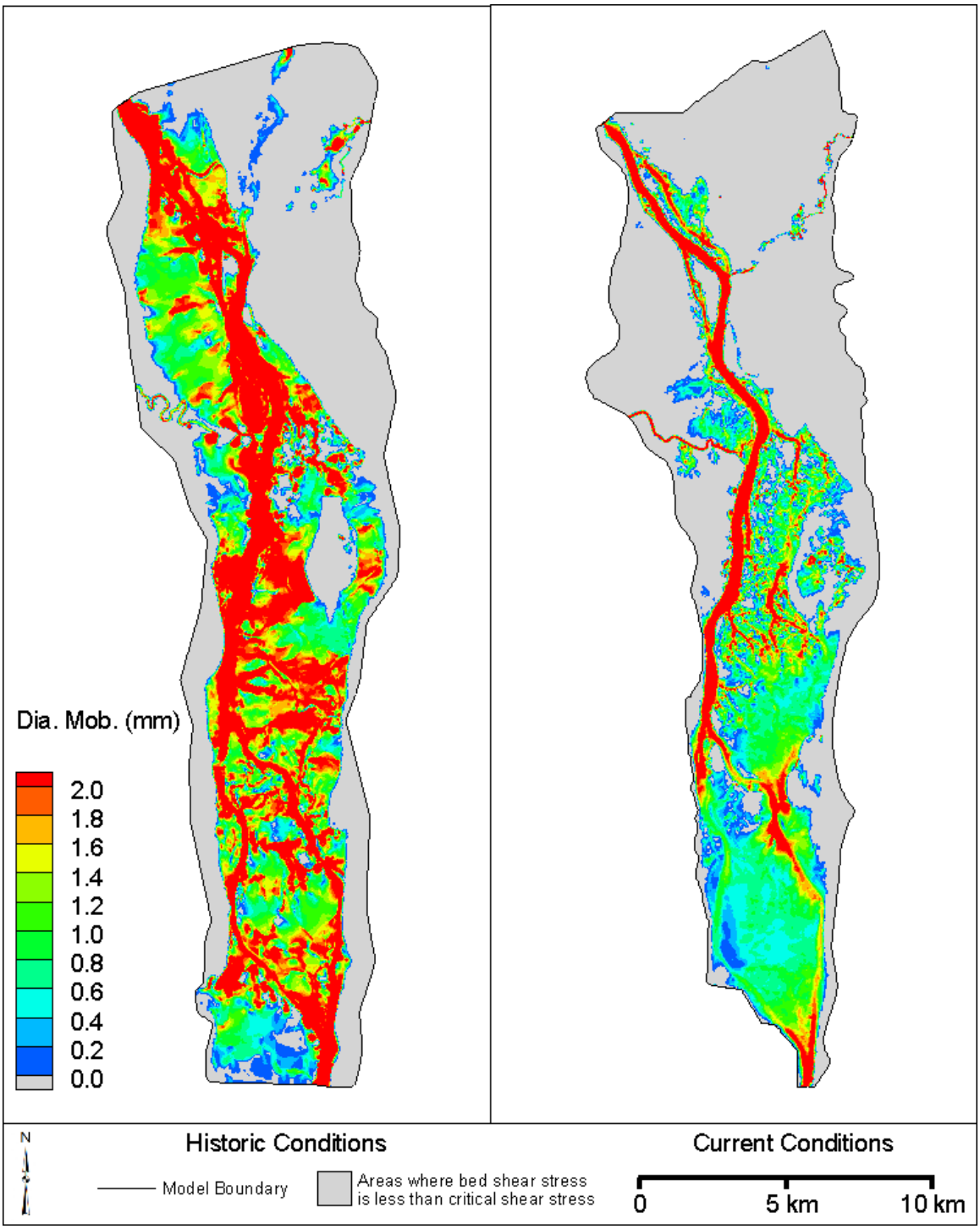

Figure 7.12: Comparison of sediment grain size (in millimeters) mobilized at 2549 m^3/s (90,000 ft^3/s) under historic and current conditions. Areas shown in gray are areas with bed shear stresses less than critical shear stress.

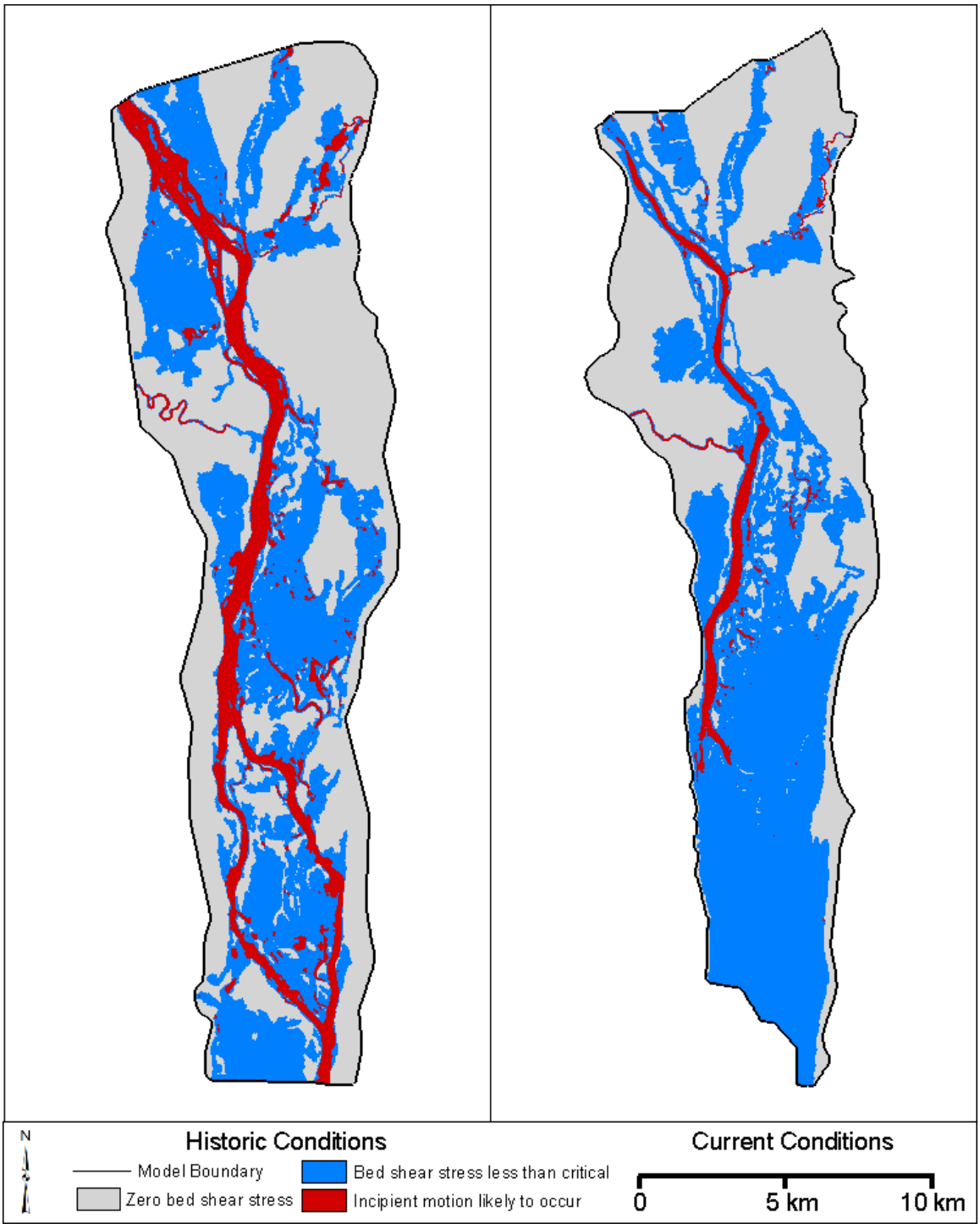

Figure 7.13: Comparison of spatial distribution of critical shear stress at 850 m^3/s (30,000 ft^3/s) under historic and current conditions. Zones shaded in red indicate areas where initiation of incipient motion is likely to occur for sediment sizes less than 0.8mm.

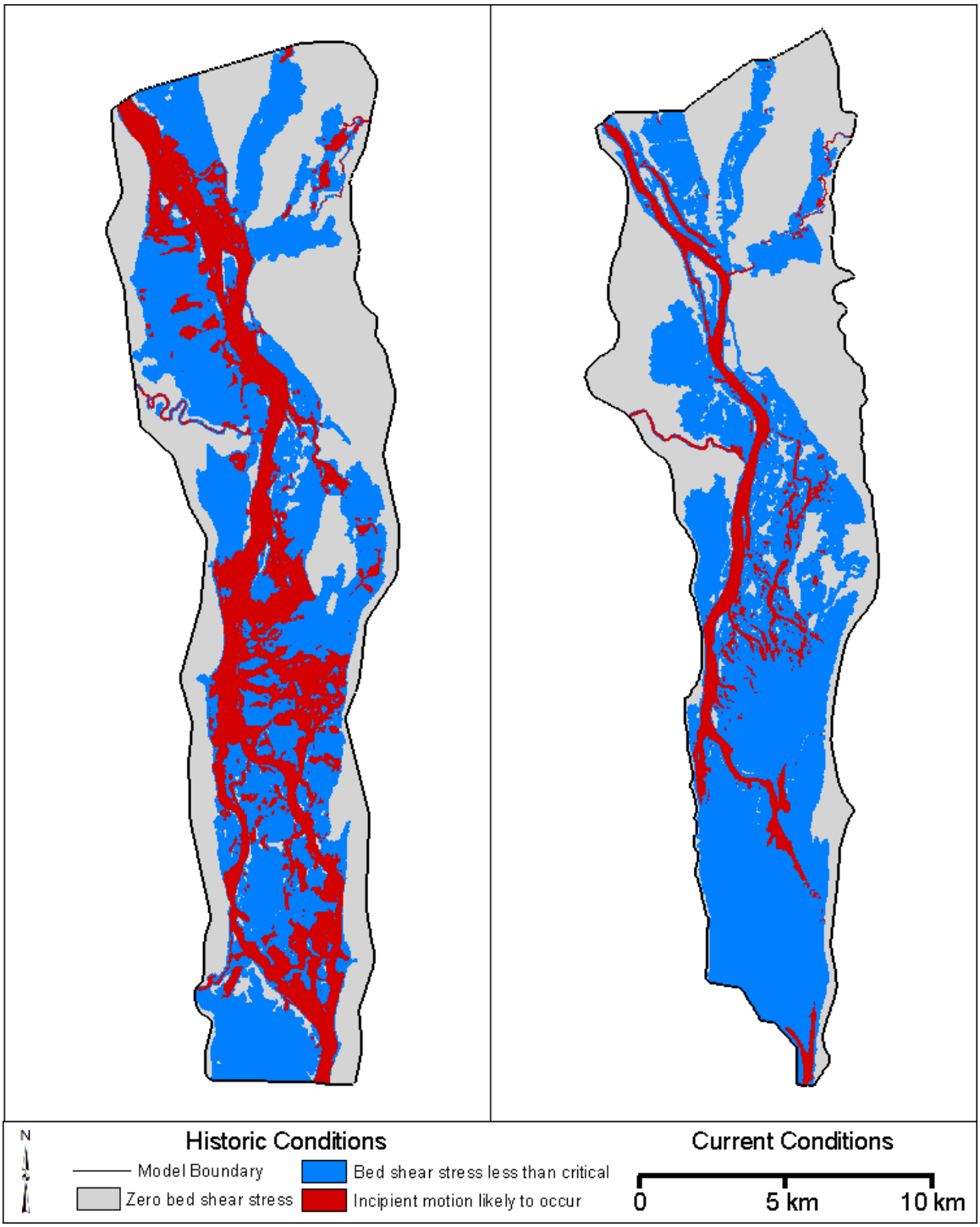

Figure 7.14: Comparison of spatial distribution of critical shear stress at 1416 m^3/s (50,000 ft^3/s) under historic and current conditions. Zones shaded in red indicate areas where initiation of incipient motion is likely to occur for sediment sizes less than 0.8mm.

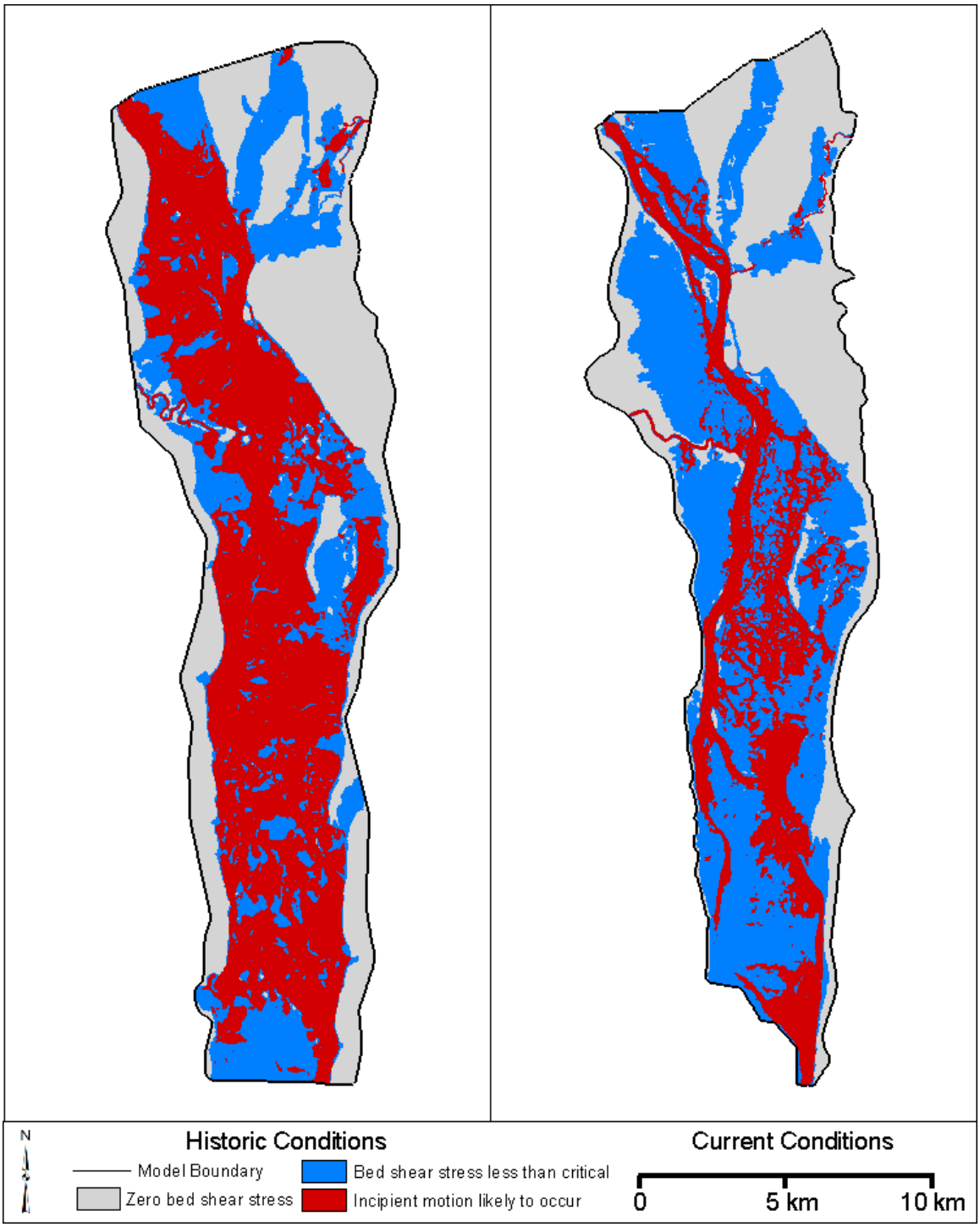

Figure 7.15: Comparison of spatial distribution of critical shear stress at 2549 m^3/s (90,000 ft^3/s) under historic and current conditions. Zones shaded in red indicate areas where initiation of incipient motion is likely to occur for sediment sizes less than 0.8mm.

mobilized in the lower part of the pool (shown in Figure 7.13) due to the lower velocities and higher depths in the inundated area. With additional information about gradation of dredged material, model results could be verified more closely.

It should be noted that many factors affect sediment transport and incipient motion. Armoring of bed sediments, gravitational force acting on particles both in the streamwise direction (longitudinal slope) and on the river banks (lateral slope), velocity fluctuations due to turbulence, and hiding effects due to bed forms or in channel obstructions all can affect sediment transport. However, Shields stress is a generally accepted, physically based relationship between the applied force due to the hydrodynamics of the flow and resisting force due to the weight of the particle. The use of Shields stress as a criteria for incipient motion is meant to demonstrate the effects that hydrodynamics have on sediment dynamics within the UMRS and how differences in pre- and post-impoundment hydrodynamics can affect transport of bed material within Pool 8.

7.5 Description of Suspended Sediment Load

Simulation results from the current and historic condition models were also used to estimate areas where silt particles would stay in suspension based on a comparison of particle settling velocities with uplift due to turbulence in the water column.

Different sediment classification systems define particles sizes of silt differently. For this study, the Subcommittee on Sediment Terminology of the American Geophysical Union recommendation of 0.062mm as the largest size of coarse silt was used (Chang, 2002). WEST Consultants (2000) cites a study by Nakato (1981) stating that 82.8 percent of suspended sediment is finer than this size for sampling performed at Lock and Dam 8.

Using Stokes law, shown in Equation (7.5), the settling velocity of coarse silt was calculated and then used with the model outputs for bed shear to calculate the Rouse number, which is shown in Equation (7.6). The Rouse number describes the shape of the

vertical sediment concentration profile. Smaller sediment sizes or more turbulent flow cause a more uniform concentration profile, indicating more sediment is in suspension. The Rouse number is based off of the assumption that mass flux of sediment in the vertical direction due to diffusion is analogous to the momentum flux due to turbulence. Further, for fine particles, the diffusion coefficient of the sediment is equal to the turbulent diffusion coefficient (Chang, 2002). These assumptions allow the transport mode of silt particles to be estimated.

Equations (7.5) through (7.7) are a function of sediment diameter and density, the properties of water at a given temperature, and the bed shear. Water temperatures in the spring months when sediment runoff is typically high ranged from approximately 5° to 20° Celsius (USACE – SP, 2012c). A temperature of 10° Celsius was chosen for the properties of water in Equation (7.5) and Equation (7.7). In the following equations, w_s is the particle settling velocity, g is the gravitational acceleration, d is the sediment particle diameter in meters, ρ_s is the sediment density, ρ is the density of water, μ is the dynamic viscosity of water, z_* is the Rouse number, κ is the Von Karman constant of 0.41, U_* is the friction (or shear) velocity, and τ_0 is the bed shear stress calculated by SRH-2D.

$$w_s = \frac{gd^2}{18}\frac{(\rho_s - \rho)}{\mu} \tag{7.5}$$

$$z_* = \frac{w_s}{\kappa U_*} \tag{7.6}$$

$$U_* = \sqrt{\frac{\tau_0}{\rho}} \tag{7.7}$$

The Rouse number is a continuum, meaning there is no definite cutoff point for different modes of transport, but general guidelines are available to allow for spatial comparisons between historic and current conditions. Three modes of sediment transport

were defined by the Rouse number range: primarily wash load (less than 0.8), primarily suspended load (0.8 to 1.2), and mixed suspended and bed load (1.2 to 2.5) (Whipple, 2004). At some point above 2.5 is when critical bed shear becomes a factor and sediment transitions from bed load to no longer being mobilized. An analysis similar to the one presented in Section 0could be performed for silt particles to more specifically determine when initiation of incipient motion occurs. A different relationship for τ_c*, which is applicable for non-cohesive silt size particles, would be necessary (ASCE, 2008).

Figure 7.16 through Figure 7.18 show the results of the Rouse number calculations. In general, the historic condition model showed more areas of wash load throughout the domain at all discharges examined. The difference between historic and current conditions is most apparent at 850 m^3/s (exceeded 50% of the time). Under current conditions, results show a significantly larger area of suspended and mixed load transport in the lower part of the pool than under historic conditions. This is due to both the decrease in velocities and increase in depths for the main channel areas (shown in Figure 7.7) under current conditions.

Differences between historic and current conditions become less apparent at higher discharges. At 1416 m^3/s (exceed about 25% of the time), areas of minimal sediment suspension are still apparent under historic conditions downstream from where the Raft Channel and main channel diverge. Under current conditions, the only areas in the same reach with minimal suspension of sediment are downstream of the island building projects. At 2549 m^3/s (exceeded 5% of the time) under current conditions, areas of suspended and mixed load are confined to backwater areas and minimal under historic conditions.

It's important to note that these results do not describe the potential for re-suspension of sediment, a problem created in the inundated areas of the navigation pools because sediments deposited during flood events are no longer able to naturally dry out and consolidate. Rather, they show the transport mode of sediment already in

suspension, which can indicate where sediment is more likely to deposit. The most important observation can be made from Figure 7.16: that for average flow conditions, more coarse silt is being transported as suspended and mixed load under current conditions than was under historic conditions. This means that sediment is more likely to fall out of suspension rather than being transported downstream.

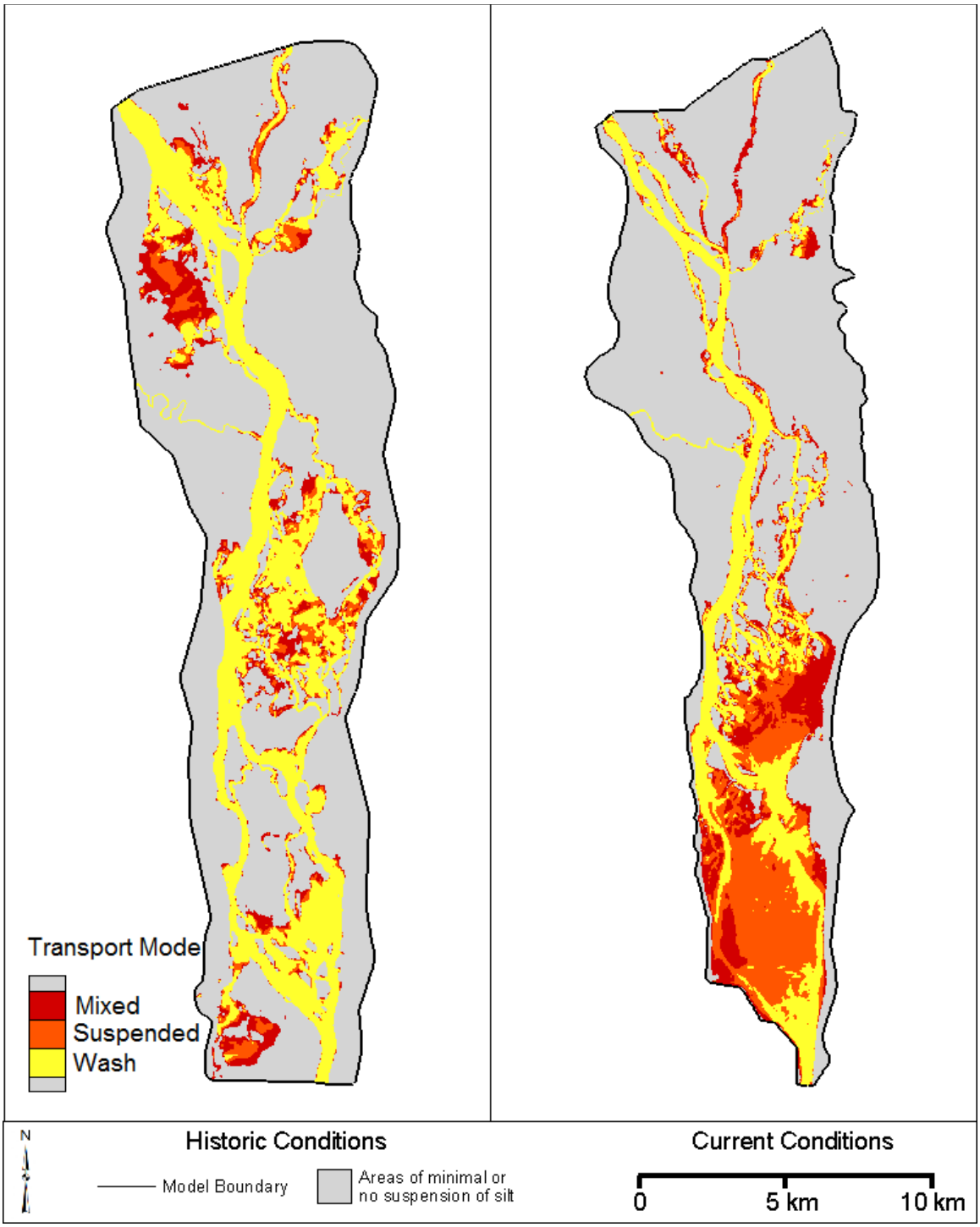

Figure 7.16: Comparison of Rouse numbers for silt particles at 850 m^3/s (30,000 ft^3/s) under historic and current conditions. Areas in yellow indicate mainly wash load, areas in orange indicate primarily suspended load, and areas in red indicate mixed suspended and bed load. Areas shown in gray are areas with no inundation or minimal suspension of silt.

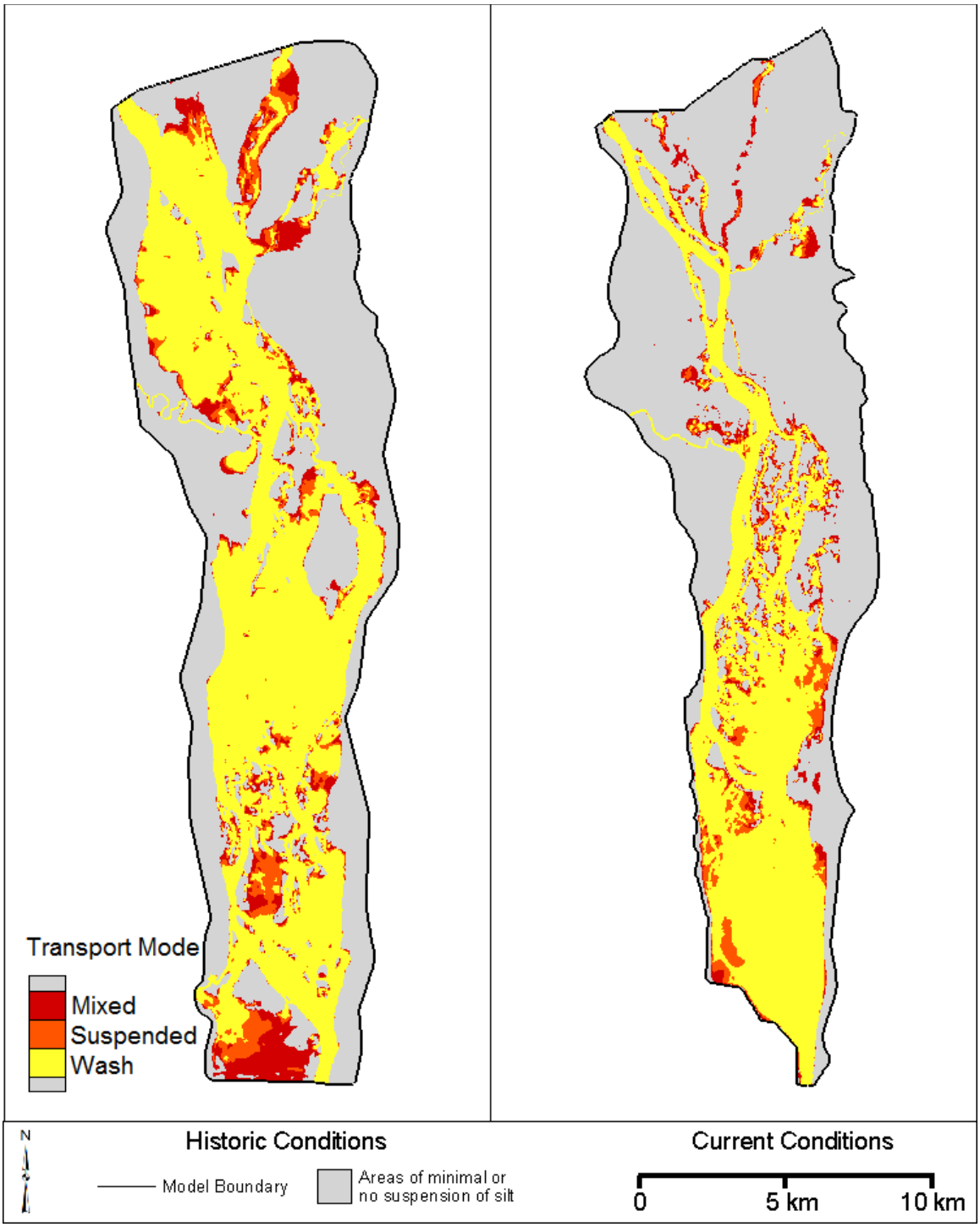

Figure 7.17: Comparison of Rouse numbers for silt particles at 1416 m^3/s (50,000 ft^3/s) under historic and current conditions. Areas in yellow indicate mainly wash load, areas in orange indicate primarily suspended load, and areas in red indicate mixed suspended and bed load. Areas shown in gray are areas with no inundation or minimal suspension of silt.

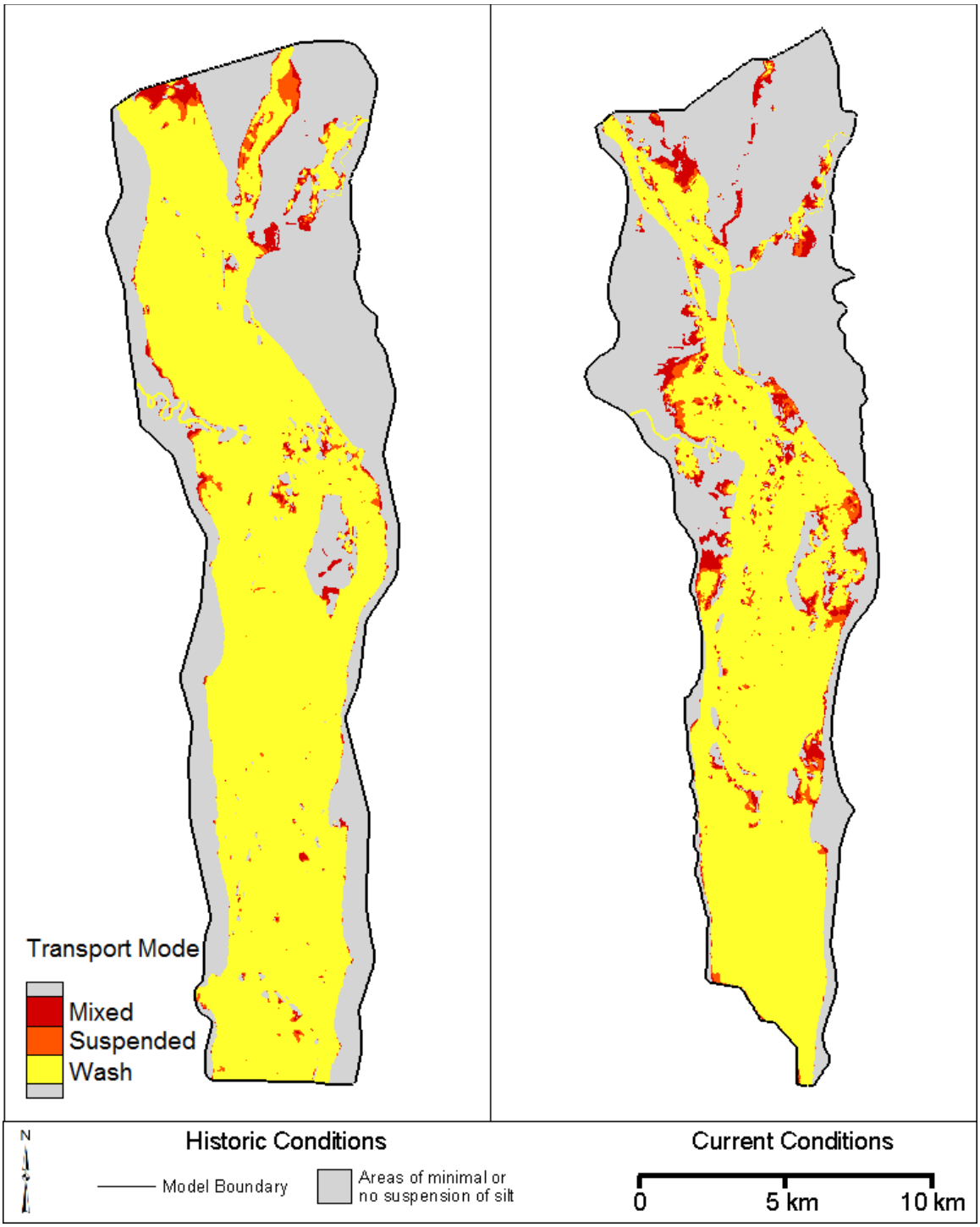

Figure 7.18: Comparison of Rouse numbers for silt particles at 2549m^3/s (90,000 ft^3/s) under historic and current conditions. Areas in yellow indicate mainly wash load, areas in orange indicate primarily suspended load, and areas in red indicate mixed suspended and bed load. Areas shown in gray are areas with no inundation or minimal suspension of silt.

CHAPTER 8: SUMMARY AND CONCLUSIONS

The Upper Mississippi River is an important resource, both as a diverse ecosystem and as an important navigation corridor. The modification of the river for navigation dates back to the early 1800s, when federally funded snag removal and dredging activities began. In the mid to late 1800s, permanent changes to the river began, with the construction of hundreds of wing dams and closing structures, intended to concentrate the river at low flows and scour the navigation channel. The most drastic changes to the river occurred during the 1930s, when the locks and dams inundated vast areas of the floodplain.

River managers acknowledge that hydrology and hydraulics are important drivers for many biological processes, and thus rehabilitation of river to support native species must recreate or preserve these physical processes. Additionally, establishment of reference conditions is an import part of the adaptive management processes. River managers have recognized that a quantitative analysis of restoration project alternatives can improve project effectiveness.

There are a few different major classes of hydrodynamic models, namely one-, two-, and three-dimensional models. Due to the highly braided characteristics of the Upper Mississippi River, a two-dimensional model hydrodynamic model was used for this study to assess the complex interactions between the main channel, side channels, and floodplain. The two dimensional model allows for spatial analysis of depths and velocities across the different habitat types found in the river corridor.

It can sometimes be difficult to ‘go back in time’ and analyze past systems. As this study demonstrated, past data can be conflicting and the methods used to gather or present that data uncertain. However, this information can be a valuable resource when proper care is taken to compare all available information. For this study, a historic map plotted in the 1890s and water surface elevations from three different sources provided

the information needed to create a two-dimensional hydrodynamic model of the Mississippi River in the area that is now Pool 8, near La Crosse, Wisconsin. The map is a valuable, pre-impoundment representation of the river channel and floodplain. It included contours and depth soundings, allowing for the generation of a raster digital elevation model (DEM) which became the elevation source for the hydrodynamic model. The water surface profiles provided an estimate of past flow events to compare to model results and assist with calibration of roughness values. Roughness values were adjusted until water surface slopes matched well through a range of discharges, and model sensitivity to bed roughness at higher discharges was examined. The model was relatively insensitive to roughness values at high discharges, as shown by the parallel slopes of the profiles for a given discharge in Figure 5.10. It was determined that the model was not sensitive to minor changes in bed topography through the process of adjusting main channel depths around wing dam areas and secondary channel depths. The calibration and sensitivity analysis provide a good understanding of how the model reacts to changes and generate confidence that the model represents the reference data well.

With the calibrated model completed, five of comparisons were made with a model of similar scope for current impounded conditions in Pool 8. A range of discharges from 283 m^3/s to 2832 m^3/s (10,000 ft^3/s to 100,000 ft^3/s) was simulated using both models and select discharges (850 m^3/s, 1416 m^3/s, and 2549 m^3/s) (30,000 ft^3/s, 50,000 ft^3/s, and 90,000 ft^3/s) were analyzed more in depth.

The discharge distribution comparison showed that the upper and middle parts of the study reach maintained much of their pre-impoundment character in terms of discharge distribution, with side channels conveying more of the discharge under current conditions due to higher connectivity in the inundated area. In the lower part of the pool, the comparison showed that a once dynamic interaction between the main channel,

secondary channel, and floodplain areas has been reduced to a constant distribution of discharge due to the near constant water levels for the range of discharges modeled.

The velocities from both the historic and current condition models were also compared spatially by classifying model outputs into three velocity classes. Those classes: low (less than 0.15 m/s (0.5 ft/s)), medium (0.15 to 0.45 m/s (0.5 to 1.5 ft/s)), and high (greater than 0.45 m/s (1.5 ft/s)) were chosen based on biological significance. The most significant difference is in the lower part of the pool. At 850 m^3/s (30,000 ft^3/s, exceeded 50% of the time), velocities in the Raft Channel fall into the medium to high range under historic conditions, while under current conditions they are much lower. Velocities don't exceed 0.45 m/s (1.5 ft/s), even for a discharge of 2549 m^3/s (90,000 ft^3/s). Also, at 2549 m^3/s (90,000 ft^3/s), most velocities are in the 0.15 to 0.45 m/s (0.5 to 1.5 ft/s) range under current conditions. The only areas of low velocities are found downstream of the restored islands near Stoddard, WI and at the head of the Raft Channel.

Using aquatic area classifications described in the same study, depths and velocities were further classified by main channel, secondary channel, and contiguous backwater areas for a discharge of 850 m^3/s (30,000 ft^3/s). The largest change in velocities and depths from historic to current conditions was observed in the main channel areas. In the upper part of the pool, a shift to deeper depths and slower velocities is observed, due primarily to dredging. In the lower part of the pool, average depths and velocities decreased significantly in main channel areas, which is due to the inundation upstream of the dam. The distribution of depths and velocities resembled a normal distribution under historic conditions but is skewed to the lower depths and velocities under current conditions. In secondary channels, a similar skew to lower velocities is observed in the upper part of the pool under current conditions. This is due to the difference in conveyance through the side channels. More conveyance in the major side channels under historic conditions caused higher velocities in those areas. In contiguous

backwater areas, the depth and velocity distributions were relatively similar. The difference between historic and current conditions is the location of the contiguous backwaters however. Under historic conditions, the backwater areas were spread out throughout the floodplain. In the lower part of the pool, many of those backwaters are permanently inundated and now the backwater areas are on the upstream end of the inundated area.

Using Shield's critical shear stress criteria, sediment size mobilized and areas where initiation of incipient motion is likely to occur were calculated using model results for bed shear stress. In general, larger sediment sizes could have been mobilized at a given discharge under historic conditions due to higher bed shear stresses. Minimal initiation of motion for coarse sand is indicated below the head of the Raft Channel at 850 m^3/s (30,000 ft^3/s). This reduction in shear stress entering the lower part of the pool coincides with the recorded dredging performed by the U.S. Army Corps of Engineers at the head of the Raft Channel and upstream to near Brownsville, MN (USACE – SP, 2011). The same analysis could be performed on other grain sizes of interest if more extensive sieve analysis of bed material composition is performed.

Finally, a comparison of spatial distribution of suspended sediment was presented. Using the Rouse number, which balances particle settling velocity with vertical velocities in the water column, a spatial distribution of sediment transport mode was modeled. The models show that coarse silt will be primarily in suspension for all of the ranges of the historic condition results presented. For the current conditions, at 850 m^3/s (30,000 ft^3/s), much of the inundated area in the lower parts of the pool shows a mixed mode of transport, and other areas show primarily bed load. As discharge increases, much of the silt becomes suspended.

One possibility for future work with the hydrodynamic model is further refinement of the DEM used as the elevation source. This study made use of the best methods currently available to digitize the floodplain and channel topography. However,

research has indicated that elliptical inverse distance weighting, anisotropic kriging, and TopoGrid have potential for use as interpolation schemes in a flow oriented coordinate system (Merwade, Maidment and Goff, 2006). It was beyond the scope of this study to develop a custom interpolation tool utilizing these schemes.

Additional future work could include applying both models to investigate the ability of different island layouts or water levels at Lock and Dam 8 to recreate the historic conditions for low velocity wake areas in the lower part of the pools. The models could also be used to investigate how these islands could help disconnect the floodplain from the main channel at average discharges, thus restoring the more dynamic interactions between the floodplain and channel areas observed by analyzing the discharge distribution in the lower part of the pool.

The model could also be applied to determine the value of the aquatic habitat to plant and animal species using habitat suitability metrics. If certain depths or velocities are known to be beneficial for a species of interest, current conditions can be compared to historic conditions within the pool to determine if and where those conditions were present.

BIBLIOGRAPHY

Anderson, J. D., Jr. *Computational Fluid Dynamics.* New York, NY: McGraw-Hill, Inc., 1995.

Anfinson, J. O. *The River We Have Wrought.* Minneapolis, MN: University of Minnesota Press, 2003.

Aquaveo. *SMS: 2D Mesh Files (*.2dm).* October 12, 2009. http://www.xmswiki.com/xms/SMS:2D_Mesh_Files_%28*.2dm%29 (accessed 2012).

ASCE. *ASCE Manuals and Reports on Engineering Practice: Sedimentation Engineering: Processes, Management, Modeling, and Practice.* Reston, VA: American Society of Civil Engineers, 2008.

Bates, P. D., and A.P.J. De Roo. "A simple raster-based model for flood inundation simulation." *Journal of Hydrology*, 2000: 54-77.

Bhowmik, N. G., and J. R. Adams. "Successional changes in habitat caused by sedimentation in navigation pools." *Hydrobiologia*, 1989: 17-27.

Brownlie, W. R. "Prediction of Flow Depth and Sediment Discharge in Open Channels." Rept. No. KH-R-43A, W.M. Keck Laboratory of Hydraulics and Water Resources, California Institute of Technology, Pasadena, CA, 1981.

Chang, H. H. *Fluvial Processes in River Engineering.* Malabar, FL: Krieger Publishing Company, 2002.

Chen, Y. H., and D. B. Simons. "Hydrology, hydraulics, and geomorphology of the Upper Mississippi River System." *Hydrobiologia*, 1986: 5-20.

Cunge, J. A., F. M. Holly, and A. Verwey. *Practical Aspects of Computational River Hydraulics.* London: Pitman Publishing Limited, 1980.

ESRI. *Applying a spline interpolation.* May 2, 2007. http://webhelp.esri.com/arcgisdesktop/9.2/index.cfm?TopicName=Applying_a_spline_interpolation (accessed 2012).

—. *ArcGIS.* [no date]. http://www.esri.com/software/arcgis (accessed 2011 - 2012).

—. *Mosaic to New Raster (Data Management).* November 29, 2010. http://webhelp.esri.com/arcgisdesktop/9.2/index.cfm?TopicName=Mosaic_To_New_Raster_%28Data_Management%29 (accessed 2012).

—. *Topo To Raster (3D Analyst).* February 9, 2011. http://webhelp.esri.com/arcgisdesktop/9.3/index.cfm?id=1243&pid=1237&topicname=Topo_To_Raster_%283D_Analyst%29 (accessed 2012).

—. *Using Topo to Raster in 3D Analyst.* January 23, 2009. http://webhelp.esri.com/arcgisdesktop/9.3/index.cfm?TopicName=Using%20topo%20to%20raster%20in%203d%20analyst (accessed 2012).

Fischer, J. R., and T. O. Claflin. "Declines in aquatic vegetation in navigation pool No. 8, upper Mississippi River between 1975 and 1991." *Regulated Rivers: Research & Management, Vol 11*, 1995: 157-165.

Galat, D. L., et al. *Environmental Science Panel Report: Establishing System-wide Goals and Objectives for the Upper Mississippi River System.* U.S. Army Corps of Engineers, Rock Island, St. Louis, and St. Paul Districts, 2007.

Gore, J. A., and F. D. Shields. "Can Large Rivers Be Restored?" *Bioscience*, 1995: 142-152.

Hendrickson, J. “Island Consruction – Rebuilding Natural Levees to Restore Connectivity in the Northern Reaches of the Upper Mississippi River.” 2nd Joint Federal Interagency Conference, Las Vegas, NV, 2010.

Hendrickson, J. S., and M. Hrdlicka. *Sediment transport monitoring for the Pool 8 water level drawdown.* Internal Report, St. Paul, MN: U.S. Army Corps of Engineers - St. Paul District, 2003.

Hutchinson, M. F. "A New Procedure for Gridding Elevation and Stream Line Data with Automatic Removal of Spurious Pits." *Journal of Hydrology*, 1989: 211-232.

Huwaldt, J. A. *Plot Digitizer.* October 13, 2012. http://plotdigitizer.sourceforge.net/ (accessed November 9, 2012).

Janvrin, J. “Personal Correspondence.” La Crosse, WI: Wisconsin Department of Natural Resources, 2011 - 2012.

Janvrin, J. A., J. Hendrickson, G. Palesh, R. Benjamin, and J. Nissen. *Upper Mississippi River Environmental Management Program Habitat Rehabilitation and Enhancement Projects: Restoration of the Ecoysystem One Project at a Time*. Unpublished Report, La Crosse, WI: Wisconsin Department of Natural Resources, [no date].

Lai, Y. G. "Two-Dimensional Depth-Averaged Flow Modeling with an Unstructured Hybrid Mesh." *Journal of Hydraulic Engineering*, 2010: 12-23.

Landwehr, K. “Personal Correspondence.” St. Paul, MN: U.S. Army Corps of Engineers - St. Paul District, 2012.

LizardTech. *About Us.* [no date]. http://www.lizardtech.com/about-us/ (accessed November 9, 2012).

Los Alamos National Laboratory. *1996 R&D 100 Awards Entry Summaries.* [no date]. http://www.lanl.gov/rd100/summaries/96_execsum.shtml#mrsid (accessed November 9, 2012).

Merwade, V. M., D. R. Maidment, and J. A. Goff. "Anisotropic considerations while interpolating river channel bathymetry." *Journal of Hydrology*, 2006: 731-741.

Merwade, V., A. Cook, and J. Coonrod. "GIS techniques for creating river terrain models for hydrodynamic modeling and flood inundation mapping." *Environmental Modeling & Software*, 2008: 1300-1311.

Nakato, T. *A review of sediment-transport studies of the GREAT-I and GREAT-II reaches of the Upper Mississippi River.* IIHR Limited Distribution Report No. 89, Iowa City, IA: Iowa Institute of Hydraulic Research, The University of Iowa, 1981.

Nestler, J. M., C. H. Theiling, K. S. Lubinski, and D. L. Smith. "Reference Condition Approach to Restoration Planning." *River Research and Applications*, 2010: 1199-1219.

Opperman, J. J., R. Luster, B. A. McKenney, M. Roberts, and A. W. Meadows. "Ecologically Functional Floodplains: Connectivity, Flow Regime, and Scale." *Journal of the American Water Resources Association*, 2010: 1-16.

Schubert, M. A. "Computational fluid dynamics applications for nitrate removal in an upper Mississippi River backwater." *MS Thesis.* Iowa City, IA: The University of Iowa, 2009.

Schnoebelen, D. J. “Personal Correspondence.” Iowa City, IA: The University of Iowa, 2011 - 2012.

Smith, T. J. "Simulation of Spatial and Temporal Trends in Hydrodynamic Conditions of Upper Mississippi River Pool 8." *MS Thesis.* Iowa City, IA: The University of Iowa, 2011.

SoftSoft Ltd. *SoftSoft.net: WinTopo Raster to Vector Converter.* [no date]. http://www.wintopo.com/ (accessed February 24, 2012).

—. *Vectorisation.* 2012. http://wintopo.com/help/html/vectorise.htm (accessed July 12, 2012).

Theiling, C. H. "Habitat rehabilitation on the Upper Mississippi River." *Regulated Rivers: Research & Management*, 1995: 227-238.

Theiling, C. H., and J. M. Nestler. "River stage response to alteration of Upper Mississippi River channels, floodplains, and watersheds." *Hydrobiologia*, 2010: 17-47.

Tockner, K, and J. A. Stanford. "Riverine flood plains: present state and future trends." *Environmental Conservation*, 2002: 308-330.

Toombes, L., and H. Chanson. "Numerical Limitations of Hydraulic Models." *34th IAHR World Congress - Balance and Uncertainty.* Brisbane, Australia: Engineers Australia, 2011. 2322-2329.

U.S. Army Corps of Engineers (USACE). *1912 and 1929 Adjustments of the US Level Net.* January 26, 1934. http://www.mvp-wc.usace.army.mil/projects/general/level_net.html (accessed 2011-2012).

U.S. Army Corps of Engineers - Army Geospatial Center (USACE - AGC). *Corpscon Version 6.0.* [no date]. http://www.agc.army.mil/corpscon/ (accessed 2011).

U.S. Army Corps of Engineers - Rock Island District (USACE - RI). *Upper Mississippi River System Ecosystem Restoration Objectives 2009.* Working Document, Rock Island, IL: U.S. Army Corps of Engineers - Rock Island District, 2011.

U.S. Army Corps of Engineers - St. Paul District (USACE - SP). *Habitat Restoration: Mississippi River, Pool 8 Islands Phase III, Wisconsin/Minnesota.* September 7, 2012a. http://www.mvp.usace.army.mil/environment/default.asp?pageid=80 (accessed November 3, 2012).

—. "Mississippi River Centerline - Headwaters to Gulf [ESRI Shapefile]." *GIS Center Data Repository.* February 2, 2010. http://www.mvp.usace.army.mil/gis/default3.asp?theme_id=2 (accessed May 16, 2012).

—. *Mississippi River Lock and Dam No. 8 Embankment Modifications - Adjusting Flow through Renow Spillway and Hastings Spillway - Hydraulic Assessment of Impacts to Reno Bottoms in Upper Pool 9.* Unpublished Report, St. Paul, MN: U.S. Army Corps of Engineers - St. Paul District, [no date, a].

—. "Mississippi River - Pool 8 (Dredge Data: 1931 - 2010) [Microsoft Excel File]." Internal Document, St. Paul, MN: U.S. Army Corps of Engineers - St. Paul District, July 12, 2011.

—. *Navigation and Ecosystem Sustainability Program (NESP).* [no date, b] http://www.mvp.usace.army.mil/navigation/default.asp?pageid=1118 (accessed November 3, 2012).

—. *Reservoir Regulation Manual - Appendix 8, Lock & Dam 8*. 1971.

—. *Upper Mississippi River Environmental Management Program, Minnesota/Wisconsin/Iowa (also known as Habitat Restoration: Upper Mississippi River Restoration).* October 16, 2012b. http://www.mvp.usace.army.mil/environment/default.asp?pageid=74 (accessed November 3, 2012).

—. *Water Control Center.* 2012c. http://www.mvp-wc.usace.army.mil/ (accessed November 2012).

U.S. Bureau of Reclamation (USBR). *SRH-2D version 2: Theory and User's Manual.* Denver, CO: U.S. Department of the Interior, 2008.

U.S. Congress. House. *Survey of Mississippi River between Missouri River and Minneapolis - December 9, 1931.* 72nd Cong., 1st sess., 1931.

U.S. Geological Survey - Upper Midwest Environmental Sciences Center (USGS – UMESC). "1890's Land Cover/Use [ESRI Shapefile]." *GIS Data - Pool 8 - Upper Mississippi River.* August 30, 1999. http://www.umesc.usgs.gov/rivers/upper_mississippi/reach_1/pool_8/p8_gis_data.html (accessed 2011-2012).

—. "1890's Map Plates - Georeferenced Images of Maps Produced by the Mississippi River Commission [ESRI Shapefile]." *GIS Data - Pool 8 - Upper Mississippi River.* October 1, 2005. http://www.umesc.usgs.gov/rivers/upper_mississippi/reach_1/pool_8/p8_gis_data.html (accessed 2011-2012).

—. "SAST River Miles [ESRI Shapefile]." *GIS Data - Pool 8 - Upper Mississippi River.* October 23, 1996. http://www.umesc.usgs.gov/rivers/upper_mississippi/reach_1/pool_8/p8_gis_data.html (accessed May 16, 2012).

U.S. Geological Survey (USGS). *Ecological status and trends of the Upper Mississippi River System 1998: A report of the Long Term Resource Monitoring Program.* LTRMP 99-T001, La Crosse, WI: U.S. Geological Survey, Upper Midwest Environmental Sciences Center, 1999.

—. *National Mapping Program Technical Instructions, Part 2-Specifications.* Washington, D.C.: Department of the Interior, 1998.

—. *The Long Term Resource Monitoring Program.* November 12, 2012. http://www.umesc.usgs.gov/ltrmp.html (accessed November 9, 2012).

Weber, L. J. “Personal Correspondence.” Iowa City, IA: The University of Iowa, 2011 - 2012.

WEST Consultants. *Upper Mississippi River and Illinois Waterway Cumulative Effects Study, Volume 1 and Volume 2.* Environmental Report #40 for the Upper

Mississippi River - Illinois Waterway System Navigation Study, Rock Island, IL: U.S. Army Corps of Engineers, Rock Island District, 2000.

Whipple, K. "Essentials of Sediment Transport." Class lecture, Massachusetts Institute of Technology, Boston, MA, September 2004.

White, F. M. *Fluid Mechanics.* New York, NY: McGraw-Hill Comapnies, Inc., 2011.

Young, N. C. "Physical Characterization of Freshwater Mussel Habitats in Upper Mississippi River Pool 16." *Ph.D. Diss.* Iowa City, IA: University of Iowa, 2006.